DISSERTATION

OH CRYOPROTECTANT, WHEREFORE ART THOU CRYOPROTECTANT? INVESTIGATION OF THE PERMEATION OF COMMON CRYOPROTECTANTS INTO LIVE RICE CALLUS CELLS BY COHERENT RAMAN MICROSCOPY

Submitted by

Fionna M. D. Samuels

Department of Chemistry

In partial fulfillment of the requirements

For the Degree of Doctor of Philosophy

Colorado State University

Fort Collins, Colorado

Summer 2023

Doctoral Committee:

Advisor: Nancy E. Levinger

Alan Van Orden
Debbie C. Crans
Jesse W. Wilson

ABSTRACT

OH CRYOPROTECTANT, WHEREFORE ART THOU?
INVESTIGATION OF THE PERMEATION OF COMMON CRYOPROTECTANTS INTO LIVE RICE CALLUS CELLS BY COHERENT RAMAN MICROSCOPY

Conserving a diverse selection of plant species is vital as climate change begins shifting the planet's ecosystems in earnest. Many plants can be preserved through maintaining their seeds in cool, dark chambers, like that of the Svalbard Seed Vault, but others do not reliably reproduce through seeds. This can include wild plants that lack seeds entirely, ferns for example, or agricultural plants where clonal propagation is the only way to conserve desirable traits, grapes, hops and bananas for example. Rather than collecting and saving seeds from these plants, researchers collect tissue samples, cool and preserve them in liquid nitrogen then warm and regrow the plants years later.

To maximize post-freezing viability, tissue samples are exposed to mixtures of cryoprotectants. Only a few cryoprotectant formulations have been used almost exclusively since their development in the early 1990s, including Plant Vitrification Solution 2 (PVS2) and Plant Vitrification Solution 3 (PVS3). Unfortunately, these formulations are not universally protective—some plant species respond extremely well to exposure while others are killed. When PVS2 or PVS3 fail to preserve a species, researchers must either empirically develop a new formulation or method of cryopreservation or settle for not conserving the species. A lack of mechanistic understanding of how these formulations work to protect tissue from extreme cold prevents straightforward development of new formulations.

Since the development of PVS2 and PVS3, advances in instrumental techniques have opened the door to improved physical characterizations of the components of these mixtures. Vibrational microscopies, like Raman or infrared microscopy, allow the direct visualization of cryoprotectants interacting with living cells. By exciting vibrations unique to the bonds in a molecule, these techniques can effectively image nearly unadulterated molecules. Through deuteration, cryoprotectants can be imaged without disturbing other molecules in the cell.

The work presented in this dissertation demonstrates how deuterated dimethyl sulfoxide (d_6-DMSO), deuterated ethylene glycol (d_6-ethylene glycol) and deuterated glycerol (d_8-glcyerol) can be directly imaged inside living rice callus cells. Readers are first introduced to the cell system, rice callus cells, and the analytical technique, coherent anti-Stokes Raman scattering (CARS) microscopy. Then, they will learn about initial static experiments searching for the location of d_6-DMSO within the callus cells. The next two chapters explore the real-time permeation of d_6-DMSO, d_6-ethylene glycol and d_8-glcyerol individually and then solvated in PVS2. The final chapter describes future experiments I think should come from this work that will increase fundamental understanding of cryoprotectant-cell interactions and streamline the process of developing new cryoprotectant formulations.

ACKNOWLEDGMENTS

This work would have been impossible without the support of my family and friends. Their support kept me going through the thick of graduate school when it was hard to see the end of the tunnel. This of course includes my Velcro pets who were always ready to give me an excuse to get out of the lab or off the computer.

I'm thankful for Dr. Nancy Levinger's guidance and flexibility. She supported my pursuit of science writing in lieu of an academic trajectory and for that I am eternally grateful.

I was and remain thrilled to have received the NSF Graduate Research Fellowship and the AAAS Mass Media Fellowship. The first kept me in graduate school and the second taught me that those "soft skills" everyone says you learn have real value outside of academia.

I was incredibly lucky to work with brilliant collaborators who helped with every aspect of this research. Thank you Dr. Gayle Volk and Remi Bonnart for opening the world of plants to me and thank you Dr. Dominik Stich for teaching me so much about microscopy.

Finally, thank you to my wonderful group members who helped in countless ways from giving me feedback on presentations and publications, to collecting data, to teaching me how to code. Y'all are amazing scientists and people; I can't wait to see all the spectacular things you accomplish!

DEDICATION

For my mom, aka my day one.

TABLE OF CONTENTS

LIST OF TABLES

LIST OF FIGURES

CHAPTER 1: Introduction

There is no question that it is vital to preserve cells and tissues from different species, from single celled organisms to higher order plants and animals. Preserved tissues and cells are used for diverse purposes, including fundamental cell research, *in vitro* fertilization (human and animal), endangered species conservation (both animal and plant), long-term agricultural security, and more.[1] The importance of plant conservation specifically was recognized by The Convention on Biological Diversity (2002), which had targets to conserve 75% of threatened plant species with *ex situ* techniques, like seed banks, and 70% of the genetic diversity of crops, wild relatives, and other economically relevant species by 2020.[2] A review published twelve years later made it clear that these goals were overly ambitious,[3] a attributed, in part, to the recalcitrance of some species to traditional seed banking. These species are known as "exceptional species" because they are exceptionally difficult to conserve.[4] They cannot be conserved through their seeds because they are 1) seedless, 2) do not survive desiccation processes associated with seed banking, 3) are short lived in cold storage, and/or 4) remain dormant for years after seed banking.[4]

For these exceptional species, collections must be grown in fields, greenhouses, or *in vitro* for preservation.[4] Unfortunately, these collections are particularly susceptible to environmental threats as well as pests and diseases. Having a secure backup of these collections is critical to their long-term sustainability.[4] When possible, cryopreservation, or long-term storage in liquid nitrogen, provides a secure, efficient backup for plant genebank collections.[4,5]

Cryopreservation has been utilized in plant genebanks for over thirty years.[5] Cryopreservation methods have been developed to maximize the number of cells that survive freezing. These methods are effective at preserving biological materials, e.g. cells and tissues, in

the liquid or vapor phase of liquid nitrogen.[1,6] Perhaps unsurprisingly, cells and tissues need help surviving the extreme temperatures of cryopreservation. Cryoprotectants are chemical compounds needed to maximize the number of viable cells after liquid nitrogen exposure for many cryopreservation systems.[7,8] During vitrification-based cryopreservation methods, cells and/or tissues are exposed to cryoprotectants then rapidly plunged into liquid nitrogen. Their exposure to cryoprotectants pulls water from the inside of the cell and the rapid cooling causes the now dehydrated cytoplasm to become glassy.[9] Unfortunately, no universal cryoprotectant solution works to protect all, or even most, samples. Cryopreservation methods must be optimized for every new species to balance the protective effects of cryoprotectants against their toxicity.[6]

In the plant community, the most commonly used cryoprotectant solutions are Plant Vitrification Solution 2 (PVS2; 30% (*wt/v*) glycerol, 15% (*wt/v*) dimethyl sulfoxide (DMSO), 15% (*wt/v*) ethylene glycol, 0.4 M sucrose)[7] and Plant Vitrification Solution 3 (PVS3; 50% glycerol, 50% sucrose),[8] but neither is universally protective. Optimizing the formulation and methods for individual plant species takes time and resources, which may not be available for endangered species. The difficulty associated with optimization is partly due to a lack of fundamental knowledge about how cryoprotectants interact with cells, particularly relating to the permeability of the cell membrane to different cryoprotectants.

Prior to the work presented in this thesis, the majority of cryoprotectant permeation studies focused on indirect evidence of permeation to explore how these molecules impact cells. Studies using brightfield and/or fluorescence microscopy to observe overall live-cell response to cryoprotectant exposure found that cells went through predictable responses with cryoprotectant exposure.[10–14] Immediately following exposure, the increased osmotic pressure from the cryoprotectant solution dehydrates cells causing the cell membrane to shrink away from the cell

wall (Figure 1.1A). This is called plasmolysis. After some time, the cell membrane starts to swell again and ultimately reaches the cell wall again—deplasmolysis (Figure 1.1C). Deplasmolysis has been attributed to cryoprotectant permeation despite the cryoprotectants being totally invisible to both brightfield and fluorescence microscopies.[10,11] This raises questions about whether cryoprotectants like glycerol, considered permeating in the animal cryopreservation community, is permeating plant cells because cells exposed to glycerol very rarely deplasmolyze. Other studies use electron microscopies to identify how cellular structures change after exposure, finding that vacuole membranes became fractured, the cytoplasm appeared denser and parts of the nucleus contained condensed chromatin, among other structural changes.[15] The question remains, where do cryoprotectants go inside plant cells?

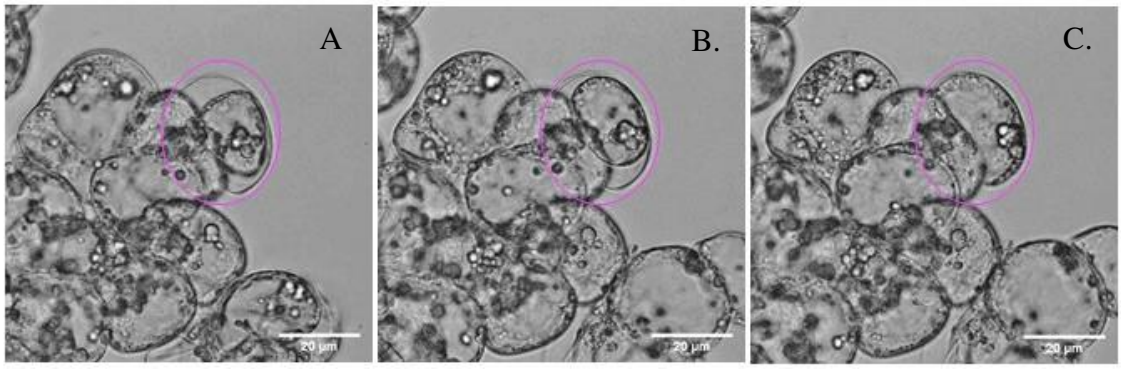

Figure 1.1: Brightfield images of plant cells exposed to a cryoprotectant mixture of 10% (*wt/v*) DMSO and 8% (*wt/v*) glucose, highlighting the plasmolysis (A.), middle of deplasmolysis (B.) and full deplasmolysis (C.) of the highlighted cell. A is 5 min after initial exposure and C is 30 min after initial exposure. Scale bar is 20 µm.

This question would be easily answered if cryoprotectants were visible through a traditional brightfield microscope—simply expose cells to cryoprotectants and see where the cryoprotectants go inside cells. However, cryoprotectant solutions are optically clear and it is impossible to determine where their components go within cells using visible light. Case in point, where is the DMSO or glucose in Figure 1.1? Fluorescent microscopy is another option that is commonly used in biology, but cryoprotectants are not inherently fluorescent and would require

the addition of a fluorescent tag to follow. For the cryoprotectants in PVS2, it is possible that the addition of such a tag would change the behavior of the cryoprotectant because of the difference in size between the cryoprotectant and tag.

Vibrational microscopies can directly measure the location and translocation of cryoprotectants in living cells. Unlike traditional fluorescence techniques, vibrational microscopies – like infrared (IR) absorbance or Raman scattering – do not require the addition of bulky fluorophores to locate molecules of interest. However, IR microscopy is limited by a large diffraction limit and the abundance of water within and around the cells. Raman scattering microscopy offers a way to directly image unadulterated-cryoprotectant interaction with living cells without interference from a water signal. To generate a signal, a laser with a frequency ω_p is impinged upon a sample causing three possible scattering events: Rayleigh, Stokes Raman and anti-Stokes Raman (Figure 1.2).[16] The Rayleigh scatter is elastic and does not contain vibrational information, while the Stokes and anti-Stokes scatter are inelastic with frequencies different than that of the original light (ω_s and ω_{as}, respectively). For spectroscopic studies, researchers take the difference between the impinged frequency and the scattered frequency to determine the difference between ground and excited vibrational states, ultimately generating a vibrational spectrum. However, there are two different approaches to using Raman scattering as a microscopy technique. The first, microspectroscopy, generates a Raman spectrum at each pixel of an image.[16,17] Different peaks in these spectra can be targeted and tracked giving researchers the ability to generate images of different cellular components from one data set. The second, simple microscopy, only collects the scattered light from a single, targeted vibrational mode and generates pixel intensity based on how much of the scattered light is collected.[16,18] All the Raman images presented in this thesis are of the simple microscopy variety.

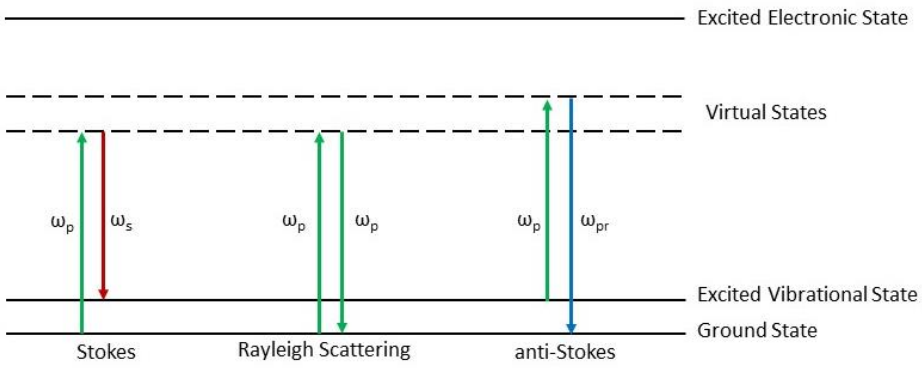

Figure 1.2: Energy diagram of the scattering processes that occur when a laser, ω_p, impinges on a sample. Rayleigh scattering is the elastic process, while the Stokes and anti-Stokes scatter are inelastic.

Unfortunately, spontaneous Raman is an inherently weak process,[18] limiting the sensitivity of the technique for imaging. Coherent anti-Stokes Raman scattering (CARS) offers orders of magnitude increase in sensitivity, while still relying on the unique vibrational modes circumventing the need for fluorescent labels.[18] CARS is a coherent nonlinear Raman scattering process wherein an anti-Stokes signal is generated by the interaction of pump, probe and Stokes fields.[18,19] Three fields with frequencies ω_p, ω_s and ω_{pr}, interact to generate the anti-Stokes shift collected in CARS microscopy such that $\omega_{as} = (\omega_p - \omega_s) + \omega_{pr}$ (Figure 1.3). The difference between ω_p and ω_{as} corresponds to a specific vibration in the molecule. Both the pump (ω_p) and probe (ω_{pr}) fields originate from the same beam, while the Stokes field is from a red-shifted beam (ω_s).[19] The two beam lines must be aligned both spatially and temporally for a signal to be generated in a sample.[19]

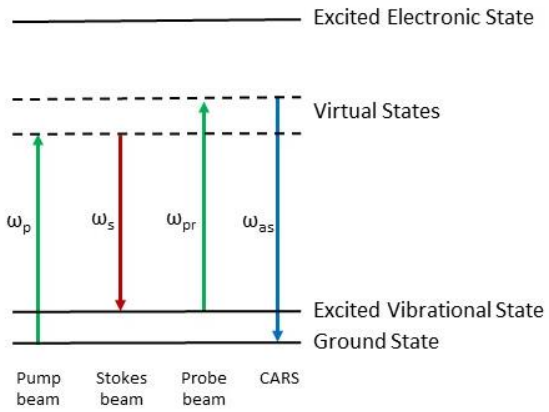

Figure 1.3: Energy diagram of the CARS process. The pump, Stokes and probe beams interact to generate a CARS signal such that $\omega_{as} = (\omega_p - \omega_s) + \omega_{pr}$.

Of course, choosing a microscopy technique is pointless without a suitable system to study. In this work, I use Asian rice (*Orzya sativa*) callus cells as a model system because callus cells are larger than cells found tissues. Callus are unorganized masses of cells that commonly form around injuries on plants (Figure 1.4).[20] These clusters can be harvested from a parent plant and grown on solid or in liquid plant growth medium.[20] In my research, callus cells appeared to continuously grow indefinitely so long as they were maintained appropriately (see Appendix IV).

Figure 1.4: An example of the callus cells used in experiments.

Classically, these clusters of cells have been considered undifferentiated cells, but there is evidence that they might be more similar to cells found in the roots of plants than to other parts of the plant regardless of where the callus forms.[21] Further, a recent study of the RNA contained within clumps of callus cells suggests that there may be some level of differentiation within each clump making the clusters heterogenous.[22] This heterogeneity seems to be between "layers" of cells going from the inside out of the entirety callus.[22] For this reason, any heterogeneity within the callus should not impact the work here because calli are broken into smaller clumps of 5-30 cells before imaging and thus each clump is more likely to be homogenous to itself. However, this should not affect the experiments described in this thesis.

Under the microscope, these cells appear as large as 20-50 μm in diameter (Figure 1.1). This makes it easy to see deuterated cryoprotectants entering the cells with CARS microscopy and measure the approximate rate of the cryoprotectant permeation. To the best of my knowledge, this work represents the first rigorous study of cryoprotectant permeation by CARS microscopy and gives us unique insights into where these molecules go within plant cells and how quickly they are getting there. By combining it with more traditional brightfield data, we are able to correlate cellular responses with the direct measurement of cryoprotectant permeation.

Chapter 2 of this work investigates how deuterated DMSO permeates live plant cells using CARS microscopy. This chapter does not incorporate kinetics and is a simple before-and-after experiment showing that the distribution of this common cryoprotectant is not uniform within plant cells.

Chapter 3 of this work combines brightfield and CARS microscope data to compare the time scale of plasmolysis and deplasmolysis to the direct observation of cryoprotectant permeation.

This chapter goes beyond DMSO and includes data from cells exposed to deuterated ethylene glycol and deuterated glycerol.

Chapter 4 of this work investigates how DMSO, ethylene glycol and glycerol behave in PVS2. This chapter aims to make this work even more relevant to current cryopreservation methods as individual cryoprotectants are always used in combination to protect cells.

Chapter 5 of this work considers the critical next steps that I believe should be taken to continue this work. The research presented here is simply the foundation for bigger and more complex future experiments.

CHAPTER 2: Non-Uniform Distribution of Cryoprotecting Agents in Rice Culture Cells Measured by CARS Microscopy

This chapter was originally published in the journal Plants.[*] The full contributions of the original authors are listed in Appendix I. I collected all the data and wrote the manuscript. Dominik D. Stich provided access and assistance with the CARS microscope. Remi Bonnart revived the callus cells from their three decades in liquid nitrogen and ensured that I knew how to maintain cell cultures. Gayle M. Volk provided insights into plant cryopreservation and helped direct the project. Nancy E. Levinger came up with the original idea to study cryoprotectant permeation with vibrational microscopy and directed the project to be successful.

2.1 Introduction

Cryoprotectants allow cells to be frozen in liquid nitrogen and cryopreserved for years by minimizing damages that occur in cooling and warming processes. Unfortunately, how the specific cryoprotectants keep the cells viable through the cryopreservation process is not entirely evident. This contributes to the arduous process of optimizing cryoprotectant formulations for each new cell line or species that is conserved. Coherent anti-Stokes Raman scattering microscopy facilitates the visualization of deuterated cryoprotectants within living cells. Using this technique, we directly imaged the location of fully deuterated dimethyl sulfoxide (d_6-DMSO), the deuterated form of a commonly used cryoprotectant, DMSO, within rice suspension cells. This work showed that d_6-DMSO does not uniformly distribute throughout the cells, rather entering the cell and sequestering within organelles, changing our understanding of how DMSO concentration varies within the

[*]Samuels, F. M. D.; Stich, D. G.; Bonnart, R.; Volk, G. M.; Levinger, N. E. Non-Uniform Distribution of Cryoprotecting Agents in Rice Culture Cells Measured by CARS Microscopy. *Plants* **2021**, *10* (3), 589. https://doi.org/10.3390/plants10030589.

cellular compartments. Variations in cryoprotectant concentration within different cells and tissues will likely lead to differing protection from liquid nitrogen exposure. Expanding this work to include different cryoprotectants and mixtures of cryoprotectants is vital to create a robust understanding of how the distribution of these molecules change when different cryoprotectants are used.

2.2 Results and Discussion

When plant cells are exposed to cryoprotectants, they can go through a process of plasmolysis and deplasmolysis,[10,12,23] as shown in Figure 2.1A. Plasmolysis is attributed to the change in osmotic pressure when a cell is exposed to a cryoprotectant solution, observable when the plasma membrane shrinks away from the cell wall. This is seen in Figure 2.1, Panel B, in the image acquired 70 s after exposure to 15% dimethyl sulfoxide (DMSO), a commonly used cryoprotectant in plant and animal cryopreservation. Following plasmolysis, the cell swells until the cell membrane reaches the cell wall in a process called deplasmolysis. Deplasmolysis is commonly attributed to cryoprotectants entering the cell,[10] as it is generally seen when cells are exposed to cell permeating cryoprotectants, like DMSO. However, simple attribution of cryoprotectants entering the cell to cause deplasmolysis does not explain why some cells, like the cell indicated by the purple arrow in Figure 2.1B, do not appear to respond to DMSO exposure with a plasmolysis/deplasmolysis cycle, while others, like the cell indicated by the red arrow, appear to respond as expected, plasmolyzing within 70 s of exposure and deplasmolyzing after 210 s of exposure, at room temperature. Both cells had movement within their cytoplasm, leading us to believe that they were both alive. This difference in response was observed in many different exposure experiments and with cells in clusters ranging from only a few cells to hundreds of cells (see Appendix I).

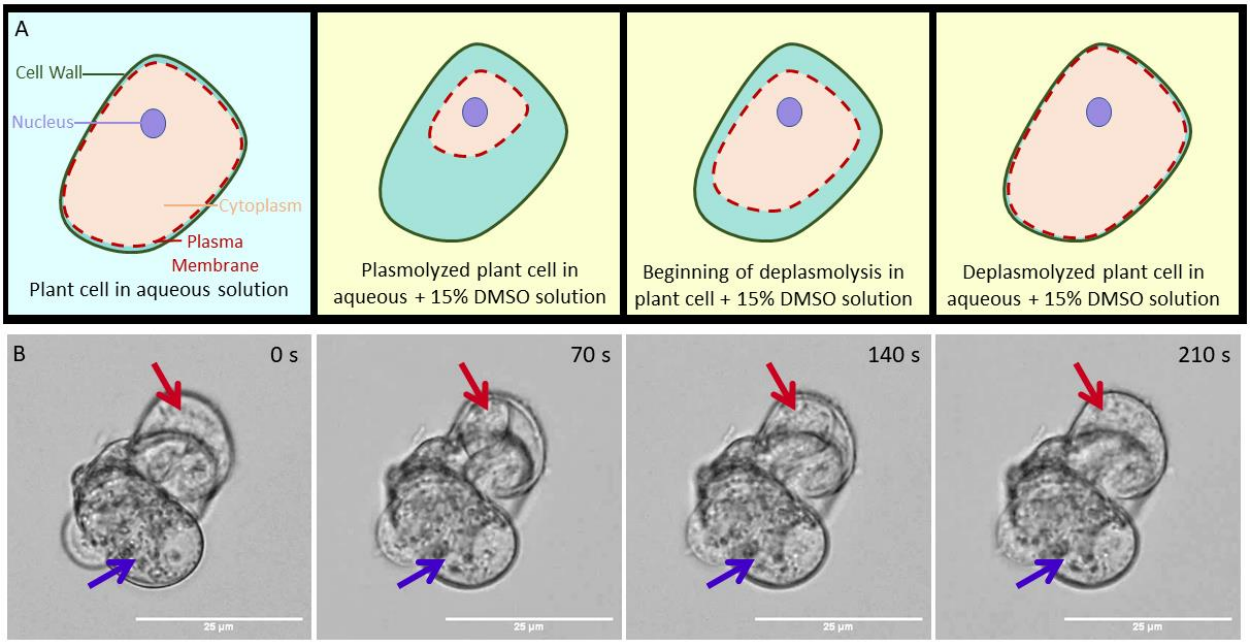

Figure 2.1: Panel A – cartoon representation of a cell undergoing plasmolysis (the pulling away of the red dashed plasma membrane from the green cell wall) and deplasmolysis (the moving of the cell membrane back to cell wall) as it is exposed to a 15% DMSO in water solution (yellow background. Panel B – brightfield microscopy images showing a small cluster of rice suspension cells 0, 70, 140, and 210 s after exposure to 15% aqueous DMSO. Red arrow: a cell that completely plasmolyzes after 70 s and deplasmolyzes after 210 s. Purple arrow: a cell that does not appear to respond to 15% DMSO in water solution.

Prior to exposure, at 0 s, the two highlighted cells appear similar, both appearing populated with small organelles which move within the cell. Thus, we might expect similar responses to the 15% DMSO solution. The question remains, did DMSO enter the unresponsive cell, or is it preferentially concentrated in the responsive cell? Although the macroscopic behavior of the cell is easily identifiable with bright field microscopy, the definitive localization of DMSO within these cells remains elusive. A primary objective of the current work is to directly observe the accumulation of DMSO within cells, as previous work has almost entirely relied on observing cellular responses to cryoprotectant exposure to understand the protective behavior of cryoprotectants.

There has been some work characterizing cellular responses to explore how cryoprotectants work to protect or destroy cells.[7,8,10,12,23–28] Bright field microscopy techniques have shown how cells respond to cryoprotectant exposure in real-time.[10] Fluorescence microscopy has identified how fluorescently-labelled organelles move and change upon cryoprotectant exposure,[24] as well as histological changes that occur.[23] Electron microscopy has been used in conjunction with fluorescence microscopy to observe ultrastructural changes within cells that occur with cryoprotectant exposure and freezing.[27,28] Toxicity studies have demonstrated the applicability of standard cryoprotectant formulations to new cell lines,[7,8] and various protein assays have determined DNA or RNA damage by cryoprotectant exposure.[25,26] All these studies inform how cells respond to and are damaged by cryoprotectant exposure, but they do not identify or determine cryoprotectant location or translocation within cells. Detailed information on cryoprotectant location and translocation within living cells, specifically which organelles are being most impacted by cryoprotectant exposure, will enable the development of highly robust and specific cryopreservation protocols that provide improved tolerance to cooling and low temperature storage.

Most cryoprotectant formulations are mixtures of small molecular components, commonly DMSO, glycerol, ethylene glycol, and sugars. These molecules cannot be directly imaged by bright field microscopy and attaching a dye molecule to any of these molecules dramatically changes their diffusion behavior, making bright field and fluorescence microscopies ill-suited for determining their exact location within cells. However, these small molecules can be imaged using vibrational microscopy, which enlists unique vibrations intrinsic to the molecules of interest to image the sample. Although IR microscopy may be used as a label-free imaging technique, its intrinsically low spatial resolution (due to long IR wavelengths) and water's high IR absorptivity

makes it challenging to image biological samples. Recent advances in IR microscopy that enlist both a mid-IR and ultraviolet laser can generate photoacoustic data with resolutions comparable to that collected with fluorescence microscopy.[29] Raman microscopy enables the imaging of live samples with wavelengths in the near-IR and visible region via the vibrations associated with specific molecules.[30] For example, the hydrocarbon in lipid molecules is highly effective for imaging cell membranes.[30] Although spontaneous Raman microscopy has been used to image live cells and tissues, it suffers from low sensitivity and contamination from endogenous sample fluorescence.

Various nonlinear coherent Raman scattering methods demonstrate dramatic enhancement in sensitivity over traditional Raman microscopy.[18,31–33] For example, coherent anti-Stokes Raman scattering (CARS), used in this work, boasts five to six orders of magnitude higher sensitivity to spontaneous Raman measurements.[18,30] Additionally, coherent Raman microscopy techniques avoid interference by endogenous fluorescence through optical filtering and also offer high spatial resolution, with optimal resolutions ≤300 nm, and high temporal resolution, <1 s, to measure location and translocation of molecules of interest.[30,33] These dramatic improvements enable real-time acquisition in live, biological samples.[34]

All coherent Raman processes require two short laser pulses, usually in the picosecond range, aligned in space and time so that both beams simultaneously impinge on the sample. When the frequency difference between the pump and Stokes beams matches a molecular vibration in the sample, CARS signal is generated (see Appendix II).[18] CARS signal is quadratically proportional to the concentration of the molecule of interest,[18] so CARS microscopy is most frequently used to image prevalent biological components in cells. Although Raman techniques have been used to image intra-cellular lipid responses to cryoprotectants,[35] freezing behavior of

water in and around live cells exposed to cryoprotectants [36–38], and bulk distributions of cryoprotectants in frozen mixtures,[39] they have yet to be applied to directly image cryoprotectants distribution within living plant cells. In the work reported here, we use CARS microscopy to image deuterated dimethyl sulfoxide (d_6-DMSO) interacting with live rice suspension cells.

As most cryoprotectants are organic molecules composed largely of carbon, hydrogen and oxygen, their vibrational modes often fall in the same frequency range as the biological sample itself. In this work, we enable selective cryoprotectant detection by deuteration. Figure 2.2A shows how deuteration in d_6-DMSO shifts the C-H stretch of DMSO (~2900 cm^{-1}) away from the broad C-H stretch region in the plant cells to the relatively quiet C-D stretch region of the spectrum (~2120 cm^{-1}). Targeting the 2120 cm^{-1} stretch ensures that CARS signal detected reflects d_6-DMSO while cell features like the cell membranes and walls block that signal. The CARS image shown in Figure 2.2B was collected after the was exposed to d_6-DMSO for approximately 3 min, which was the amount of time it took to prepare the sample and begin collecting data. The d_6-DMSO signal appears as yellow, while blue features indicate places where no d_6-DMSO is present or components of the cell or other cells block the d_6-DMSO signal. Figure 2.2C shows an expanded view of the cell highlighted by the light blue square in Figure 2.2B. In this cell, the d_6-DMSO signal appears to pool in subcellular organelles. That is, rather than remaining dispersed throughout the cytoplasm, the d_6-DMSO preferentially accumulates in specific organelles. The blue outlines around these pools and in other parts of the image arise from areas where cellular components, such as lipid membranes and cell walls, block the d_6-DMSO signal. Figure 2.2D contrasts the pixel intensity along the pink and dark blue lines drawn in Figure 2.2C. The pink line intercepts three obvious d_6-DMSO-rich organelles while the blue line goes through a relatively uniform background part of the cell, contrasting the inside of the organelles to the surrounding cytoplasm.

It is clear that there is a higher concentration of d_6-DMSO inside those organelles than in the surrounding cytoplasm. This demonstrates that d_6-DMSO is not uniform in the cell interior, preferentially pooling inside organelles within the cell. Other than a ~8% increase in mass, the properties of d_6-DMSO differ little from H_6-DMSO. Thus, we expect the same effect when cells are exposed to H_6-DMSO, as the molar mass is not significantly changed by deuteration.

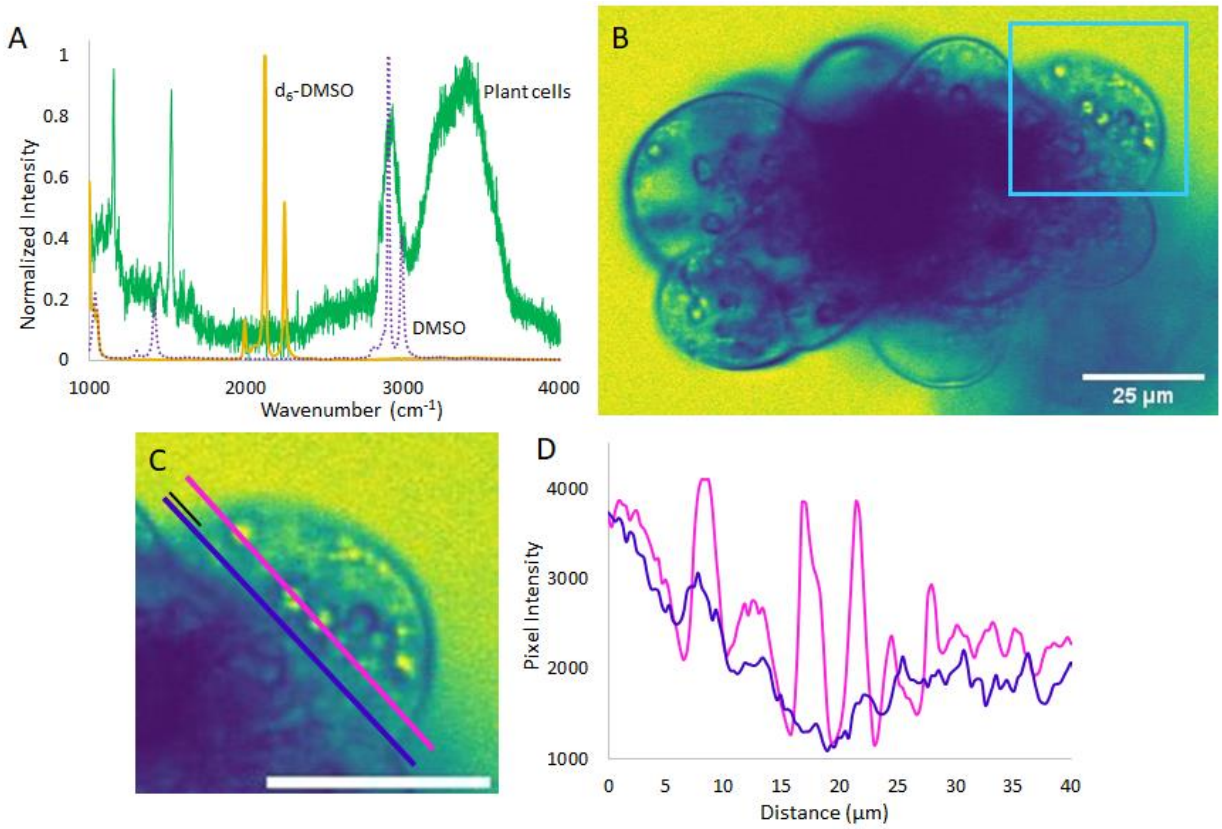

Figure 2.2: A: Spontaneous Raman spectra of d_6-DMSO (yellow), DMSO (purple, dashed) and the rice cells (green), showing the shift in DMSO vibrational frequency upon deuteration away from significant peaks in the cell spectrum. B: Representative CARS microscopy image of rice cells imaged in resonance with the d_6-DMSO stretching vibrational mode (yellow trace in A) Signal from d_6-DMSO appears yellow while places blocking d_6-DMSO signal appear blue. C: Expanded view of cell outlined in light blue in B. Parallel pink and dark blue line profiles bisect three organelles and relatively uniform space away from organelles, respectively. Both lines start 5 µm outside of the cell, a distance shown with the small black line, and stretch, parallel, across approximately 40 µm. D: Pixel intensity along pink and dark blue line profiles from C as a function of distance along the line. Scale bars in C and D are 25 µm. Images artificially colored with ImageJ LUT, mpl-viridis.[40]

The CARS images collected of d_6-DMSO indicate that DMSO is pooling in specific organelles within the live cells. On the basis of bright field microscopy experiments (shown in Appendix I), we suspect that the organelles preferentially taking-up DMSO are amyloplasts and/or starch bodies. Additionally, there is evidence in the literature suggesting that DMSO interacts with glucose and amylose, both components of starch.[41,42] An increase in DMSO concentration in these organelles may increase the amount of protection afforded to the organelles as DMSO is known to disrupt the hydrogen bond network of water and support vitrification—or freezing the cells in a glassy state—over ice crystallization. This result may also indicate that these organelles are at a higher risk of damage from DMSO toxicity, as DMSO has been shown to cause cell death[43] and, at high concentrations, presumed to disrupt cell membranes.[44,45] Furthermore, the apparent sequestration of DMSO inside these organelles challenges the assumption of equal DMSO distribution throughout the cell. The preferential localization of the DMSO cryoprotectant has ramifications in all disciplines that use cryopreservation – an unequal distribution of cryoprotectants in cells and tissues have different implications depending on the specific system. In cells that do not contain these organelles, DMSO uptake may be more uniform or different organelles may be preferentially sequestering the cryoprotectant. Previous research on cellular responses to cryoprotectants have made it obvious that assuming cryoprotectants to work equally and effectively in all cell types is flawed,[7,8] and this result may partially explain the differences in cellular response seen in brightfield studies like those in Figure 2.1.

2.3 Conclusions

Using CARS microscopy, we visualized sequestration of d_6-DMSO in organelles within living rice suspension cells that were originally cryopreserved in 1981. After 37 years of cryostorage, the cells were thawed in 2018, and grew vigorous, friable calli. Both macroscopic

signs of growth and generated autofluorescence within cells demonstrated the viability after rewarming and cryoprotectant exposure experiments. These cells serve as a model system for our first experiments demonstrating the value of direct visualization of cryoprotectants in living systems. Localization of cryoprotectants like DMSO in cell organelles may explain how these substances induce changes in cellular processes.[26,43] The nonuniform distribution of cryoprotectant in the cells implies that any assumption of an equal cryoprotectant dispersion with a cell, and consequently equal protection afforded by the cryoprotectant throughout the cell, is flawed. Continued investigation into the exact location of various cryoprotectants within a broad range of living cells and tissues will likely illuminate why cellular response varies with cryoprotectant exposure, something applicable to both animal and plant cells. The establishment of cellular responses to cryoprotectant exposure has the potential to streamline development of cryopreservation protocols for newly endangered plant and animal species, allowing goals such as those set by The Convention on Biological Diversity to be more readily achievable, and enable more species to be conserved as we face our current climate crisis.

2.4 Materials and Methods

2.4.1 Growth and Maintenance of Oryza sativa (Asian Rice) Cells

2.4.1.1 Rewarming Cells and Initial Plating

Rice callus cells were acquired from the USDA-ARS National Laboratory for Genetic Resources Preservation in Fort Collins, CO. The cell line was originally produced by G. Schaeffer, U.S. Dept. of Agriculture, Beltsville, Md in 1981.[46] The rice cells used in this work were originally cryopreserved by Finkle and Ulrich in 1981 using PGD (10% w/v polyethylene glycol, 8% w/v glucose, and 10% w/v DMSO)[47] and a slow-cool procedure. Rice callus cells (A7 line) were removed from liquid nitrogen and immediately warmed in a 40 °C water bath for 2 min, until the

solid cryoprotectant solution inside the vial was liquid. The cryoprotectant solution and cells were then diluted with 0.5 mL of wash solution made with 30 g L^{-1} sucrose (Alfa Aesar, Ward Hill, MA) and Murashige and Skoog basal plant medium with vitamins (MS Media, M519; PhytoTechnology Laboratories, Lenexa, KS) in distilled water at 22 °C and incubated for 10 min, before 1 mL of wash solution was added at 22 °C. The solution was then allowed to sit for 10 min. The vial was then centrifuged for 1 min at 1000 rpm. The supernatant was removed with a pipette and 1 mL of wash solution was added to the remaining cells and incubated at 22 °C for 10 min. The liquid was removed from the vial with a pipette and the cells were scooped from the vial onto a sterile filter paper and blotted to remove excess liquid. The semi-dry cells were then plated onto solid modified MS Media (PT046; HiMedia Laboratories, Lincoln University, PA) supplemented with 1 mg L^{-1} each of 2,4-dichlorophenoxyacetic acid (2,4-D, Sigma-Aldrich, St. Louis, MO), indoleactetic acid (IAA, TCI America, Portland, OR) and kinetin (TCI America), 146 mg L^{-1} glutamine (Acros Organics, Geel, Belgium), 30 g L^{-1} sucrose and 8 g L^{-1} agar (BD Diagnostics, Franklin Lakes, NJ) at pH 5.7. The plated cells were placed in a light-free container and were confirmed to be alive after growth was visible (approximately 3 weeks after plating).

2.4.1.2. Cell Culture

The cells were grown as suspension cultures or as callus. For both suspension and plated cultures, modified MS medium (PT046) was supplemented with 1 mg L^{-1} each of 2,4-D, IAA and kinetin, 146 mg L^{-1} glutamine, 30 g L^{-1} sucrose and 8 g L^{-1} agar (removed for suspension cells) at pH 5.7. After autoclaving, 10 mL of medium was placed in 6 cm diameter Petri dishes and allowed to set for 30 min before being stored in the refrigerator. Rice callus cells were transferred to new solid media every 4-6 weeks depending on growth of the callus. When they were transferred, growth appearing the lightest in color was selected from the callus with sterile tweezers and placed

onto the new medium. The cells were grown at room temperature in a closed drawer, maintaining constant darkness and used in experiments as necessary. Suspension cells were grown using the same formulation of modified Murashige and Skoog medium, without the addition of agar. To grow cells in suspension, approximately a gram of the lightest colored rice callus cells was removed from plates and placed in Erlenmeyer flasks with 50 mL liquid media. Cells were culture grown on a shaker continuously rotating at 140 rpm. The Erlenmeyer flasks with suspension cells were wrapped in aluminum foil to ensure the cells would be grown in the dark. Suspension medium was replaced every 1-2 weeks, and the cells were moved to new suspension cultures at that time, depending on growth. When creating a new culture, flasks were removed from the shaker and allowed to settle for about 10 minutes before excess media was removed with a pipette. Cells were removed from the flask, blotted on sterile filter paper to remove excess medium and about 1 cm^3 of cells was placed in a new flask.

2.4.2 Cryoprotectant Solutions

For bright field images, 15% (w/v) DMSO in distilled water was used. For all cryoprotectant exposures imaged with the CARS microscope, 15% (w/v) d_6-DMSO (MilliporeSigma, St. Louis, MO) in distilled water was used. This is the concentration of DMSO found in PVS2[7] and was chosen for the broad applicability of DMSO to both animal and plant cryopreservation.

2.4.3 Cell Imaging

Bright field images were acquired using an Olympus IX73 fluorescence microscope (Olympus Corporation, Tokyo, Japan) in the Chemistry Department Cell Culture Facility at Colorado State University. A rudimentary perfusion chamber was developed to image cells as exposure to cryoprotectant solutions occurred. The rudimentary perfusion chambers were made

using a microscope slide, cover slip, and silicone grease, as shown in Figure 2.3. After creating a central channel using silicone grease, the channel was coated in 1% poly-L-lysine (Electron Microscopy Sciences, Hatfield, PA) to immobilize the rice cells while solutions flowed through the chamber. The slide was cleaned with methanol, then a large drop – enough to cover the entire area under the coverslip – of poly-L-lysine was placed on the slide and allowed to set for 24 hours. After setting, the poly-L-lysine was rinsed away with distilled water and the slide was air dried and immediately used for imaging the cells. Both cells grown on plates and suspension cultures were used. Callus cells were suspended in a small amount of MS Media by placing a small amount of friable callus in a vial with 1 mL of media and vigorously shaking. Suspension cells were placed on microscope slides directly from the cellular suspension. After placing the cells on the microscope slide, a 25×50 mm cover slip was placed onto the slide, creating a wide channel through which cryoprotectant mixtures could be wicked. Approximately 0.5 mL of the 15% DMSO solution was placed on the edge of the coverslip while a Kim Wipe was held to the other end. This created flow and images were acquired as the solution travelled across the perfusion chamber and the cryoprotectant solution was allowed to sit in the chamber. This was repeated five times with 15% DMSO in water and a total of 35 cells were clearly visible. Of these cells, 8 appeared dead, 22 cells (61%) had a visible response to the solution, and 3 cell (8%) had a full plasmolysis/deplasmolysis cycle. A visible response was considered a rapid shrinking and expansion where there was no visible plasmolysis. For more on the number of cells responding to cryoprotectant mixtures, see Appendix I.

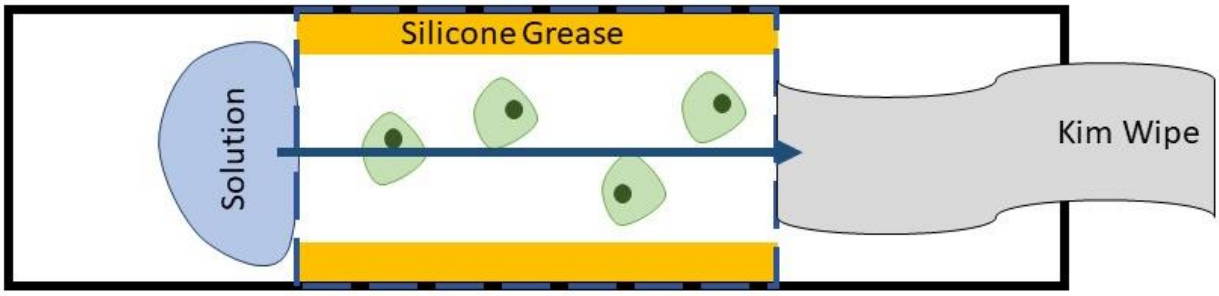

Figure 2.3: Rudimentary perfusion chamber showing plant cells in green, silicone grease in yellow, wicked solution in blue, and KimWipe in grey on a white microscope slide (outlined in solid black). 25×50 mm cover slip placed on top of grease shown in blue dashed lines.
See Appendix I for a CARS microscopy instrument description.

2.4.4 IKI Staining

Cells were stained with an iodine solution prepared with 100 mL distilled water, 1 g of iodine chips (Fisher Scientific, Fair Lawn, NJ) and 2 g KI (Fisher Scientific), for 1.5 to 5 minutes. After staining, the cells were rinsed with water before mounting and imaging.

CHAPTER 3: Direct measurement of rice (*Oryza sativa*) callus cell responses to common molecular cryoprotectants

This chapter was originally published in the journal Cell Reports Physical Sciences in June, 2023.[†] *The full contributions of the original authors are listed in Appendix II. I collected all the CARS data, analyzed both the CARS and the brightfield data, and wrote the manuscript. Both Kylie C. Pearce and Stephanie Soderlund collected the brightfield data that appear here. Again, Dominik D. Stich provided access and assistance with the CARS microscope. Remi Bonnart provided callus cells to us after mine died from neglect during the first year of the COVID-19 pandemic. Again, Gayle M. Volk provided insights into plant cryopreservation and helped direct the project. And finally, it was Nancy E. Levinger's idea to expand the original paper beyond just DMSO permeation and she ultimately directed the project to success.*

3.1. Introduction

Cryoprotectants are vital to ensuring that undifferentiated plant cells and organized shoot tips can survive liquid nitrogen exposure during cryopreservation and subsequent warming. The fundamental interaction between cryoprotectants and cells and shoot tips is an understudied area and the exact mechanism for protection remains elusive. By coupling coherent anti-Stokes Raman scattering (CARS) microscopy with brightfield microscopy, we determine how quickly the widely used cryoprotectants dimethyl sulfoxide, ethylene glycol, and glycerol permeate into living plant cells and how this permeation correlates with cellular responses. Some cellular responses observed with brightfield microscopy, such as plasmolysis and deplasmolysis, occur in response to

[†] Samuels, F. M. D.; Pearce, K. C.; Soderlund, S.; Stich, D. G.; Bonnart, R.; Volk, G. M.; Levinger, N. E. Direct Observation of Common Cryoprotectant Permeation into Rice Callus by CARS Microscopy. *Cell Reports Physical Science* **2023**, 101469. https://doi.org/10.1016/j.xcrp.2023.101469.

cryoprotectant permeation. The observational results from the combination of brightfield and coherent anti-Stokes Raman microscopy reported here show that cellular response and cryoprotectant permeation occur on different timescales and that cryoprotectant molecules permeate virtually all cells, even those displaying no response in brightfield microscopy.

To assess and compare the timescales of cellular response to different cryoprotectants, this chapter reports both brightfield and CARS microscopy data from cells exposed to cryoprotectant solutions in a perfusion chamber. Cellular response is widely attributed to the permeation of cryoprotectants, but this relationship has not previously been directly visualized in plant cells. Brightfield images allow us to determine the probability of three different cellular responses and CARS data show when and where cryoprotectants permeate cells. A statistical analysis of how quickly cellular responses occur compared to how rapidly cryoprotectants permeate cells suggests that the relationship between responses observed in brightfield microscopy and cryoprotectant exposure may be more complex than simple osmotic pressure gradients. In contrast, our CARS microscopy data show that cryoprotectants penetrate all cells, even those that do not exhibit responses typically associated with permeation. Combining the two techniques gives a robust picture of how cellular responses relate to cryoprotectant permeation. Ultimately, understanding how cryoprotectant permeation correlates to easily observed cellular responses could help make the arduous process of optimizing cryopreservation methods more efficient. These findings both contribute to the field of cryopreservation by adding to a growing body of work focused on cryoprotectant-cell interactions and demonstrate the power of combining multiple analytical techniques with statistical analysis.

3.2. Results and Discussion

3.2.1 Brightfield Microscopy

Herein, we report the responses of rice callus cells to individual components of PVS2 and PVS3 cryoprotectant solutions measured using brightfield microscopy. We observe variable cellular responses and response times. This is consistent with previous literature that measured sweet potato suspension cell responses to cryoprotectants.[9] Unlike previous studies, the data reported here were collected as the cryoprotectant solutions flowed across the cells.[43] The resulting videos allow cellular response to be visualized in real-time. However, brightfield microscopy does not show when the cryoprotectant enters the perfusion chamber nor when the media initially present in the perfusion chamber has been completely replaced by the cryoprotectant solution because both solutions are clear and colorless when viewed through the microscope. This makes it difficult to establish exactly when the cryoprotectant solution first enters the field of view, the ideal time zero. Thus, for the brightfield experiments, we estimate time zero—the time when the cryoprotectant solution enters the field of view—as the first time the cells showed any response to cryoprotectant introduction into the perfusion chamber. This generally appears as the entire cluster of cells shrinking slightly before any individual cells show a response and occurs with any cryoprotectant exposure. We note that this time could be after the cryoprotectant actually entered the perfusion chamber.

There are three expected responses when cells are exposed to cryoprotectants: a slight deformation of the membrane, plasmolysis, and deplasmolysis. The first two responses occur at or after the initial cryoprotectant exposure and the third, deplasmolysis, can only occur after the cells first plasmolyze in response to the cryoprotectant. A cartoon illustration in Figure 3.1 demonstrates these responses beginning with an untreated cell. Figure 3.1a shows one possible observation upon

exposure to a cryoprotectant: slightly deformed cells, where the plasma membrane deforms and slightly pulls away from the cell wall before returning to its initial shape. Although this could be interpreted as some level of plasmolysis, in real cells it is frequently difficult to tell if the membrane fully pulls away from the cell wall, as expected during plasmolysis.[10] Rather than representing this action as full plasmolysis, we call this a "crumpling" and do not include any cells that respond in this manner in plasmolysis or deplasmolysis counts in the statistical analyses. Alternatively, a cryoprotectant solution-treated cell may plasmolyze and then deplasmolyze (Figure 3.1b). Cells that respond in this way are counted as both plasmolyzing and deplasmolyzing in subsequent statistical analyses. Finally, a cryoprotectant solution-treated cell may plasmolyze and then fail to deplasmolyze within the observed timeframe (Figure 3.1c). In this case, the cell would only be counted as plasmolyzing.

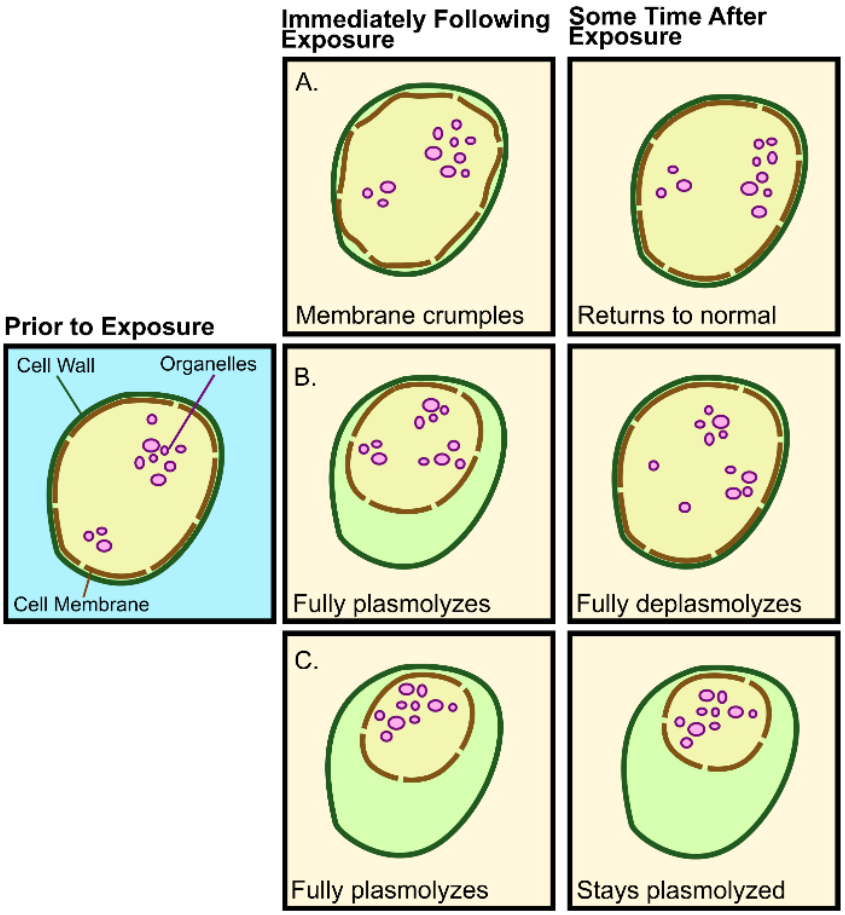

Figure 3.1: A cartoon representation of a cell undergoing the three responses observed from rice callus cells: a. slight deformation or crumpling response that differs from true plasmolysis because the cell membrane only deforms slightly away from the cell wall, b. plasmolysis (cell membrane contracts away from the cell wall) and subsequent deplasmolysis (cell membrane returns to cell wall), c. plasmolysis with no deplasmolysis. The timescales for the processes vary. Note: we omit the tonoplast because it is not always visible in brightfield or CARS images making its behavior difficult to elucidate.

3.2.2 Overall Brightfield Observations

The collected brightfield data show that the responses of individual cells in a cell cluster to cryoprotectant exposure vary. Table 3.1 provides the results from a generalized linear model correlating plasmolysis and deplasmolysis to cryoprotectant exposure. This model shows how likely we are to observe each response when exposed to each individual cryoprotectant: a crumpling/slight deformation response (% crumpled), plasmolysis (% plasmolysis) and deplasmolysis (% deplasmolysis). For example, although it is unlikely, the brightfield data show

that some cells exposed to glycerol deplasmolyze. The generalized linear model was generated from 10 glycerol, 13 ethylene glycol, and 5 DMSO exposure experiments, comprising 101, 113, and 45 clearly visible cells, respectively. The data and model give insights into how response, plasmolysis and deplasmolysis depends on the type of cryoprotectant to which the cells are exposed.

Table 3.1: Summary of generalized linear model results used to predict the percentage of cells that undergo a crumpling response, plasmolysis, or deplasmolysis based on the cryoprotectant used. Response and plasmolysis are based on the total number of visible cells analyzed while deplasmolysis values reflect only the cells that have plasmolyzed. The number of cells that go through each response are shown in parentheses.

	N	**% Crumpled***	**% Plasmolysis**	**% Deplasmolysis**
DMSO	45	36.4 *(n=17)*	63.6 *(n=28)*	96.4 *(n=27)*
ethylene glycol	113	47.8 *(n=53)*	52.2 *(n=59)*	100.0 *(n=59)*
glycerol	101	20.8 *(n=20)*	79.2 *(n=80)*	20.0 *(n=16)*

* Cells counted as undergoing a crumpling response are not included in the plasmolysis or deplasmolysis numbers.

3.2.3 Response to DMSO

When a 15% (*wt/v*) DMSO solution was flowed across live rice callus cells, 36.4% of the observed cells exhibit crumpling, 63.6% of the observed cells exhibit plasmolysis, and 96.4% of the plasmolyzed cells also deplasmolyzed (Table 3.1).

An example of these responses is shown in a series of images in Figure 3.2. Four cells of interest are indicated in the first frame. We identify the cell membrane location with a colored line just inside of the cell membrane. The line type is solid prior to exposure, dashed at the end of plasmolysis, and dash-dot at the end of deplasmolysis or a crumpling response. The first image at t = -0.4 min, shows the cells prior to the initial overall cluster response (t = 0). Cell 1 (light pink) crumples slightly before expanding to its previous size; this response is not captured in these still images because it occurs within 30 s of t = 0 min. This demonstrates the necessity for high time-resolution imaging techniques as some cell responses occur relatively quickly. Cells 2, 3 and 4 all

plasmolyze and deplasmolyze. Although all these cells plasmolyze, the larger cells (3 and 4) take longer to plasmolyze than the smaller cell (2). Cell 2 completes plasmolysis after 1 min and deplasmolysis after 2 min. Cells 3 and 4 both finish plasmolyzing after 2 min then deplasmolyze after 10 and 8 min, respectively. We observed movement within all the cells throughout the entire process, indicating that these cells are likely alive throughout the experiment.

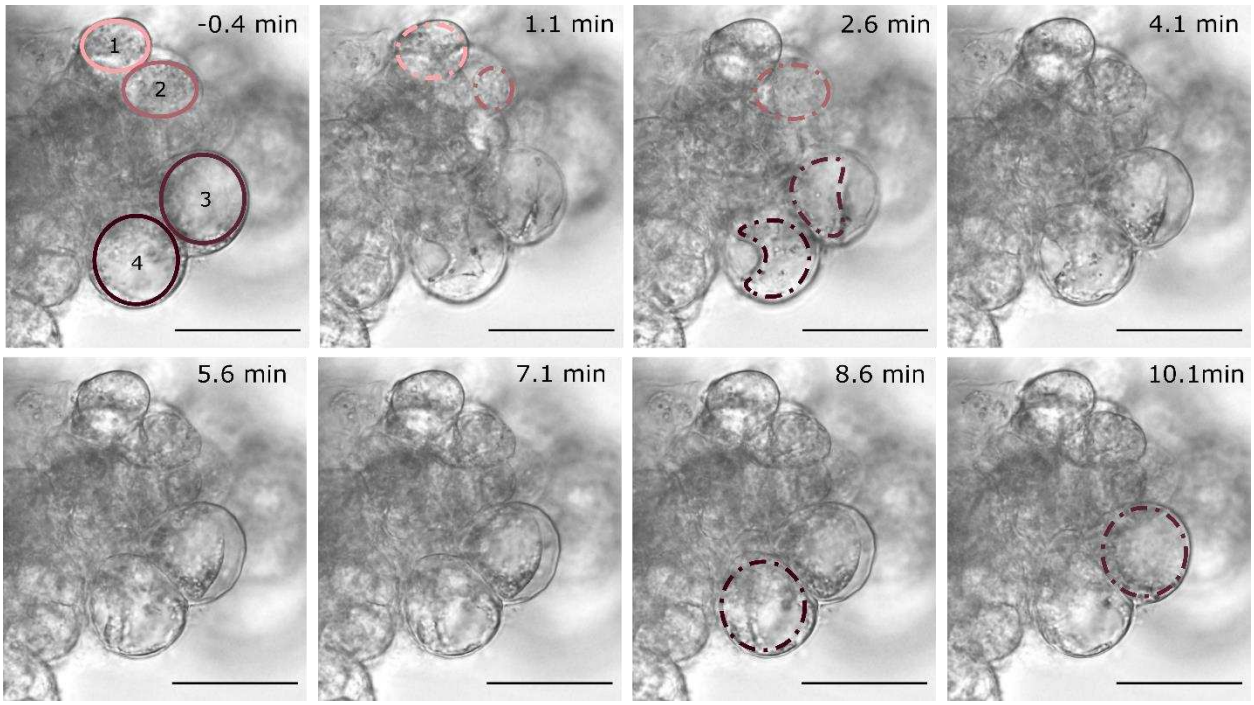

Figure 3.2: Brightfield images of live rice callus cells responding to 15% (*wt/v*) DMSO over 10 min. Solid lines in -0.4 min indicate the initial location of the plasma membrane in each cell of interest. Dashed lines indicate the location of the plasma membrane after complete plasmolysis, and the dashed-dotted lines indicate when each cell of interest is finished deplasmolyzing. Each line is drawn just-inside the cell membrane. Scale bar is 25 µm.

3.2.4 Response to ethylene glycol

Rice callus cells exposed to 15% (*wt/v*) ethylene glycol respond in a similar manner as those exposed to DMSO. Of the 113 cells that were observed after exposure to ethylene glycol, 47.8% were crumpled, 52.2 % were plasmolyzed, and 100% of the plasmolyzed cells displayed deplasmolysis (Table 3.1). Four cells exemplify these processes in Figure 3.3. All four cells exhibit some level of plasmolysis and deplasmolysis. In contrast to the DMSO exposures, many of the cell

responses occur much more quickly. In fact, cells 2, 3, and 4 all plasmolyze and deplasmolyze in under one minute. Cell 1 takes longer, fully plasmolyzing by 3 min after initial exposure and only completing deplasmolysis after 6 min of exposure (Figure 3.3). The short timescale of these responses again indicates the need for a high time-resolution microscopy technique to capture early responses.

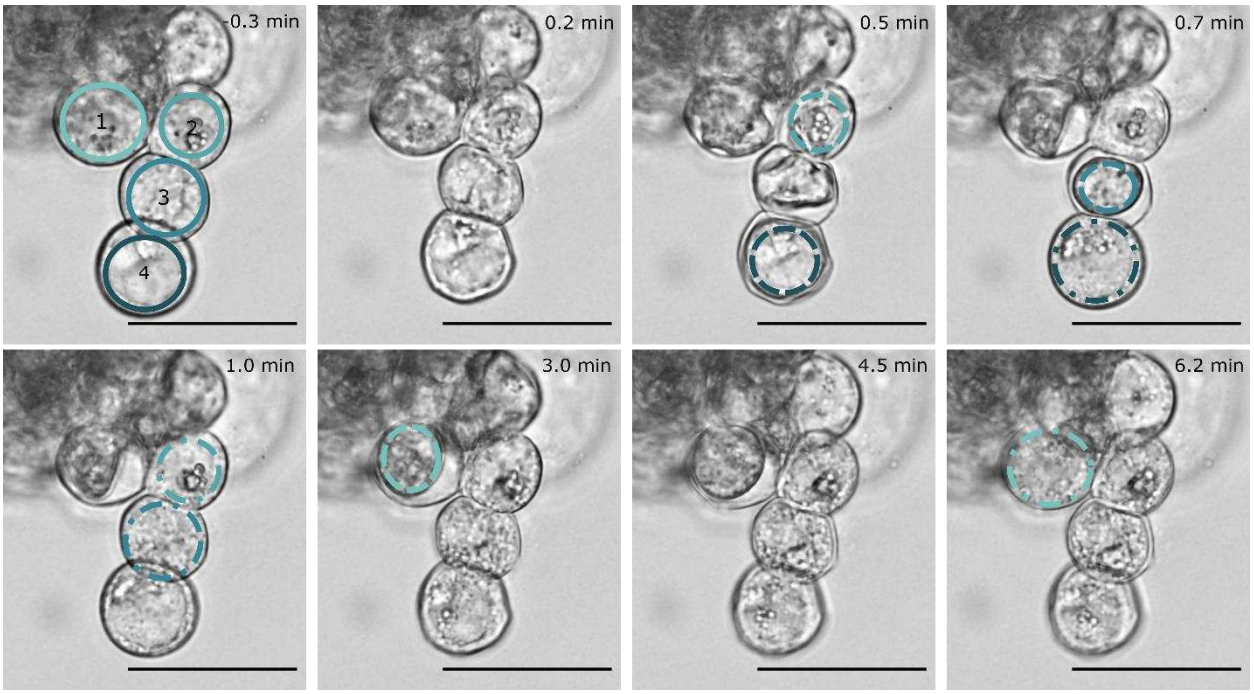

Figure 3.3: Brightfield images of live rice callus cells responding to 15% (*wt/v*) ethylene glycol over the course of 6.2 min. The solid lines in -0.3 min indicate where the cell membrane begins in each cell of interest. The dashed lines indicate where each cell of interest finishes plasmolyzing, and the dashed-dotted lines indicate when each cell of interest is finished deplasmolyzing. Each line is drawn just-inside the cell membrane. Scale bar is 25 µm.

3.2.5 Response to glycerol

Of a total of 101 cells measured after exposure to 30% (*wt/v*) glycerol, 20.8% were crumpled, 79.2% were plasmolyzed, and only 20.0% of the plasmolyzed cells exhibited deplasmolysis (Table 3.1). We observed plasmolysis for each of the four cells marked in Figure 3.4, as well as several unmarked cells visible in the background. All the cells appear to be fully plasmolyzed after 0.65 min and they remain visually the same for the course of the entire

experiment, which ran for an additional 19 min after the initial shrinking response. When deplasmolysis occurs after exposure to glycerol solution, the cells either rapidly deplasmolyze, apparently in under 3 s, or slowly deplasmolyze, taking over 5 min. The rapid deplasmolysis response may indicate the membrane breaking, although persistent movement visible inside the cell after this response suggests that the cell is alive.

The variability in cell response makes it challenging to know the expected response of the cells during CARS data collection, especially because it can be difficult to see the individual cells while using CARS to image deuterated cryoprotectants. This is because the cell signal does not significantly contribute to the overall signal detected, leaving us to rely on lack of signal (or darkness) to identify cell walls and membranes. As a result of the response variability observed in brightfield images, it is helpful to use a model to predict how likely a specific cellular response is when cells are exposed to each cryoprotectant.

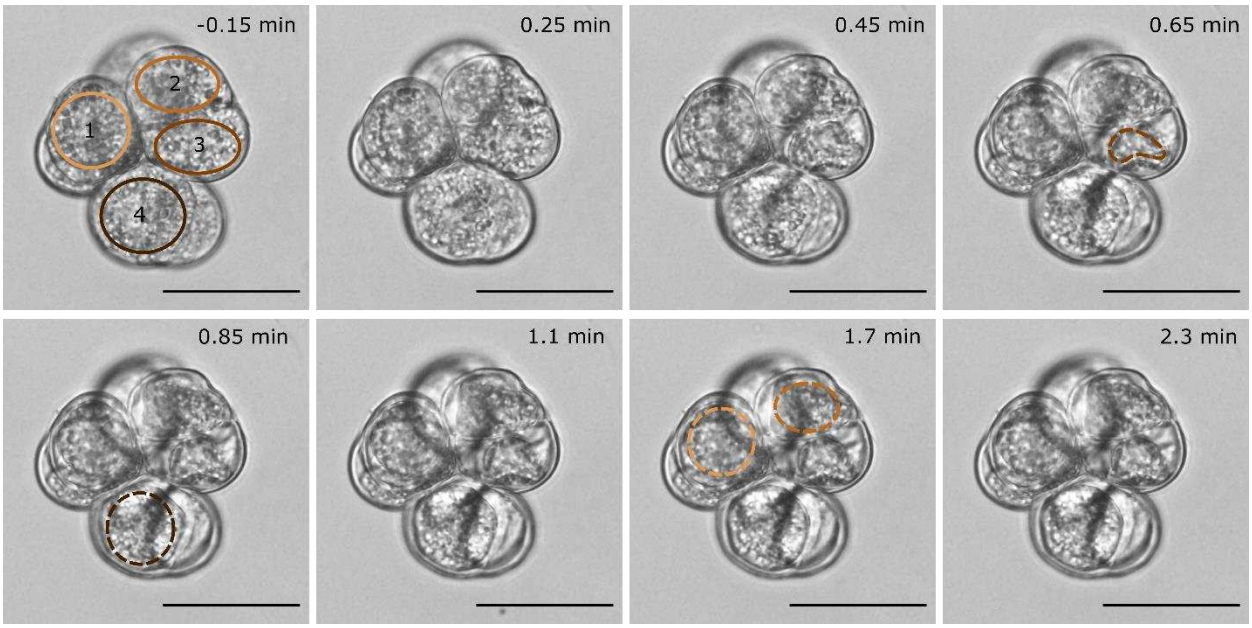

Figure 3.4: Brightfield images of live rice callus cells responding to 30% (*wt/v*) glycerol over the course of 2.3 min. The solid lines in -0.15 min indicate where the cell membrane begins in each cell of interest. The dashed lines indicate where each cell of interest finishes plasmolyzing, and the dashed-dotted lines indicate when each cell of interest finishes deplasmolyzing. Each line is drawn just-inside the cell membrane. Scale bar is 25 µm.

3.2.6 Brightfield Response Timescales

In addition to the varied responses displayed by the cells, the timing of the various responses to each cryoprotectant exposure is also of interest. To compare the timing of each response, the end of each response was manually determined as the last frame where the cell membrane moves. This includes movement inwards (plasmolysis) or movement outwards (crumpling responses and deplasmolysis). Figure 3.5 contrasts the end of the crumpling response, end of plasmolysis, and end of deplasmolysis for each kind of cryoprotectant exposure matching the color schemes used in Figures 3.2, 3.3, and 3.4. In brightfield microscopy we have no way to quantitatively determine precisely when the cryoprotectant solution enters the perfusion chamber. This makes it impossible to accurately establish how quickly the crumpling response or plasmolysis starts after exposure to the cryoprotectant. For the brightfield studies, we estimate t = 0 occurs at the first visible cluster response. Although this response tends to occur before individual cellular responses, appearing as an overall shrinking of the cluster, the cryoprotectant may have entered earlier.

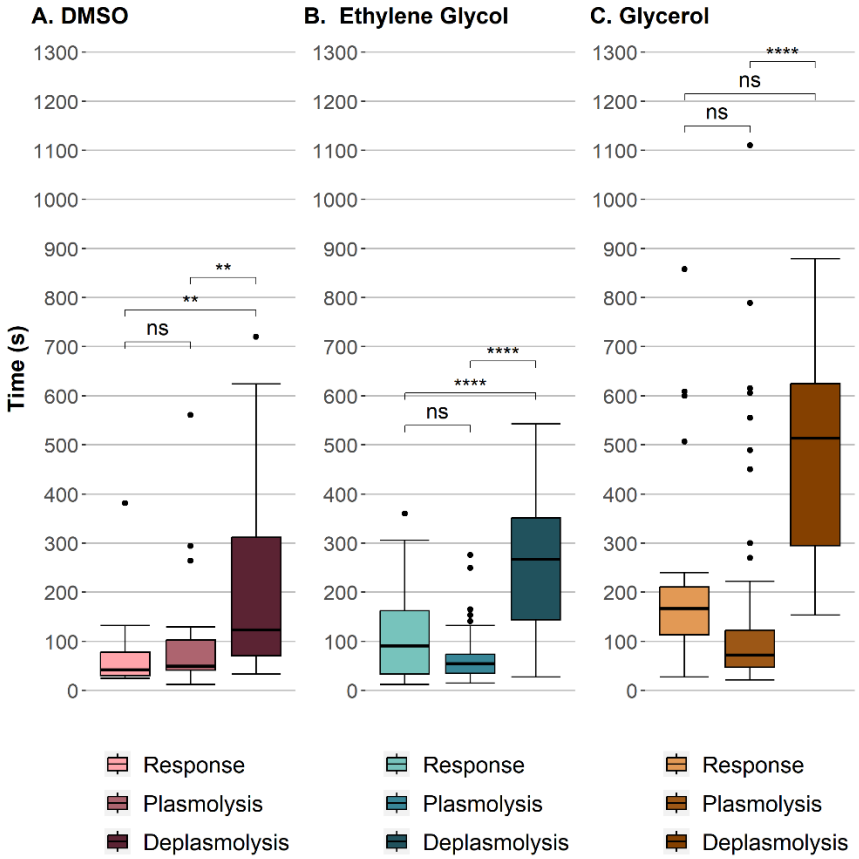

Figure 3.5: Box-and-whisker plots showing the median (line in box), the interquartile range (IQR; 25% quartile to 75% quartile) and the hinges ± 1.5 IQR (whiskers) of each group of data: a. end of the response, plasmolyis and deplasmolysis in cells exposed to 15% (*wt/v*) DMSO, b. end of the response, plasmolyis and deplasmolysis in cells exposed to 15% (*wt/v*) ethyelene glycol, and c. end of the response, plasmolyis and deplasmolysis in cells exposed to 30% (*wt/v*) glycerol. Significance levels: ns – not significant, ∗ – p <0.05, ∗∗ – p <0.01, ∗∗∗ – p <0.001, ∗∗∗∗ – p <0.0001.

For exposures to 15% (*wt/v*) DMSO, the crumpling and plasmolysis responses occur on the same timescale; with interquartile ranges of 30-78 s and 40.5-103.5 s, respectively (Figure 3.5a). Deplasmolysis events finish statistically later, with an interquartile range of 70.5-312 s (Figure 3.5a). Similarly, for exposures to 15% (*wt/v*) ethylene glycol, the crumpling and plasmolysis responses have interquartile ranges of 33-162 s and 34.5-73.5 s, respectively; deplasmolysis occurs later, with an interquartile range of 144-351 s (Figure 3.5b). For 30% (*wt/v*) glycerol exposures, the crumpling and plasmolysis responses occur over a statistically similar timescale, with interquartile ranges of 100.5-220.5 s and 46.5-124.5 s, respectively. When it

occurs, deplasmolysis happens later (283.5-634.5 s), although this response was only statistically significant to plasmolysis (Figure 3.5c).

The crumpling responses appear as small, rapid, shrinking (*i.e.*, an osmotic response) followed by rapid expansion. (*i.e.*, cryoprotectant permeation, analogous to deplasmolysis), which could be interpreted as occurring to the cell that cryoprotectants enter most rapidly. In all cases the crumpling response finishes statistically sooner than deplasmolysis. However, the brightfield data cannot determine if the concentration of cryoprotectants within these cells differs from the concentration within neighboring cells. Additionally, as deplasmolysis has been attributed to cryoprotectant permeation, it is expected that both DMSO and ethylene glycol permeate the cells because they regularly cause deplasmolysis.[9] Because cells rarely deplasmolyze when exposed to glycerol, it is not obvious that glycerol enters most cells. However, glycerol is widely cited as permeating in systems where aquaporin-3 is expressed,[44,45] and as a permeating cryoprotectant in mammalian systems.[46,47] If a deformation response (*i.e.*, deplasmolysis) indicates cryoprotectant permeation, but cells do not deplasmolyze with glycerol exposure, it provides conflicting evidence about the response from cells exposed to glycerol.

3.2.7 CARS Microscopy

CARS microscopy provides a complementary approach for observing cellular responses to cryoprotectant solutions. Previous studies on plasmolysis/deplasmolysis suggest that deplasmolysis occurs when the cryoprotectant enters a cell, removing the osmotic pressure gradient.[9,10] This raises the question of whether glycerol, widely considered a permeating cryoprotectant, enters cells that do not deplasmolyze. Further, it suggests that there are differing rates of permeation for cells that deplasmolyze more quickly than their neighbors. Vibrational microscopy gives us a unique opportunity to investigate both questions directly.

We directly image specific cryoprotectants in rice cells with coherent anti-Stokes Raman scattering (CARS) microscopy using deuterated cryoprotectant components.[43] Prior to collecting CARS images, it is critical to collect spontaneous Raman spectra to ensure that we target the vibrational mode associated with the deuterated molecules. The spectra in Figure 3.6 show how deuteration shifts the peaks associated with carbon-hydrogen bonds of each cryoprotectant into a relatively quiet region of the plant spectrum; the spectrum of rice cells in 30% (*wt/v*) sucrose solution (green) contrasts the nondeuterated (yellow) and deuterated (purple) cryoprotectants. The most intense peaks in each non-deuterated (yellow) spectrum lie under a broad peak of the plant spectrum at 2900 cm^{-1}, the region of the Raman spectrum associated with C-H vibrations (Figure 3.6).[48] The plant cells have a strong signal in this region due to the C-H bonds in the cellulose comprising the cell wall[49] and lipids of the membranes within the plant,[48] among other biomolecules. The plant spectrum also has a broad peak from 3100-3700 cm^{-1} that is attributed to the O-H bonds present in the cells, mostly from water, but also from cellulose, sugars, or other biomolecules in the cells. Both the ethylene glycol and glycerol spectra also display a broad peak in the 3100-3600 cm^{-1} region (Figure 3.6) because both molecules have O-H bonds.

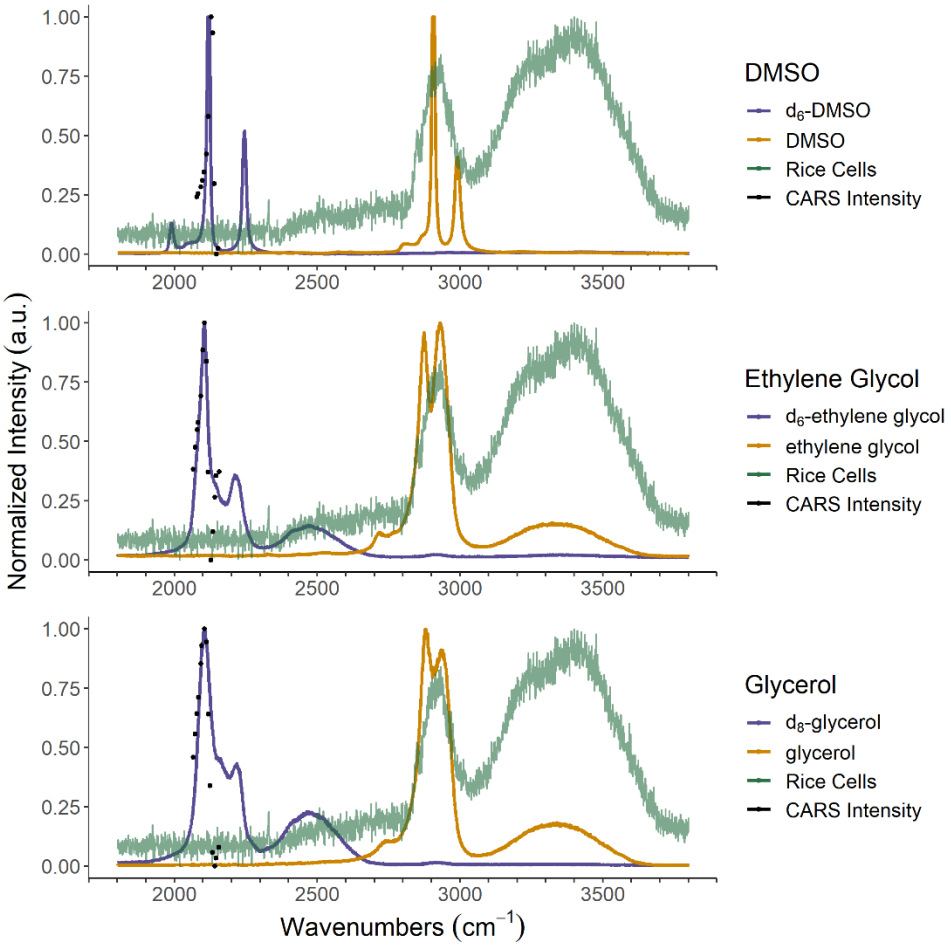

Figure 3.6: Raman spectra of each cryoprotectant used in this study. Plant cell spectrum in green is the same in every graph; non-deuterated cryoprotectant spectra are yellow, and deuterated cryoprotectant spectra are purple. Black dots show normalized CARS intensity at different Raman frequencies.

The purple traces show that exchanging hydrogen for the heavier isotope, deuterium, shifts all the target peaks to around 2100 cm^{-1}, the quiet region of most Raman spectra.[48] The d_6-ethylene glycol and d_8-glycerol spectra also show a broad, O-D peak from 2300-2700 cm^{-1}. Because the O-D groups rapidly exchange with water O-H groups in the aqueous cryoprotectant solution,[50] this peak includes contributions from both water and the cryoprotectants. Thus, we do not use the O-D peak to determine the cryoprotectant location. We target these specific deuterated cryoprotectants and directly image those molecules as they interact with living plant cells using CARS microscopy.[12,43]

Images were collected using the CARS signal from live cells exposed to each individual cryoprotectant as the solution flowed across the cells in the perfusion chamber (Figures 7-9). In the CARS images in each figure, blue coloration is correlated with low CARS signal and yellow coloration correlates with high CARS signal. Due to the quadratic relationship between CARS signal and concentration,[26] and the variability of the laser (e.g., laser drift, minor power changes, etc.) between experiments and on different days, we do not quantify the CARS signal beyond "low" and "high". The average intensity of selected regions of interest (ROIs) are shown in the CARS images (Figures 7-9). The intensity of each cell ROI is normalized to minimum and maximum of the average intensity of 2-3 background ROIs (Equation 3.1). In addition, all the traces are shifted to equivalent time zero positions (t = 0), defined as the moment the deuterated cryoprotectant enters the field-of-view (see Methods). This is the first moment cells could be exposed to the cryoprotectant.

3.2.8 DMSO Exposure

Five images in the time series from experiments investigating each of the three cryoprotectant components are shown in Figs. 8-10, along with intensity data from each ROI, illustrating how the intensity data correspond to images. Each vertical, red-dashed line in the intensity data corresponds to one of the images above the intensity plot. The first line shows the field of view before the background's first change point and the subsequent lines show the field of view at subsequent intervals. The intervals are not uniform because much of the intensity changes occur at earlier times.

Over the course of the time series of cells exposed to d_6-DMSO, the background goes from low CARS intensity (deep blue) to high CARS intensity (yellow) (top of Figure 3.7). The background intensities (BK1, BK2, and BK3) display a sigmoidal response (Figure 3.7). One cell,

C3, also appears to increase in intensity at the same rate as the background (the C3 trace is nearly impossible to differentiate from the BK3 trace because the points lie on top of each other). This response, in addition to a complete lack of autofluorescence from the cell, suggests that C3 was likely empty and dead. Autofluorescence and movement inside the rest of the cells indicate that these cells remain alive before, during, and after flowing the d_6-DMSO solution across them, and as they respond to the addition of d_6-DMSO (Figure 3.7, see Appendix II).

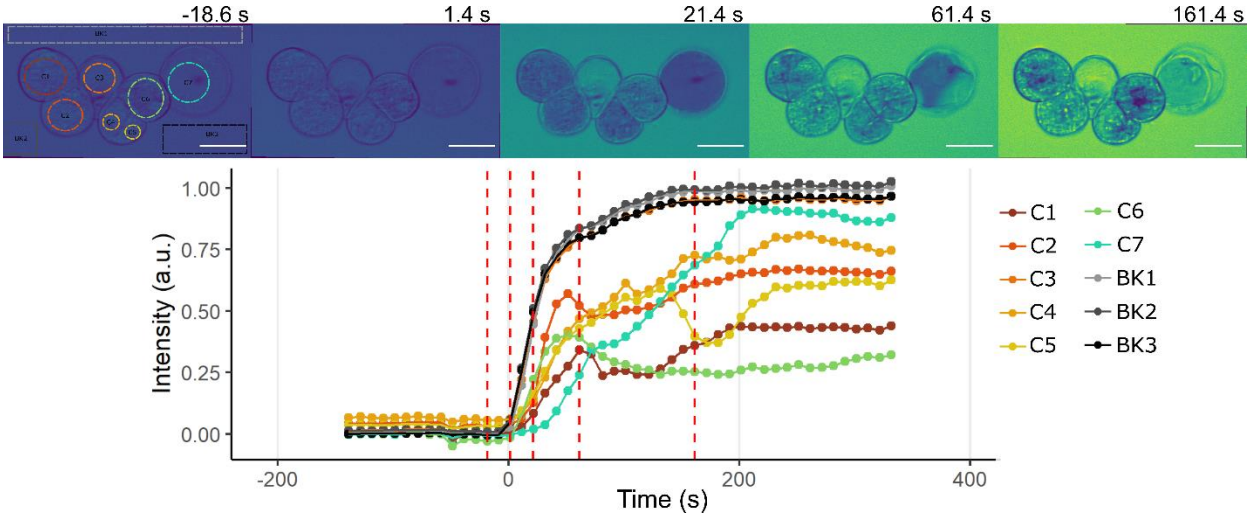

Figure 3.7: (Top) CARS images of rice callus cells responding to d_6-DMSO. Top image shows seven regions of interest chosen within the cells and three background regions of interest (ROI). (Bottom) background-normalized intensity of each cell ROI (rainbow) and the background ROIs (grey-scale). The vertical, red dashed lines indicate on the graph the times when top images were captured. Objective: 20x air, image size: 596 x 520 pixels, 3.9370 pixels/micron, 2121 cm^{-1} target wavenumber.

Individual cells exhibit slightly different responses to the cryoprotectant exposure. The average intensity in cells C1, C2, C5, C6 display a dip between the lowest level at $t \leq 0$ s and the highest level occurring at $t > 200$ s. These dips likely correspond to the clustering of the components inside the cells that either block or absorb the signal. At first glance, C4 and C5 appear to belong to one singular cell, but upon exposure to DMSO, a barrier within the region becomes apparent suggesting that a cell has recently divided so that the regions respond independently. Cells C4 and C7 exhibit increasing intensity after $t = 0$ and C7 also clearly shows plasmolysis and

deplasmolysis over the course of the entire experiment. The other cells all appear to experience a crumpling response, save for C3 which is presumed dead. Further, C7 has the highest intensity of all the cells after 200 s. This could suggest that it has the highest concentration of d_6-DMSO at the end of the exposure, the most uniform distribution of d_6-DMSO, or it could be that there are no places within the ROI where cellular components block the signal.

Overall, this collection of cells shows how a dead cell (C3), a cell that does not appear to contain densely packed components (C7), dense cells (C1, C2, C5, C6), and possibly recently divided cells (C4/C5) all respond to d_6-DMSO exposure. Although each cell responds in slightly different ways, all display an increase in d_6-DMSO signal inside the cell. This suggests that macroscopic observations of how cells respond—plasmolysis and deplasmolysis—to DMSO exposure is not an indication of DMSO permeation but instead may indicate the viability of the cell upon exposure to the cryoprotectant and the density of the cellular contents.

3.2.9 Ethylene Glycol Exposure

Using CARS microscopy, we see that rice cells respond to ethylene glycol in a manner similar to the DMSO response (Figure 3.8). Signals from background ROIs (black and grey traces) follow a largely sigmoidal line-shape as d_6-ethylene glycol enters the perfusion chamber and the CARS signal increases from low to high intensity. The gap in the data that occurs from t = 267 - 277 s comes from the acquisition of z-stack data (for more information, see Appendix II). Like Figure 3.7, all the cell ROIs in Figure 3.8 increase in intensity as d_6-ethylene glycol exposure continues, though the traces do not follow a completely uniform line shape. Cells C3 and C4 both dip in intensity just after 61.2 s before climbing and eventually reaching a plateau. In contrast, C1a – the lower half of the first cell – displays a rapid rise in intensity between 22.0 and 61.2 s. After this jump, C1a stays relatively consistent, with small variations possibly due to organelles moving

in and out of the ROI that block the CARS signal. The upper half of the first cell – C1b – appears to follow a relatively gentle trajectory to its maximum intensity. This region of the first cell appears to contain fewer organelles than C1a, which likely minimizes how frequently organelles enter the ROI and change the average intensity. Overall, the CARS intensity from d_6-ethylene glycol increases over the course of the experiment for all the cells.

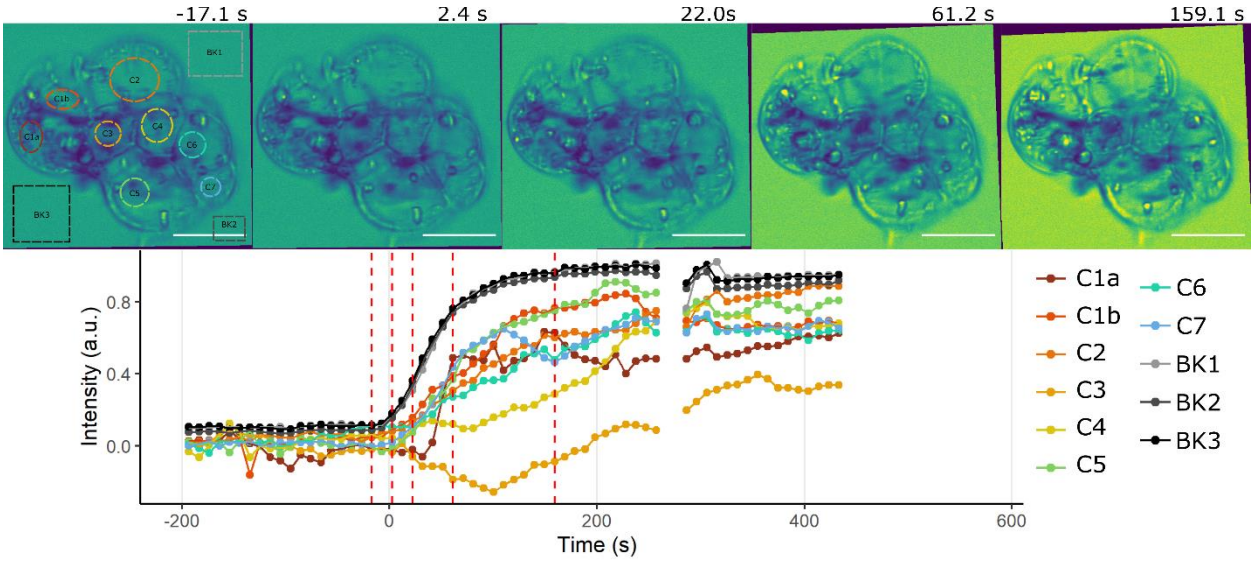

Figure 3.8: (Top) CARS images of rice callus cells responding to d_6-ethylene glycol. Top image shows eight regions of interest chosen within the cells and three background regions of interest (ROI). (Bottom) background-normalized intensity of each cell ROI (colors) and the background ROIs (grey-scale). The vertical, red dashed lines indicate on the graph the times when top images were captured. The gap in the intensity vs. time graph represents a period where z-stack data were collected. Objective: 20x air, image size: 593 x 319 pixels, 4.4444 pixels/micron, 2090 cm^{-1} target wavenumber.

When compared to the images of d_6-DMSO (Figure 3.7), it is apparent that the initial background signal for d_6-ethylene (Figure 3.8) appears brighter. This is because the Raman signal for d_6-ethylene glycol is inherently weaker than that of d_6-DMSO, in part because ethylene glycol has fewer C-D bonds[26] and also because the deuterated methyl ($-CD_3$) stretch in DMSO gives a stronger signal than the deuterated methylene ($-CD_2$) stretches in ethylene glycol. The lower signal from ethylene glycol requires a different microscope optimization, increasing the initial signal from the sample. We are primarily interested in the time it takes for cryoprotectants to permeate

the cells and for the cells to respond, rather than directly comparing the concentrations between different cryoprotectants, so the different microscope optimizations do not affect the interpretation of our results.

3.2.10 Glycerol Exposure

The background ROIs for cells exposed to d_8-glycerol follow a sigmoidal trend as it enters the perfusion chamber, as shown in Figure 3.9. For the most part, the selected cell ROIs show only plasmolysis and cells remained plasmolyzed for the timescale of the experiments (up to 19 min). The gaps in the data that occur starting at t = 158.6 s, ~280 s, and ~320 s come from the acquisition of z-stack data. The collected z-stacks confirmed that deuterated glycerol permeated the cell clusters. After d_8-glycerol exposure, the signal within each ROI generally increases in intensity and then plateaus without many dips or spikes in the intensity traces; all traces remain at a lower intensity than the background signals. The exceptions are C1 and C4, which spike at t = 580 s and drop at t = 300 s respectively. These responses are clear in the collected videos.

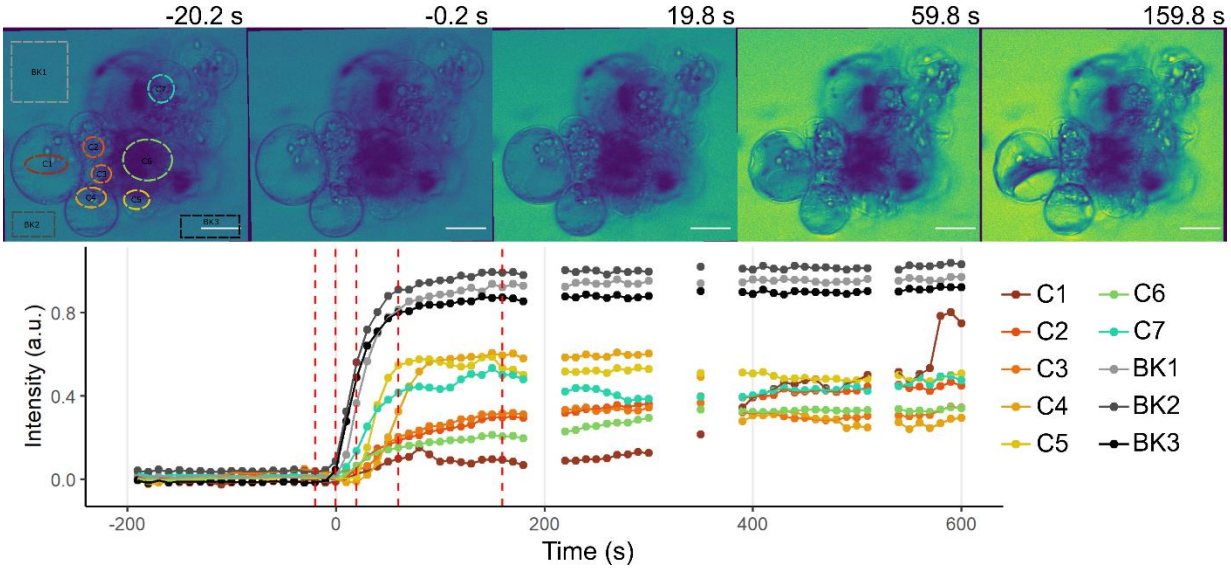

Figure 3.9: (Top) CARS images corresponding to d_8-glycerol exposure. The first image shows the seven regions of interest chosen within the cells and the three background regions of interest. (Bottom) The background-normalized intensity of each cell ROI (colors) and the background ROIs (grey-scale). The vertical, red dashed lines indicate times on the graph the top images were captured. The gap in the intensity vs. time graph represents a period where z-stack data were

collected. Objective: 20x air, image size: 515 x 465 pixels, 6.0606 pixels/micron, 2090 cm^{-1} target wavenumber.

For the same reasons as d_6-ethylene glycol, the signals from d_8-glycerol have lower overall Raman intensity compared to d_6-DMSO,[26] requiring the modification of the instrument parameters that leads to a higher starting background signal compared to d_6-DMSO. Multiple data points are removed from these traces creating three gaps. In each case, the data were removed because usable CARS data were not being collected.

Two traces in Figure 3.10 deviate significantly from the intensity profiles we generally capture. Cell C1 displays a dramatic intensity increase at about t = 550 s whereas the intensity of C4 drops rapidly during the gap associated with z-stack acquisition at approximately 280 s. In the video of the CARS images, C1 appears to deplasmolyze rapidly, but it is difficult to distinguish exactly what occurs to this cell because the response occurs in under the 10 s period between captured frames. This makes it appear as though the cell goes from completely plasmolyzed to completely deplasmolyzed. It is impossible to tell if a rupture occurred that caused the rapid expansion of the cell membrane, or if the membrane were compromised. In a similar fashion, Cell C4 responds to the glycerol influx by rapidly deplasmolyzing. However rather than increasing the intensity within the ROI, the CARS intensity decreases. This may reflect the dispersal of organelles in the cell that previously formed an apparent bright band within the ROI. After the cellular response, material in cell C4 – most likely organelles – appear to coagulate, creating a shadow and further decreasing the measured intensity of d_8-glycerol. Despite these varied responses, the increasing CARS signal after d_8-glycerol exposure demonstrates permeation by d_8-glycerol into all the cells in Figure 3.9.

Historically, researchers have interpreted deplasmolysis as an indication of cryoprotectants entering the cell.[9,51] However, the CARS data demonstrate unequivocally that d_8-glycerol enters

the cells despite the absence of partial or complete deplasmolysis. Although the cells exposed to glycerol do not fully deplasmolyze, some cells appear to undergo a process wherein the cell membrane fully separates from the cell wall and then regains some turgidity, leading to a smooth circular or elliptical cell membrane. It is possible that a certain amount of glycerol, less than the 30% (*wt/v*) in the surrounding solution, can enter the cell, but not enough enters to cause a full deplasmolysis, just enough to cause the cell membrane to become more spherical. This could cause the internal intensity to increase until it plateaus at a level lower than the background. Alternatively, it is possible that once glycerol enters the cell it prevents deplasmolysis through an unknown mechanism while still remaining at a lower concentration than the surrounding solution. If the second case were true, it would suggest that the cell is actively maintaining a lower concentration of glycerol.

3.2.11 CARS Exposure Timescales

The major result of CARS microscopy experiments is that all the tested cryoprotectants enter the interior of the individual cells, crossing both the cell wall and the cell membrane. The intensity within the cells increases, indicating cryoprotectant permeation, although the intensity of the cryoprotectant signal is not uniform within specific cells nor across all cells in each sample. We previously reported observation of nonuniform distribution of DMSO in rice callus cells, specifically hypothesizing pooling of the DMSO cryoprotectant in organelles such as starch granules.[43] Although the cell line used for studies reported here appears to have fewer starch granules than cells used for our previous report, we still observe some intracellular locations that display this pooling phenomenon.[43] It is also visually evident in the work presented here that the CARS signal in the space between the cell wall and cell membrane increases indicating that all the cryoprotectants cross the cell wall, although we did not thoroughly investigate this phenomenon.

All the intracellular intensities appear to increase over the course of exposure, and eventually the intensity appears to plateau. When image collection was continued, the intensity often remained at the plateau level for up to 7 min (see Appendix II) but rarely did the average intensity of ROIs within cells reach the level at or above those of the normalized background (see Appendix II).

Although the exact concentrations of each cryoprotectant within the cells cannot be determined, they can be compared to their own respective background traces. It appears that the intensity within the cells exposed to DMSO and ethylene glycol plateau closer to the background intensity than those exposed to glycerol, despite the higher glycerol concentration in the cryoprotectant solution. Comparing the intensity within cells to the background ROIs in this way suggests that it is rare for the average internal concentration of cryoprotectant to exceed the external concentration. Further it suggests that, although d_8-glycerol enters the cells, the final glycerol concentration within the cells may be lower than the concentration of DMSO or ethylene glycol within cells in comparable experiments, even though the concentration of glycerol, 30 *w/v* %, exposed to the cells is higher than the concentrations of either DMSO or ethylene glycol (each 15 *w/v* %). This might account for the higher probability of DMSO and ethylene glycol exposure to cause deplasmolysis. Future experiments aim to address this by quantifying the cryoprotectant concentrations.

Although the average intensity values can only be compared qualitatively, we can quantitatively compare the time behavior of cryoprotectant permeation through the change points in the data. Figure 3.10 shows the boxplot distribution of background ROIs and cell ROIs during each cryoprotectant exposure.

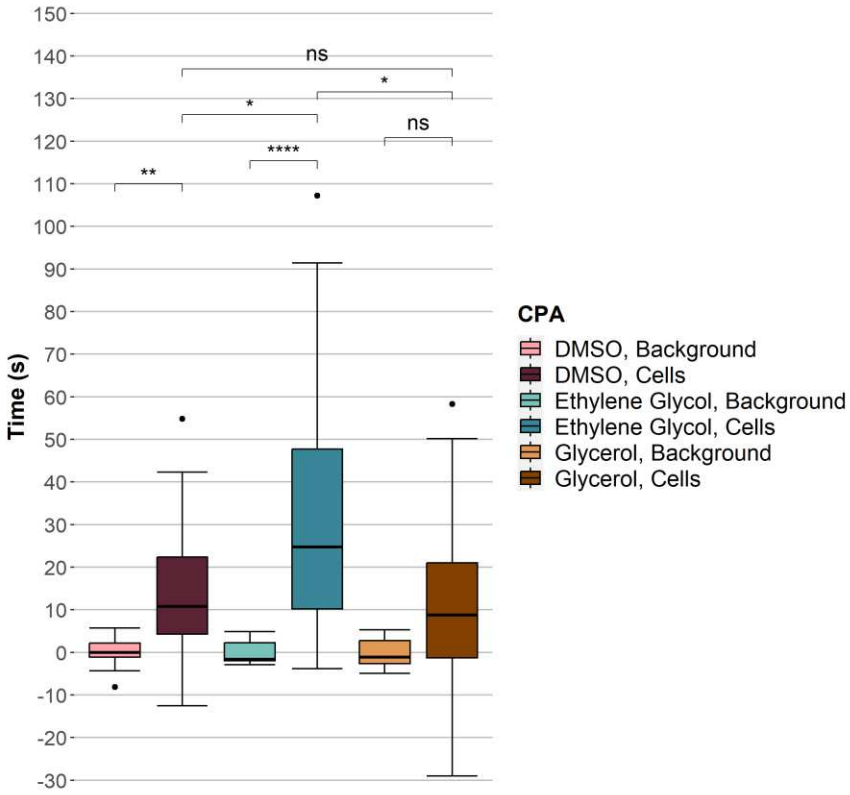

Figure 3.10: Boxplot showing the distribution of change point data extracted from the intensity traces of the background and cell ROIs for each cryoprotectant. DMSO background values are in light red (n=19) and cell values are in dark red (n=47). Ethylene glycol background values are in light green (n=11) and cell values are in dark green (n=36). Glycerol background values are in light orange (n=11) and cell values are in dark orange (n=27). Significance levels: ns – not significant, ∗ – p <0.05, ∗∗ – p <0.01, ∗∗∗ – p <0.001, ∗∗∗∗ – p <0.0001.

Generally, the first background change point is considered to occur at t = 0. However, it is important to note that the first change point for the background data may differ depending on the background ROI because rastering an entire frame takes 10 s. If a deuterated cryoprotectant enters the field of view in this period, the intensity increases as a gradient across the background. Thus, different background ROIs have different change points within 10 s of each other. Significance testing shows that the background change points collected in both d_6-DMSO and d_6-ethylene glycol experiments occur on shorter timescales than the first change point of the cells, indicating that permeation by DMSO or ethylene glycol occurs after the cryoprotectant flows into the sample.

However, the background and cell first change points of the d_8-glycerol display no statistical difference. Comparison between the different cryoprotectants reveals that the first change point of cells exposed to d_6-ethylene glycol is statistically longer than the change points of cells exposed to d_6-DMSO and d_8-glycerol while the change points of d_6-DMSO and d_8-glycerol are not statistically different.

3.2.12 Implications of Brightfield and CARS Microscopy Results

CARS microscopy allows us to assess the penetration of cryoprotectants beyond simply visualizing images of cellular responses. The CARS intensity inside the cells always begins to change before plasmolysis is fully complete. Table 3.2 shows that the median times for processes observed using the two different imaging methods, brightfield and CARS microscopy, differ significantly; the times reported from CARS experiments are much shorter than those from brightfield microscopy. The values in Table 3.2 reflect the end of plasmolysis and end of deplasmolysis as reported in Figure 3.5, while the first change point from CARS experiments reflect times given in Figure 3.10. Note that there is no equivalent brightfield value to the CARS background change point because we cannot see when the cryoprotectant solution enters the field of view; our brightfield t = 0 occurs likely after our CARS t = 0 because the brightfield value is defined as the first response from the cells.

Table 3.2: Median time in seconds of the data sets of the end of plasmolysis visible in brightfield imaging and the first change point of both average cell ROIs and background ROIs calculated from CARS imaging for each tested cryoprotectant. (BF) = measurement by brightfield imaging; (CARS) = measurement by coherent anti-Stokes Raman scattering imaging.

	Median time (s)		
Process observed	**DMSO**	**Ethylene Glycol**	**Glycerol**
End Plasmolysis *(BF)*	49.5	54	72
End Deplasmolysis *(BF)*	123	267	513
First Cell Change point *(CARS)*	10.8	24.7	8.8
Background Change point *(CARS)*	0	-1.6	-1.1

Commonly, plasmolysis and deplasmolysis are considered indicative of cells dehydrating due to an increase of osmotic pressure and penetration of cryoprotectants, respectively.[9] This suggests that during plasmolysis water leaves the cell cytoplasm and only after plasmolysis is complete do the cryoprotectants enter the cells, causing full deplasmolysis. By this logic, we predict the first cellular change point measured with CARS microscopy would align with the end of plasmolysis as the internal CARS intensity began to increase with the permeation of cryoprotectants. However, in all three cases, the median time value for the first CARS change point occurs well before the end of plasmolysis, showing that cryoprotectants permeate the cell membrane much more quickly than the cells respond to that permeation by deplasmolyzing. We observe cryoprotectant penetration into the cells even when plasmolysis and deplasmolysis do not occur. This suggests that cryoprotectants enter the cell simultaneously as water is leaving the cell and that cryoprotectants continue to enter the cell through both plasmolysis and deplasmolysis. The results from CARS microscopy experiments disagree with the common interpretation of plasmolysis and deplasmolysis from brightfield experiments.[16]

Several new questions arise from the results reported here. First, many plant cryopreservation protocols dose plant material with cryoprotectant solutions at or near 0 ˚C. Without a cold stage compatible with the CARS microscope, we have only performed perfusion experiments at room temperature (20-25 ˚C). We hypothesize that cryoprotectant penetration should occur more slowly at 0 ˚C,[52] if only due to increased solution viscosity.[53] It will be interesting and useful follow cryoprotectant flow at lower temperatures. Second, using CARS microscopy precludes quantitative determination of intracellular cryoprotectant concentrations. However, stimulated Raman scattering (SRS) microscopy should enable the quantitative determination of cryoprotectant concentrations within cells as a function of time,[48] and could be

used in future experiments. Finally, the next logical step to the work reported here will use a Raman microscopy technique observe how PVS2, with all three cryoprotectants combined, permeates plant cells; generally, the cryoprotectants used here are used in combination rather than individually.

3.3 Conclusions

Results reported here indicate using caution when attributing cellular response to cryoprotectant permeation.[9] It is likely that the two are intimately entwined, but it is evident that cryoprotectant permeation occurs more rapidly than cellular responses and that even cells that do not deplasmolyze—like most of those exposed to glycerol—still experience cryoprotectant permeation. Specifically, our CARS results demonstrate effective cryoprotectant permeation occurring for all three systems on timescales much less than one minute. This suggests that if cryoprotectant permeation is one key to successful cryopreservation, then the vitrification step of cryopreservation may be able to occur much faster than standard protocols follow.

3.4 Materials and Methods

3.4.1 Cell culture

Orzya sativa (Asian rice) callus cells were obtained from the U.S. Dept. of Agriculture, Agricultural Research Service (USDA-ARS) National Laboratory for Genetic Resources Preservation (Fort Collins, CO, USA). The cell line was originally produced by Schaeffer at USDA (Beltsville, MD) in 1981; the line was cryopreserved in 1982 by Finkle and Ulrich at USDA-ARS (Berkeley, CA).[41] After warming in 2021, cells were grown on modified Murashige and Skoog basal plant medium with vitamins (MS Media, M519; PhytoTechnology Laboratories, Lenexa, KS), supplemented with 1 mg L^{-1} each of 2,4-dichlorophenoxyacetic acid (2,4-D, Sigma-Aldrich, Laramie, WY), indoleactetic acid (IAA, TCI America, Portland, OR), and kinetin (TCI America),

146 mg L^{-1} glutamine (Acros Organics, Geel, Belgium), 3% *wt/v* sucrose (Alfa Aesar) and 8 g L^{-1} agar (BD Diagnostics, Franklin Lakes, NJ). The modified MS medium was autoclaved prior to pouring into Petri plates and used within a month of being poured. Plated cells were placed in the dark at room temperature (22-25 °C) and allowed to grow until the callus had at least doubled in size. Friable, white callus cells were selected for re-plating every 4-6 weeks based on growth.

3.4.2 Cryoprotectant solutions

Three solutions of cryoprotectant components were used in brightfield studies: 15% *wt/v* DMSO (Fisher Scientific, Hampton, NH), 15% *wt/v* ethylene glycol (Sigma-Aldrich), and 30% *wt/v* glycerol (Mallinckrodt Chemical, Phillipsburg, NJ, USA), each prepared in distilled water. Deuterated cryoprotectant solutions were used in CARS studies: 15% *wt/v* d_6-DMSO (EMD Millipore, Burlington, MA, USA), 15% *wt/v* d_6-ethylene glycol (Sigma-Aldrich), and 30% *wt/v* d_8-glycerol (Sigma-Aldrich), each prepared in distilled water.

3.4.3 Spontaneous Raman Spectra

Spontaneous Raman spectra from rice callus cells, DMSO, d_6-DMSO, ethylene glycol, d_6-ethylene glycol, glycerol, and d_8-glycerol were collected on a Horiba TeraHertz Raman System (Horiba, Kyoto, Japan) with a 532 nm excitation. Each spectrum was collected from 1000-4000 cm^{-1}, capturing the region where the non-deuterated cryoprotectants and rice cells have strong vibrational modes (>2500 cm^{-1}) associated with C-H and O-H bonds, the “quiet region” (2000-2500 cm^{-1}) where deuterated cryoprotectants have large vibrational modes associated with C-D bonds, and the fingerprint region (<2000 cm^{-1}) where lower frequency vibrational modes appear. Spectra were normalized for comparison to each other.

3.4.4 Coherent anti-Stokes Raman scattering (CARS) imaging

CARS microscopy images were recorded at the Advanced Light Microscopy Core at the University of Colorado, Anschutz Medical Campus, using an Olympus FV1000 FCS/RICS modified with a picoEmerald laser system (Angewandte Physik & Elektronik GmbH, Berlin, Germany) for CARS imaging. This laser and microscope system is described more comprehensively elsewhere.[43] The microscope can record CARS images and volumetric datasets (z-stacks) in epi- and forward direction, two-photon excitation fluorescence in the epi-direction and second harmonic generation in forward direction. In all experiments, forward CARS and two-photon excitation fluorescence inherent to the sample (autofluorescence) were collected. Additional information about the microscopy as well as collected autofluorescence and z-stacks is provided in the Supporting Information.

The C-D stretch mode of deuterated PVS2 components was visualized by CARS. The fixed Stokes beam at 1030 nm was used in combination with the probe beam at 845.3 nm to image the deuterated DMSO, and at 847.5 nm to image d_6-ethylene glycol and d_8-glycerol entering the cells. These parameters tuned the instrument to measure molecular vibrations at 2121 cm^{-1} for d_6-DMSO and 2090 cm^{-1} for the other deuterated cryoprotectant components. Background due to laser light passed by filters into the detector was determined by detuning the temporal overlap of Stokes and pump laser pulses. Two-photon excitation epi-fluorescence images were acquired simultaneously with the CARS images, capturing any autofluorescence emitted by the cells. Images were acquired at 10-15 s intervals showing the cryoprotectants as they entered the cells.

"Sticky-Slide" perfusion chambers (ibidi, Fitchburg, WI, USA) were used to flow the cryoprotectant solutions over cells at room temperature. Prior to flow, plated callus cells were prepared in the same manner to the rudimentary perfusion chamber mentioned above.

Additionally, about 0.5 mL of this suspension was placed onto a Sticky-Slide before a coverslip coated in poly-L-lysine was placed over the slide, sealing in the contents. Aqueous solutions (up to 2 mL) of deuterated PVS2 components, 15% *wt/v* d_6-DMSO, 15% *wt/v* d_6-ethylene glycol or 30% *wt/v* d_8-glycerol, were flowed over the cells as they were imaged with CARS microscopy.

3.4.5 Brightfield imaging

A rudimentary perfusion chamber was used to flow cryoprotectant solutions over cells at room temperature as brightfield images were collected on an Olympus IX73 fluorescence microscope (Olympus, Tokyo, Japan). The perfusion chamber consisted of a microscope slide, cover slip, and silicone grease, as shown in Figure 3.8. To prepare the perfusion chamber, the microscope slide was cleaned with methanol, ~5 mm of silicone grease was added to the long slide edges, and 1% poly-L-lysine (Electron Microscopy Sciences, Hatfield, PA) was placed in the area that would comprise the center of the chamber. After 24 h, the poly-L-lysine solution was rinsed off the slide with distilled water and the slide was air dried. Using the prepared slide within 24 h of rinsing ensured that cells adhered to the slide throughout cryoprotectant flow.

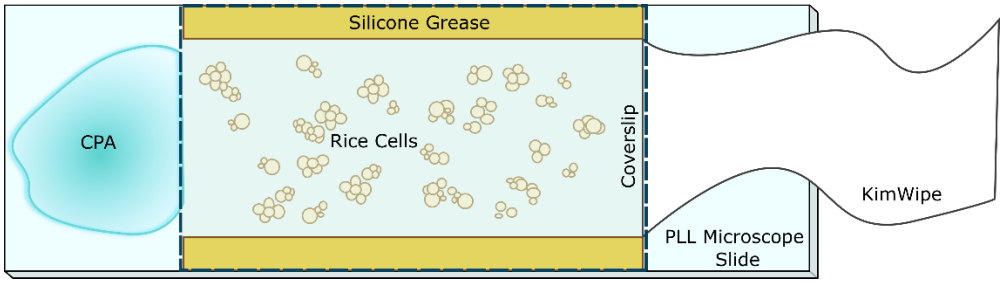

Figure 3.11: Rudimentary perfusion chamber used on the brightfield microscope to flow cryoprotectant solutions over rice callus cells; CPA = cryoprotectant solution.

To prepare plated cells for flow, a pea-sized amount of callus from a healthy plate (plated 4-6 weeks prior) was transferred into a 2 mL microfuge tube and gently mixed with ~1.5 mL of liquid, non-supplemented MS media (M519, PhytoTechnology Laboratories) until the cells were suspended. About 0.5 mL of this suspension was transferred to a poly-L-lysine prepared slide, a

coverslip was placed over the suspension solution and gently pressed into the silicone grease, sealing the perfusion chamber along the long edges. The chamber was placed onto the microscope and ~0.5 mL of the chosen cryoprotectant solution was placed on one side of the chamber. It was wicked through the chamber with a KimWipe. Brightfield images were captured every 3 s over the course of 15-25 min. This was repeated at least five times for each cryoprotectant solution. Three different individuals followed the protocol described in the SI to count cell responses reported in Tables 1 and 2.

3.5 Data Processing

3.5.1 CARS Images

3.5.1.1 ImageJ

All image data were extracted from .oib files to .tiff files using Fiji.[35,54] Brightness and contrast were adjusted and the images were cropped. To accurately measure the change in signal within specific cells, we used the ImageJ "StackReg" plugin, which anchors all subsequent images to be matched in space, to stabilize and align the CARS image stack based on the first image.[35,55]. This effectively stabilizes any movement from the cells throughout exposure to the cryoprotectant solution. This ensured that individual cells in images used for analysis appeared stationary throughout each time sequence. [7,9]

After stabilizing images, cells that were visible throughout the time series were selected for further analysis. We selected regions of interest (ROIs) within visible cells so that the ROI remained within the cell membrane throughout the entire time series as the cell responded to the cryoprotectant solution. This ensured that the CARS signal captured by the ROI represented only the signal within the cell, not the background signal or the CARS signal between the cell wall and plasmolyzed membrane. The average intensity of each ROI was extracted for every time point,

saved as a .csv file, then analyzed with custom written code in R that is available on GitHub. The total number of ROIs analyzed was based on the number of visible cells plus 2-3 ROIs recording background data. The cell ROIs were drawn to minimize the area of the ROI outside of the cell membrane after the largest cellular response. For example, if a cell plasmolyzed completely, the ROI was drawn so that it remained inside the plasmolyzed membrane. In this way, we capture the signal of any deuterated cryoprotectant permeating both the cell wall and membrane, rather than the cryoprotectant only crossing the cell wall.

3.5.1.2 R

An R script was written to normalize the extracted intensity data to the background intensity.[56] First, the minimum and maximum intensity for each background ROI were determined; these values were averaged for each experiment and the minima and maxima were used in Equation 3.1 to normalize the data, where I_{cell} is the average intensity of the cell ROI, I_{BK_min} is the average minimum intensity of the background ROIs, and I_{BK_max} is the average maximum intensity of the background ROIs.

$$I_{norm} = \frac{I_{cell} - I_{BK\_min}}{I_{BK\_max} - I_{BK\_min}} \qquad \text{Eq. 3.1}$$

After normalization, we determined the change point in the background intensities using a segmented linear fit (*segmented.R*).[57–59] Modelling the change point yielded a time at which the relatively constant background intensity started to increase due to deuterated cryoprotectants entering the field of view that caused an increase in the intensity. Comparing the background change points to the cell change points—calculated by modelling the internal cell intensities to the segmented linear fit (*segmented.R*)—showed how quickly the deuterated cryoprotectant entered the cells.

An alignment in time was achieved by setting the first change point equal to the average of the first change points of two to three background ROI traces. To do this, we averaged the first changepoint for every background ROI in a single experiment then shifted all the intensity data (including the background ROIs) so that the background average was t = 0 in the intensity data. In some cases, this leads individual background change points to appear slightly offset from zero.

3.5.2 Brightfield Images

3.5.2.1 ImageJ

Brightfield images were imported into ImageJ and converted from .tiff files to .avi files at 7 fps.[35] Brightness and contrast were adjusted, the images were cropped, and scale bars were added.

3.5.2.2 R

An R script was written to model cell responses based on cryoprotectant exposure and is available on GitHub.[49] The logit model, glm, from the aod R package were used for 10 glycerol, 13 ethylene glycol, and 5 DMSO exposure experiments, comprising 101, 113, and 45 clearly visible cells, respectively. This generalized linear model was used to predict cellular response, cellular plasmolysis and cellular deplasmolysis based on cryoprotectant exposure. Responses were considered binary: a cell either did or did not respond, did or did not plasmolyze, and did or did not deplasmolyze. The model considered the nested nature of these responses, *i.e.,* a cell could not deplasmolyze if it did not initially plasmolyze.

3.5.3 Statistics

Prior to significance testing, a Shapiro-Wilk test (*stats.R*) was conducted on each set of data. The null hypothesis was rejected for multiple data sets (see R code) indicating a non-normal distribution. To ensure we were not assuming normal distributions, we performed the non-

parametric Kruskal-Willis test (*stats.R*) to determine when data sets contained statistically different groups (see R code). An *ad hoc* Dunn test with Benjamini-Yekutieli adjustment (*rstatix.R*) was performed to determine statistically different groups.[60,61] The results of this test for every data set are described in the SI.

CHAPTER 4: Permeation of deuterated cryoprotectants solubilized in Plant Vitrification Solution 2

The data presented in this chapter are currently in preparation and will be included in a paper in collaboration with co-authors of the previous two chapters. The authors are currently working on the fully developed work which will include brightfield data collected and analyzed by Kylie C. Pearce, including Figure 3.3. All the CARS data presented here were collected and analyzed by F. M. D. Samuels.

4.1 Introduction

As previously discussed, cryopreservation is widely used to conserve cells and tissues from a variety of species.[6] For living material to be successfully conserved, it must first be exposed to cryoprotectants—permeating and non-permeating molecules that mediate damages associated with freezing.[6] In the previous chapter, the permeation of individual cryoprotectants was investigated and it was clear that the sampled cryoprotectants (dimethyl sulfoxide, ethylene glycol and glycerol) all permeated the cell, crossing both the plant cell wall and the cell membrane. Further, the permeation of these molecules appeared to begin before cell responses traditionally associated with permeation, namely deplasmolysis (see Chapter 3).[10,11]

However, it is rare to find a cryopreservation protocol for plants that does not dose living material with a *mixture* of cryoprotectants.[6,50] For example, plants are generally preserved with mixtures like Plant Vitrification Solution 2 (PVS2) which contains dimethyl sulfoxide (DMSO), ethylene glycol, glycerol and sucrose, or Plant Vitrification Solution 3 (PVS3) which contains glycerol and sucrose.[7,8] It is possible that the permeability of the cell membrane to different cryoprotectants changes when these molecules are used together. For example, DMSO is known to generally increase the permeability of membranes.[51] This raises the question: is it necessary to

include DMSO in cryoprotectant solutions to ensure the permeation of other cryoprotectants? The data presented in Chapter 3 suggest that DMSO is not strictly necessary for the permeation of ethylene glycol or glycerol; both those cryoprotectants readily entered the cell on their own. Does this mean that the permeation of each cryoprotectant alone is the same as in a mixture? Cell responses that we have observed would suggest otherwise.

Here, I explore the timescales of permeation for cells exposed to PVS2, which consists of 15% (*wt/v*) DMSO, 15% (*wt/v*) ethylene glycol, 30% (*wt/v*) glycerol and 0.4 M sucrose[7] using coherent anti-Stokes Raman scattering (CARS) microscopy. As described in previous chapters, deuterated cryoprotectants were used to ensure that collected CARS signal arose from the cryoprotectant of interest. However, it would be ill-advised to create PVS2 mixtures where every cryoprotectant was deuterated because a single cryoprotectant could not be targeted because any CARS signal would come from all the molecules. Instead, three PVS2 solutions were used wherein a single cryoprotectant of interest—DMSO, ethylene glycol or glycerol—was deuterated and the others were left fully protonated. This allowed us to see how a specific cryoprotectant permeated the cells when used in tandem with the other cryoprotecting molecules in PVS2. Unlike what we observed using individual cryoprotectant solutions, the CARS images from each of these solutions were incredibly similar.

4.2 Results and Discussion

As discussed in Chapter 3, we have previously observed three general cell responses to individual cryoprotectants: crumpling, plasmolysis and deplasmolysis (see Figure 3.1). Plasmolysis is generally attributed to the rapid loss of water from within the cell, which causes the protoplast to shrink.[10,11] Deplasmolysis has, in the past, been attributed by the permeation of cryoprotectants back into the cell, causing the protoplast to expand back to the cell wall.[10,11] This

has led some researchers to classify a few cryoprotectants as "non-permeating" because they do not cause deplasmolysis.[10,11] Our past work (presented in Chapter 3) demonstrates that the individual cryoprotectants in PVS2 *all* permeate the cell membrane despite some (*i.e.,* glycerol) not causing deplasmolysis (see Chapter 3).[10,11] Additionally, the timescale of deplasmolysis for DMSO and ethylene glycol is well after the beginning of cryoprotectant permeation.

Unlike exposure to single cryoprotectant solutions (see Chapter 3), the only response we observe when cells are exposed to PVS2 is plasmolysis. Despite the lack of deplasmolysis, CARS imaging shows that all the tested cryoprotectants permeate into the cell. This is consistent with the behavior we see from individual cryoprotectants. In fact, the average intensity sampled within cells appears to be more uniform when the cryoprotectants are combined than when cells are exposed to individual solutions (Figure 3.7-3.9 compared to Figure 4.1). For example, images show that cells exposed to d_6-DMSO in PVS2 appear to go from uniformly having no signal to a level that is almost indistinguishable from the background in only 29.4 s (Figure 4.1A). The corresponding intensity traces show that the average intensity within the cells follows the same shape as the background, though the first increase in intensity (first changepoint) in the cells occurs later than the background. The similar shape of the traces suggests that all the cells are experiencing permeation of d_6-DMSO in a similar way. This is different from cells exposed to single cryoprotectants (Chapter 3), which often had intensity traces that were markedly different than the background trace. For example, the intensity traces of cells exposed to d_6-DMSO in water do not appear sigmoidal like the background (Figure 3.7). Instead, these cells go through a period of dipping and rising in intensity before ultimately reaching something like an asymptote.

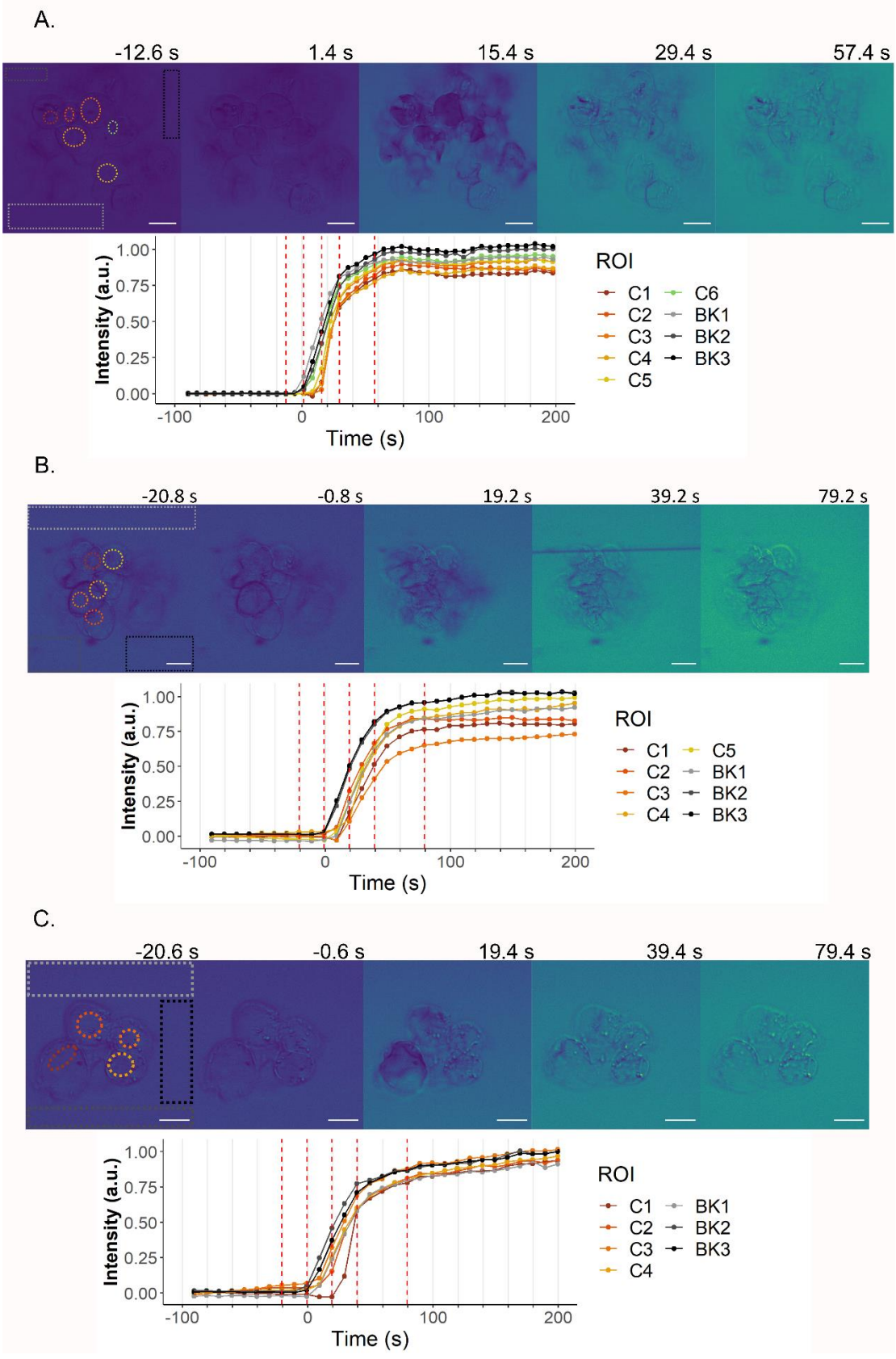
A.
-12.6 s
1.4 s
15.4 s
29.4 s
57.4 s
Intensity (a.u.)
1.00
0.75
0.50
0.25
0.00
-100
0
100
200
Time (s)
ROI
C1
C2
C3
C4
C5
C6
BK1
BK2
BK3
B.
-20.8 s
-0.8 s
19.2 s
39.2 s
79.2 s
Intensity (a.u.)
1.00
0.75
0.50
0.25
0.00
-100
0
100
200
Time (s)
ROI
C1
C2
C3
C4
C5
BK1
BK2
BK3
C.
-20.6 s
-0.6 s
19.4 s
39.4 s
79.4 s
Intensity (a.u.)
1.00
0.75
0.50
0.25
0.00
-100
0
100
200
Time (s)
ROI
C1
C2
C3
C4
BK1
BK2
BK3

Figure 4.1: Examples of cells exposed to A. d_6-DMSO, B. d_6-ethylene glycol and C. d_8-glycerol and their corresponding intensity traces. The vertical red dashed lines on the intensity graphs correspond to times for the images above the graph. In those images, high intensity is yellow while low intensity is blue. Dashed lines in the images indicate the regions of interest (ROIs) within which the intensity is averaged and plotted on the graph below. The color of the ROIs corresponds to the color of its intensity trace.

Just like the cells exposed to d_6-DMSO in PVS2 (Figure 4.1A), both d_6-ethylene glycol (Figure 4.1B) and d_8-glycerol (Figure 4.1C) appear to permeate rice cells quickly and uniformly when in combination with other components of PVS2. And, like d_6-DMSO, the intensity within the cells appears to closely follow the background intensity for the other two cryoprotectants, rather than going through a series of dips before reaching a plateau (Figures 3.7 and 3.8).

In the previous chapter, we suggested the final relative intensity of the traces within the cells could be compared to the relative background intensity because all the traces were normalized to average maximum and minimum of the background intensities. In the cases of DMSO and ethylene glycol, there were cells that reached relative intensities comparable to the background (Figures 3.7 and 3.8). Based on the associated cell images collected, it also seemed like lower plateaued intensities within cells were due to the signal being blocked rather than a true lower concentration. In contrast, the cells exposed to glycerol never reached relative intensities comparable to that of the background traces (Figure 3.9) even when it was clear that there were no other cells blocking the signal. We suggested that it was possible that a lower percentage of the glycerol permeated into the cell from the external solution than other cryoprotectants (*i.e.,* half of 30% glycerol compared to all of 15% DMSO or ethylene glycol). This is not the case for glycerol solvated in PVS2.

The combination of glycerol and other PVS2 components change the final CARS intensity from d_8-glycerol inside the cell. Rather than plateauing below well below the normalized background intensity (Figure 3.9), the CARS intensity within cells exposed to glycerol in PVS2 plateaus at, or near, the background (Figure 4.1C). This suggests that the concentration of glycerol

within cells is higher when glycerol is combined with the other cryoprotectants in PVS2. In fact, regardless of which cryoprotectant is imaged, the CARS intensity within the cells plateaus near the final intensity of the background suggesting that the final concentration of each cryoprotectant is close or equal to the concentration of the cryoprotectant in PVS2. Although solutions of DMSO and ethylene glycol alone also reach intensities inside cells to comparable the background traces, they appear to plateau more rapidly when used in tandem. In individual cryoprotectant solutions, a plateau was reached by 200 s of exposure regardless of cryoprotectant (Chapter 3). In contrast, the CARS intensity of cells exposed to PVS2 reaches a plateau by 100 s regardless of which cryoprotectant is being investigated.

The dips and rises seen in the intensity traces of cells exposed to individual cryoprotectants were largely attributed to clustering organelles blocking the light (dip) or other organelles that displayed higher CARS intensities entering the ROI (rise). The lack of these dips and rises, combined with how quickly the CARS intensity plateaus suggests that DMSO, ethylene glycol and glycerol all permeate more rapidly and uniformly when used in combination in PVS2. This suggests that the membrane becomes more permeable to all the cryoprotectants when exposed to PVS2. DMSO is known to make tissues more permeable to drugs and is often referred to as a penetration enhancer.[52–54] Molecular dynamics simulations have shown that DMSO can form pores in membranes, which could explain its success as a penetration enhancer.[51,55,56] It is possible that DMSO is enhancing the penetration of both ethylene glycol and glycerol. This is particularly important for the permeation of glycerol which, when alone, does not appear to permeate the cell membrane particularly well (Chapter 3).

Interestingly, despite the apparent increased permeability of the cryoprotectants when mixed, when the intensity first increases inside the cells is comparable to the individual components. The

changepoint analysis first introduced in Chapter 3 was used probe when the cryoprotectants in PVS2 first permeate the cells. Like in the previous chapter, the first changepoint of the background intensity trace was compared to the first changepoint of the cell traces (Figure 3.2). In all cases, the first changepoint from the background traces (Figure 4.2, lighter tones) appeared statistically earlier than the first cell changepoint (Figure 4.2, darker tones). For both the DMSO data (reds) and the ethylene glycol data (greens), the first cell changepoints occurred about 10 s after the first background changepoints. For glycerol (browns), the difference was a bit longer at 15 s. None of the background changepoints were statistically different from each other nor were the first cell changepoints.

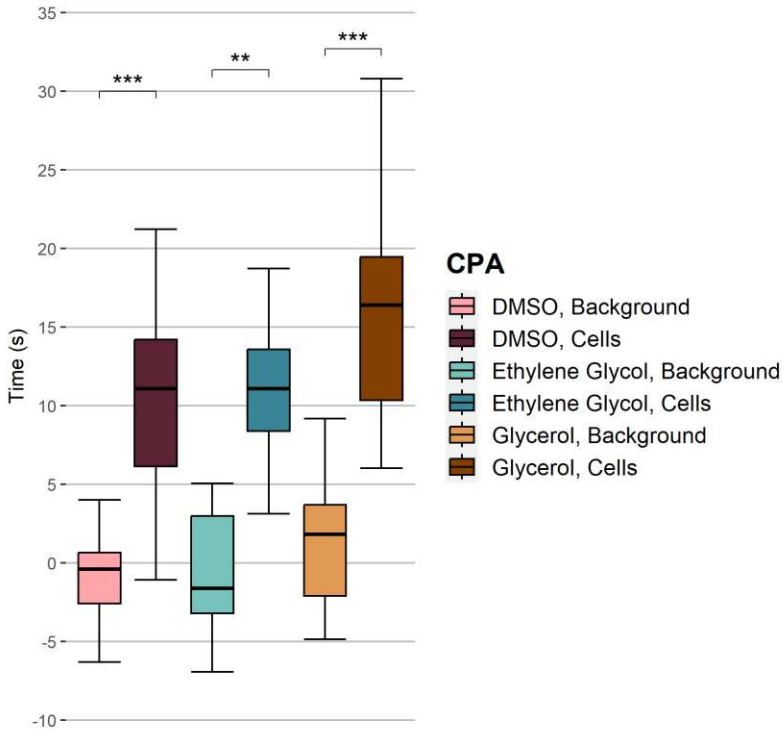

Figure 4.2: Boxplot showing the distribution of changepoint data extracted from the intensity traces of the background and cell ROIs for each cryoprotectant. DMSO background values are in light red and cell values are in dark red. Ethylene glycol background values are in light green and cell values are in dark green. Glycerol background values are in light orange and cell values are in dark orange. Only significant relationships are highlighted. Significance levels: ∗ – p <0.05, ∗∗ – p <0.01, ∗∗∗ – p <0.001, ∗∗∗∗ – p <0.0001.

We have not seen these cells deplasmolyze when they are exposed to PVS2. Because we do not expect deplasmolysis when cells are exposed to PVS2, we cannot compare these times to this particular cellular response. However, we can compare these points to the brightfield data collected by K.C. Pearce. She collected data from 95 cells and saw four different responses: crumpling (Figure 3.1), initial plasmolysis (Figure 3.1), slow shrinking of the protoplast and slow swelling of the protoplast. Cells that experienced crumpling did not experience any other response, but cells that experienced initial plasmolysis could go on to experience slow shrinking or slow swelling of the protoplast. Cells could also initially experience slow shrinking and then no other response or go on to experience slow swelling. Importantly, the protoplast never swelled back to the cell wall (*i.e.,* deplasmolysis never occurred). Figure 4.3 shows the timescales of each of these responses.

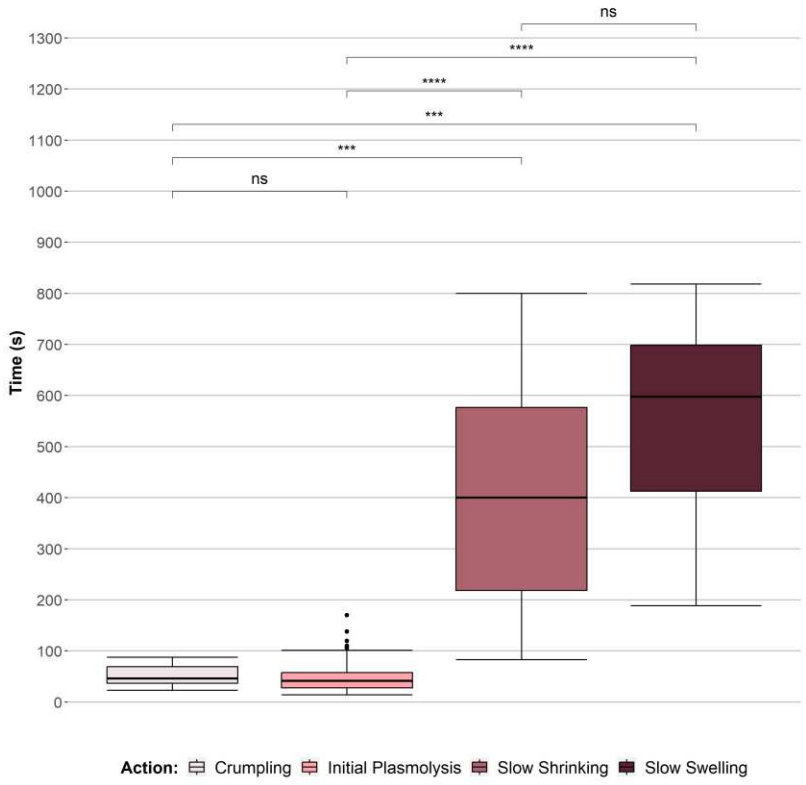

Figure 4.3: Box and whiskers plots showing the median (line in box), interquartile range (IQR; 25% quartile to 75% quartile) and the hinges ± 1.5 IQR (whiskers) of the end of each brightfield

response observed by K.C. Pearce. The lightest pink corresponds to the end of the crumpling response (n = 7), the middle-tone pink corresponds to the end of the initial plasmolysis (n = 71), the pink corresponds to the end of the slow shrinking response (n = 59), and the dark-pink corresponds to the end of the slow swelling response (n = 18). Significance levels: ns – not significant, ∗ – p <0.05, ∗∗ – p <0.01, ∗∗∗ – p <0.001, ∗∗∗∗ – p <0.0001.

It is clear that the end of these cellular responses occurs well after the beginning of cryoprotectant permeation (Figure 4.2 and 4.3). In fact, the last cells stop responding after 800 s, almost 100 times later than the first change point within the cell. Like results presented in the previous chapter, cellular response does not seem indicative of cryoprotectant permeation and permeation is likely occurring simultaneously to water removal.

We can also compare the changepoints of this data to the changepoints measured in Chapter 3. The boxplot values of Figure 4.2 and Figure 3.10 are presented in Table 4.1. It is important to note that there are almost double the number of cells presented in Chapter 3 compared to results presented here, which limits statistical power.

Table 4.1: Values presented in Figure 4.2 and Figure 3.10. The values from Figure 4.2 are presented as "CPA in PVS2" and the values from Figure 3.10 are presented as "CPA." n = sample size; Min = lower whisker; First Quartile = bottom of box; Median = median value; Third Quartile = top of box; Max = upper whisker.

	DMSO	**DMSO in PVS2**	**Ethylene glycol**	**Ethylene glycol in PVS2**	**Glycerol**	**Glycerol in PVS2**
n	47	20	36	12	27	13
Min	-12.5	-1.1	-3.8	3.1	-29.0	6.0
First Quartile	4.3	5.7	10.2	7.5	-1.3	10.3
Median	10.8	11.1	24.7	11.1	8.8	16.4
Third Quartile	22.4	14.3	47.7	14.4	21.0	19.5
Max	42.3	21.2	91.4	18.7	50.2	30.8

Interestingly, the median changepoint value for DMSO alone is comparable to DMSO in PVS2 (10.8 s and 11.1 s, respectively), but the value for ethylene glycol alone is more than double that of ethylene glycol in PVS2 (24.7 s and 11.1 s, respectively) and the median for glycerol in

PVS2 is double that of glycerol alone (8.8 s and 16.4 s, respectively). In all cases, there is less spread in the data (*i.e.,* the range is smaller) for cells exposed to PVS2. This may be due to the uniformity of response between cells, though this conclusion would be made stronger with more sampling.

4.3 Implications and Conclusion

The data presented here show that there is a difference between the permeability of cryoprotectants exposed to cells individually compared to their permeability in combination with other components of PVS2, most markedly the final concentration of glycerol within cells. Although we cannot directly quantify how much of each cryoprotectant ends up in cells due to the quadratic relationship between CARS signal and concentration,[19,57] comparing the intensity within cells to the intensity external to cells gives us an idea of relative concentrations. In combination with other cryoprotectants, the final concentration of glycerol within cells is closer to the background intensity than when cells are exposed to glycerol alone. This may be due to DMSO facilitating the crossing of more glycerol across the cell membrane as DMSO is known to increase the permeability of membranes. This facilitation may also explain why all the intensity traces look similar regardless of what cryoprotectant is being targeted—DMSO threw the doors open for easy permeation of all the cryoprotectants.

This raises questions for practitioners of cryopreservation in the field. There is a push to move away from DMSO as a cryoprotectant because it is more toxic than other molecules.[43] This has led to more use of PVS3, a mixture of 50% (*wt/v*) glycerol and 50% (*wt/v*) sucrose, which can also protect some plant species from freezing damage.[8] However, the difference in glycerol permeation when the cryoprotectant is alone compared to in concert with DMSO shown here suggests that a pure glycerol solution may not maximize the protective nature of glycerol. Rather

than eliminating DMSO completely, it may be prudent to study how lowering the concentration of DMSO impacts glycerol's permeability. Perhaps there is a sweet spot where DMSO toxicity is minimized, and glycerol permeation is maximized.

4.4 Materials and Methods

4.4.1 Cell culture

The same *Orzya sativa* (Asian rice) callus cells used in Chapter 3 were used for experiments described here. They were originally gifted by the U.S. Dept. of Agriculture, Agricultural Research Service (USDA-ARS) National Laboratory for Genetic Resources Preservation (Fort Collins, CO, USA). The cell line used here is one of many produced by Schaeffer at USDA (Beltsville, MD) in 1981; Finkle and Ulrich at USDA-ARS (Berkeley, CA) cryopreserved this line in 1982.[46] These cells were rewarmed in 2022 by Remi Bonnart and have since been grown on modified Murashige and Skoog basal plant medium with vitamins (MS Media, M519; PhytoTechnology Laboratories, Lenexa, KS), supplemented with 1 mg L^{-1} each of 2,4-dichlorophenoxyacetic acid (2,4-D, Sigma-Aldrich, Laramie, WY), indoleactetic acid (IAA, TCI America, Portland, OR), and kinetin (TCI America), 146 mg L^{-1} glutamine (Acros Organics, Geel, Belgium), 3% *wt/v* sucrose (Alfa Aesar) and 8 g L^{-1} agar (BD Diagnostics, Franklin Lakes, NJ).

Plates were split every 4-6 weeks. Prior to splitting, new plates were prepared with autoclaved MS media. Once plated, cells were placed into a dark drawer and kept at room temperature (22-25 °C) until they were split again. After being split once, cells were disposed of properly.

4.4.2 Cryoprotectant solutions

To make the singly-deuterated PVS2 solutions either 15% *wt/v* d_6-DMSO (EMD Millipore, Burlington, MA, USA), 15% *wt/v* d_6-ethylene glycol (Sigma-Aldrich), and 30% *wt/v* d_8-glycerol (Sigma-Aldrich) were combined with their respective non-deuterated components. These were 15% *wt/v* DMSO (Fisher Scientific, Hampton, NH), 15% *wt/v* ethylene glycol (Sigma-Aldrich), 30% *wt/v* glycerol (Mallinckrodt Chemical, Phillipsburg, NJ, USA), and 4 M sucrose (Alfa Aesar). The appropriate components (*i.e.,* one deuterated cryoprotectant, plus the corresponding two non-deuterated cryoprotectants and sucrose) were combined in a volumetric flask, which was then filled to the mark with distilled water.

4.4.3 Coherent anti-Stokes Raman scattering (CARS) imaging

An Olympus FV1000 FCS/RICS modified with a picoEmerald laser system (Angewandte Physik & Elektronik GmbH, Berlin, Germany) housed and maintained by the Advanced Light Microscopy Core at the University of Colorado, Anschutz Medical Campus, was used for CARS imaging (described in detail in Appendix I).[58] See Chapter 3 for more information about microscope capabilities and how the laser was tuned to the correct cryoprotectant signal.

As described in Chapter 3, "Sticky-Slide" perfusion chambers (ibidi, Fitchburg, WI, USA) were used to flow the cryoprotectant solutions over cells at room temperature. Prior to flow, cells were gently suspended in the same MS medium described above but made without adding agar.

4.5 Data Processing

4.5.1 CARS Images

4.5.1.1 ImageJ

Unlike the processing described in Chapter 3, after extracting .oib files to .tiff files using Fiji,[40,59] the brightness and contrast were not adjusted nor were the images stabilized. This was in

an attempt to make accurate calibration plots, but unfortunately the focal plane of the calibration was likely different than that of the cells making the calibration plots non-viable (see Appendix III).

Just like Chapter 3 describes, I selected regions of interest (ROIs) within visible cells. The cell ROIs were drawn to minimize the area of the ROI outside of the cell membrane after the largest cellular response. For some experiments this required manually moving the ROI because there was so much cell movement (see Appendix III, Figure AIII.1), and the images were not stabilized. In these situations, the intensity traces from each ROI were cut together based on the frame in where a new ROI was required. For example, if at frame 10 a cell moved so that the ROI was no longer in the cell membrane, I manually moved the ROI so that it was contained in the membrane. Later, the first 10 frames of the intensity trace captured by the first ROI location would be spliced to the remaining frames of the second ROI location. In this way, we capture the signal of any deuterated cryoprotectant permeating both the cell wall and membrane, rather than the cryoprotectant only crossing the cell wall.

The total number of ROIs analyzed was based on the number of visible cells plus 2-3 ROIs recording background data.

4.5.1.2 R

The script used and described in Chapter 3 was modified to be used to analyze the data presented here. The basic steps were not changed, but the script had variable names specific for the data presented in Chapter 3 so those were changed to fit the data presented here.

CHAPTER 5: Future Directions

The research presented in this thesis is entirely novel to our group. Over the course of my studies, Dr. Nancy Levinger and I developed this research from an idea into a fully-fledged, multi-member project. We had to decide what microscopy system to use and settled on coherent anti-Stokes Raman scattering for the reasons laid out in Chapter 1. We had to decide what model cells to use and, for a moment, I maintained human cancer cells (biosafety level 2) and even brought them to the CARS microscope in Denver. They were a suboptimal system to use to develop an entirely new project. Although they were easy to maintain, they were difficult to transport and had some biosafety risk. It was a blessing when we established a relationship with Dr. Gayle Volk and began using plant cells. These cells were even easier to maintain and presented no risk to humans or animals. There was also minimal risk to plants because we were not infecting the cells with pathogens. But the cells didn't stick to glass and I could not find any literature about how to get live callus cells to adhere to glass. So, I developed a procedure to get the cells to stick to glass by drying poly-L-lysine on the surface of my glass slides and coverslips. That became the foundation for all the other procedures I developed for this research would have been possible.

That said, if there is one thing I wish I could change about those procedures it is the temperature at which we were collecting data. The majority of cryopreservation techniques expose cells to cryoprotectants at temperatures closer to 0 °C, not room temperature.[6] However, this requires a specialized microscopy stage able to be transferred between two different microscope set ups—the brightfield and the coherent anti-Stokes Raman scattering microscopes. Although this may seem trivial, each microscope had different physical specifications, ranging from the distance of the condenser to the stage, to the structure of the stage itself, to the necessity of covering the

microscope during data collection. Unfortunately there was no appropriate stage available at the time I was collecting data.

Although these data were not collected at 0 °C, I do believe they are still informative with regards to the general permeability of plant cells to different cryoprotectants. I expect that had the cells and solutions been cooled to lower temperatures it would simply take longer for the cells to respond to the cryoprotectants, as demonstrated in other work.[12] Because we've demonstrated that permeation occurs more quickly than cellular response, it is possible that the permeation of the cryoprotectants would not be slowed at cooler temperatures, but it is difficult to know without further studies. Future experiments should try to lower the exposure temperature to at least 0 °C to more closely match the temperature cryobiologists use to prepare cells for cryopreservation.

Another obvious step from this research is observing how sucrose interacts with the cells. There is some debate about sucrose permeation[12,37,60] and it would be interesting to directly observe the difference between permeation in a purely sucrose solution versus in combination with the other cryoprotectants in PVS2. Sucrose is widely considered a key player in protecting plants from the frigid temperatures of cryopreservation.[61,62] Plants (and some animals) naturally produce sucrose and other sugars as natural cryoprotectants. Sugars, including glucose, sucrose and trehalose, are generally less toxic than the other cryoprotectants we use[61–63] and if it is possible to determine if they permeate and how quickly it could lead to avenues of research that maximize protection and minimize toxicity.

Finally, this research used the simplest system we could get our hands on—rice callus cells. Although I think callus cells are interesting, and in some cases are capable of re-growing entire plants,[64] they are not the cells that will save the world's biodiversity in the face of climate change. Instead, future research must focus on tissues. Tissues are significantly more complex than callus

cells. They contain differentiated cells that may respond to cryoprotectants in different ways. Tissues are also much thicker than anything presented in this work, and it will likely take longer times for cryoprotectants to permeate into the center of the tissue compared to the edge simply because there is more material to permeate. The toxicity of a cryoprotectant is directly correlated with exposure time[6,63] so the edge of a tissue may die before the center becomes protected. This necessitates the development of a cryoprotectant solution that maximizes permeability while minimizing toxicity. Knowing how quickly different cryoprotectants permeate tissues and how those permeation times change when multiple molecules are combined will be vital in finding this solution.

All these future studies will benefit greatly from the use of coherent Raman microscopies to directly image the location of cryoprotectants, but stimulated Raman scattering (SRS) provides a superior method to CARS microscopy.[48] CARS suffers from a quadratic relationship between concentration and intensity making calibrating for concentration challenging.[19,57,65] SRS has a simple linear relationship between concentration and intensity.[66,67] In an attempt to generate quantitative data, calibration plots were collected prior to each experiment. Although these plots were quadratic as expected, moving from the calibration slide to the ibidi perfusion chamber changed the focal plane of the images, changing their relative intensities and rendering the calibrations only useful for setting up the instrument rather than quantifying the intensity of the CARS images. It would be simpler to use the perfusion of the deuterated cryoprotectant in the chamber as a calibration within the sample because we can accurately predict the starting concentration, 0%, and the final concentration 15% or 30%. However, it is difficult to successfully predict concentration from the intensity of the surrounding solution without knowing the coefficient for the linear term in our quadratic equation.[68]

With the simple linear relationship between concentration and intensity in SRS data, the background intensity traces within an image could easily be used as an internal calibration. With this kind of calibration, the difference in concentration between cells and between cryoprotectant mixtures could be determined and thereby investigated. SRS also benefits from a reduction in non-resonant background,[66,67,69] which is particularly important when studying plant tissues which contain much higher levels of autofluorescence due to the presence of chloroplasts.

Overall, I believe this work lays the foundation for a plethora of other studies. I am thrilled that multiple Levinger group members are pursuing some of these directions and I hope that their work is incredibly fruitful.

REFERENCES

(1) Lewis L. Coriell; Arther E. Greene; Ruth K. Silver. Historical Development of Cell and Tissue Culture Freezing. *Cryobiology* **1964**, *Volume 1* (Issue 1), 72–79.

(2) Global Strategy for Plant Conservation. The Targets 2011-2020. *Convention on Biological Diversity* **2011**.

(3) Sharrock, S. *Plant Conservation Report 2020: A Review of Progress in Implementation of the Global Strategy for Plant Conservation 2011-2020*; Technical Series No. 95; Secretariate of the Convention on Biological Diversity: Montreal, Canada, 2020; p 68.

(4) Pence, V. C.; Meyer, A.; Linsky, J.; Gratzfeld, J.; Pritchard, H. W.; Westwood, M.; Bruns, E. B. Defining Exceptional Species—A Conceptual Framework to Expand and Advance Ex Situ Conservation of Plant Diversity beyond Conventional Seed Banking. *Biological Conservation* **2022**, *266*, 109440. https://doi.org/10.1016/j.biocon.2021.109440.

(5) Reed, B. M. Plant Cryopreservation: A Continuing Requirement for Food and Ecosystem Security. *In Vitro Cellular & Developmental Biology: Plant* **2017**, *53* (4), 285–288. https://doi.org/10.1007/s11627-017-9851-4.

(6) *Cryopreservation and Freeze-Drying Protocols*, Third Edition.; Day, J. G., Stacey, G., Eds.; Methods in molecular biology; Humana Press: New York, 2015.

(7) Sakai, A.; Kobayashi, S.; Oiyama, I. Cryopreservation of Nucellar Cells of Navel Orange (Citrus Sinensis Osb. Var. Brasiliensis Tanaka) by Vitrification. *Plant Cell Reports* **1990**, *9* (1), 30–33. https://doi.org/10.1007/BF00232130.

(8) Nishizawa, S.; Sakai, A.; Amano, Y.; Matsuzawa, T. Cryopreservation of Asparagus (Asparagus Officinalis L.) Embryogenic Suspension Cells and Subsequent Plant Regeneration by Vitrification. *Plant Science* **1993**, *91* (1), 67–73. https://doi.org/10.1016/0168-9452(93)90189-7.

(9) Zamecnik, J.; Faltus, M.; Bilavcik, A. Vitrification Solutions for Plant Cryopreservation: Modification and Properties. *Plants* **2021**, *10* (12), 2623. https://doi.org/10.3390/plants10122623.

(10) Volk, G. M.; Caspersen, A. M. Cryoprotectants and Components Induce Plasmolytic Responses in Sweet Potato (Ipomoea Batatas (L.) Lam.) Suspension Cells. *In Vitro Cell.Dev.Biol.-Plant* **2017**, *53* (4), 363–371. https://doi.org/10.1007/s11627-017-9834-5.

(11) Levitt, J. Plasmolysis Shape in Relation to Freeze-Hardening of Cabbage Plants and to the Effect of Penetrating Solutes*. *Plant, Cell & Environment* **1983**, *6* (6), 465–470. https://doi.org/10.1111/1365-3040.ep11588112.

(12) Volk, G. M.; Caspersen, A. M. Plasmolysis and Recovery of Different Cell Types in Cryoprotected Shoot Tips of Mentha × Piperita. *Protoplasma* **2007**, *231* (3), 215–226. https://doi.org/10.1007/s00709-007-0251-1.

(13) Lang, I.; Sassmann, S.; Schmidt, B.; Komis, G. Plasmolysis: Loss of Turgor and Beyond. *Plants (Basel)* **2014**, *3* (4), 583–593. https://doi.org/10.3390/plants3040583.

(14) Lang-Pauluzzi, I. The Behaviour of the Plasma Membrane during Plasmolysis: A Study by UV Microscopy. *Journal of Microscopy* **2000**, *198* (3), 188–198. https://doi.org/10.1046/j.1365-2818.2000.00677.x.

(15) Kaplan, F.; Lewis, L. A.; Wastian, J.; Holzinger, A. Plasmolysis Effects and Osmotic Potential of Two Phylogenetically Distinct Alpine Strains of Klebsormidium (Streptophyta). *Protoplasma* **2012**, *249* (3), 789–804. https://doi.org/10.1007/s00709-011-0324-z.
(16) Jones, R. R.; Hooper, D. C.; Zhang, L.; Wolverson, D.; Valev, V. K. Raman Techniques: Fundamentals and Frontiers. *Nanoscale Research Letters* **2019**, *14* (1), 231. https://doi.org/10.1186/s11671-019-3039-2.
(17) Massonnet, G.; Buzzini, P.; Monard, F.; Jochem, G.; Fido, L.; Bell, S.; Stauber, M.; Coyle, T.; Roux, C.; Hemmings, J.; Leijenhorst, H.; Van Zanten, Z.; Wiggins, K.; Smith, C.; Chabli, S.; Sauneuf, T.; Rosengarten, A.; Meile, C.; Ketterer, S.; Blumer, A. Raman Spectroscopy and Microspectrophotometry of Reactive Dyes on Cotton Fibres: Analysis and Detection Limits. *Forensic Science International* **2012**, *222* (1), 200–207. https://doi.org/10.1016/j.forsciint.2012.05.025.
(18) Evans, C. L.; Xie, X. S. Coherent Anti-Stokes Raman Scattering Microscopy: Chemical Imaging for Biology and Medicine. *Annual Review of Analytical Chemistry* **2008**, *1* (1), 883–909. https://doi.org/10.1146/annurev.anchem.1.031207.112754.
(19) Cheng, J.-X.; Xie, X. S. Coherent Anti-Stokes Raman Scattering Microscopy: Instrumentation, Theory, and Applications. *The Journal of Physical Chemistry B* **2004**, *108* (3), 827–840. https://doi.org/10.1021/jp035693v.
(20) Ikeuchi, M.; Sugimoto, K.; Iwase, A. Plant Callus: Mechanisms of Induction and Repression. *The Plant Cell* **2013**, *25* (9), 3159–3173. https://doi.org/10.1105/tpc.113.116053.
(21) Sugimoto, K.; Jiao, Y.; Meyerowitz, E. M. Arabidopsis Regeneration from Multiple Tissues Occurs via a Root Development Pathway. *Dev Cell* **2010**, *18* (3), 463–471. https://doi.org/10.1016/j.devcel.2010.02.004.
(22) Zhai, N.; Xu, L. Pluripotency Acquisition in the Middle Cell Layer of Callus Is Required for Organ Regeneration. *Nat. Plants* **2021**, *7* (11), 1453–1460. https://doi.org/10.1038/s41477-021-01015-8.
(23) Salma, M.; Engelmann-Sylvestre, I.; Collin, M.; Escoute, J.; Lartaud, M.; Yi, J.-Y.; Kim, H.-H.; Verdeil, J.-L.; Engelmann, F. Effect of the Successive Steps of a Cryopreservation Protocol on the Structural Integrity of Rubia Akane Nakai Hairy Roots. *Protoplasma* **2014**, *251* (3), 649–659. https://doi.org/10.1007/s00709-013-0565-0.
(24) Kratochvílová, I.; Kopečná, O.; Bačíková, A.; Pagáčová, E.; Falková, I.; Follett, S. E.; Elliott, K. W.; Varga, K.; Golan, M.; Falk, M. Changes in Cryopreserved Cell Nuclei Serve as Indicators of Processes during Freezing and Thawing. *Langmuir* **2019**, *35* (23), 7496–7508. https://doi.org/10.1021/acs.langmuir.8b02742.
(25) Zilli, L.; Schiavone, R.; Zonno, V.; Storelli, C.; Vilella, S. Evaluation of DNA Damage in Dicentrarchus Labrax Sperm Following Cryopreservation. *Cryobiology* **2003**, *47* (3), 227–235. https://doi.org/10.1016/j.cryobiol.2003.10.002.
(26) Verheijen, M.; Lienhard, M.; Schrooders, Y.; Clayton, O.; Nudischer, R.; Boerno, S.; Timmermann, B.; Selevsek, N.; Schlapbach, R.; Gmuender, H.; Gotta, S.; Geraedts, J.; Herwig, R.; Kleinjans, J.; Caiment, F. DMSO Induces Drastic Changes in Human Cellular Processes and Epigenetic Landscape in Vitro. *Scientific Reports* **2019**, *9* (1), 4641. https://doi.org/10.1038/s41598-019-40660-0.
(27) Kaczmarczyk, A.; Rutten, T.; Melzer, M.; Keller, E. R. J. Ultrastructural Changes Associated with Cryopreservation of Potato (Solanum Tuberosum L.) Shoot Tips. *Cryoletters* **2008**, *29* (2), 145–156.

(28) Halmagyi, A.; Coste, A.; Tripon, S.; Crăciun, C. Low Temperature Induced Ultrastructural Alterations in Tomato (Lycopersicon Esculentum Mill.) Shoot Apex Cells. *Scientia Horticulturae* **2017**, *222*, 22–31. https://doi.org/10.1016/j.scienta.2017.04.019.
(29) Shi, J.; Wong, T. T. W.; He, Y.; Li, L.; Zhang, R.; Yung, C. S.; Hwang, J.; Maslov, K.; Wang, L. V. High-Resolution, High-Contrast Mid-Infrared Imaging of Fresh Biological Samples with Ultraviolet-Localized Photoacoustic Microscopy. *Nature Photonics* **2019**, *13* (9), 609–615. https://doi.org/10.1038/s41566-019-0441-3.
(30) Cheng, J.-X.; Xie, X. S. Vibrational Spectroscopic Imaging of Living Systems: An Emerging Platform for Biology and Medicine. *Science* **2015**, *350* (6264), aaa8870. https://doi.org/10.1126/science.aaa8870.
(31) Zhang, D.; Wang, P.; Slipchenko, M. N.; Cheng, J.-X. Fast Vibrational Imaging of Single Cells and Tissues by Stimulated Raman Scattering Microscopy. *Acc. Chem. Res.* **2014**, *47* (8), 2282–2290. https://doi.org/10.1021/ar400331q.
(32) Lee, H. J.; Cheng, J.-X. Imaging Chemistry inside Living Cells by Stimulated Raman Scattering Microscopy. *Methods* **2017**, *128*, 119–128. https://doi.org/10.1016/j.ymeth.2017.07.020.
(33) Zhang, C.; Cheng, J.-X. Perspective: Coherent Raman Scattering Microscopy, the Future Is Bright. *APL Photonics* **2018**, *3* (9), 090901. https://doi.org/10.1063/1.5040101.
(34) Potma, E. O.; de Boeij, W. P. Real-Time Visualization of Intracellular Hydrodynamics in Single Living Cells. 6.
(35) Mokrousova, V. I.; Okotrub, K. A.; Amstislavsky, S. Y.; Surovtsev, N. V. Raman Spectroscopy Evidence of Lipid Separation in Domestic Cat Oocytes during Freezing. *Cryobiology* **2020**, *95*, 177–182. https://doi.org/10.1016/j.cryobiol.2020.03.005.
(36) Dong, J.; Malsam, J.; Bischof, J. C.; Hubel, A.; Aksan, A. Spatial Distribution of the State of Water in Frozen Mammalian Cells. *Biophysical Journal* **2010**, *99* (8), 2453–2459. https://doi.org/10.1016/j.bpj.2010.08.035.
(37) Yu, G.; Li, R.; Hubel, A. Interfacial Interactions of Sucrose during Cryopreservation Detected by Raman Spectroscopy. *Langmuir* **2019**, *35* (23), 7388–7395. https://doi.org/10.1021/acs.langmuir.8b01616.
(38) Yu, G.; Yap, Y. R.; Pollock, K.; Hubel, A. Characterizing Intracellular Ice Formation of Lymphoblasts Using Low-Temperature Raman Spectroscopy. *Biophysical Journal* **2017**, *112* (12), 2653–2663. https://doi.org/10.1016/j.bpj.2017.05.009.
(39) Karpegina, Yu. A.; Okotrub, K. A.; Brusentsev, E. Yu.; Amstislavsky, S. Ya.; Surovtsev, N. V. Cryoprotectant Redistribution along the Frozen Straw Probed by Raman Spectroscopy. *Cryobiology* **2016**, *72* (2), 148–153. https://doi.org/10.1016/j.cryobiol.2016.01.002.
(40) Schindelin, J.; Arganda-Carreras, I.; Frise, E.; Kaynig, V.; Longair, M.; Pietzsch, T.; Preibisch, S.; Rueden, C.; Saalfeld, S.; Schmid, B.; Tinevez, J.-Y.; White, D. J.; Hartenstein, V.; Eliceiri, K.; Tomancak, P.; Cardona, A. Fiji: An Open-Source Platform for Biological-Image Analysis. *Nature Methods* **2012**, *9* (7), 676–682. https://doi.org/10.1038/nmeth.2019.
(41) Vasudevan, V.; Mushrif, S. H. Insights into the Solvation of Glucose in Water, Dimethyl Sulfoxide (DMSO), Tetrahydrofuran (THF) and N,N-Dimethylformamide (DMF) and Its Possible Implications on the Conversion of Glucose to Platform Chemicals. *RSC Advances* **2015**, *5* (27), 20756–20763. https://doi.org/10.1039/C4RA15123B.
(42) Tusch, M.; Krüger, J.; Fels, G. Structural Stability of V-Amylose Helices in Water-DMSO Mixtures Analyzed by Molecular Dynamics. *J. Chem. Theory Comput.* **2011**, *7* (9), 2919–2928. https://doi.org/10.1021/ct2005159.

(43) Galvao, J.; Davis, B.; Tilley, M.; Normando, E.; Duchen, M. R.; Cordeiro, M. F. Unexpected Low-Dose Toxicity of the Universal Solvent DMSO. *The FASEB Journal* **2014**, *28* (3), 1317–1330. https://doi.org/10.1096/fj.13-235440.
(44) Cheng, C.-Y.; Song, J.; Pas, J.; Meijer, L. H. H.; Han, S. DMSO Induces Dehydration near Lipid Membrane Surfaces. *Biophysical Journal* **2015**, *109* (2), 330–339. https://doi.org/10.1016/j.bpj.2015.06.011.
(45) Gurtovenko, A. A.; Anwar, J. Modulating the Structure and Properties of Cell Membranes: The Molecular Mechanism of Action of Dimethyl Sulfoxide. *J. Phys. Chem. B* **2007**, *111* (35), 10453–10460. https://doi.org/10.1021/jp073113e.
(46) Schaeffer, G. W.; Frank T. Sharpe, Jr. Lysine in Seed Protein from S-Aminoethyl-L-Cysteine Resistant Anther-Derived Tissue Cultures of Rice. *In Vitro* **1981**, *17* (4), 345–352.
(47) Finkle, B. J.; Ulrich, J. M. Cryoprotectant Removal Temperature as a Factor in the Survival of Frozen Rice and Sugarcane Cells. *Cryobiology* **1982**, *19* (3), 329–335. https://doi.org/10.1016/0011-2240(82)90161-4.
(48) Saar, B. G.; Contreras-Rojas, L. R.; Xie, X. S.; Guy, R. H. Imaging Drug Delivery to Skin with Stimulated Raman Scattering Microscopy. *Mol Pharm* **2011**, *8* (3), 969–975. https://doi.org/10.1021/mp200122w.
(49) R Core Team. *R: A language and environment for statistical computing*. https://www.r-project.org/.
(50) Benelli, C. Plant Cryopreservation: A Look at the Present and the Future. *Plants* **2021**, *10* (12), 2744. https://doi.org/10.3390/plants10122744.
(51) Hughes, Z. E.; Mark, A. E.; Mancera, R. L. Molecular Dynamics Simulations of the Interactions of DMSO with DPPC and DOPC Phospholipid Membranes. *J. Phys. Chem. B* **2012**, *116* (39), 11911–11923. https://doi.org/10.1021/jp3035538.
(52) Kligman, A. M. Topical Pharmacology and Toxicology of Dimethyl Sulfoxide—Part 1. *JAMA* **1965**, *193* (10), 796–804. https://doi.org/10.1001/jama.1965.03090100042010.
(53) Williams, A. C.; Barry, B. W. Penetration Enhancers. *Advanced Drug Delivery Reviews* **2012**, *64*, 128–137. https://doi.org/10.1016/j.addr.2012.09.032.
(54) Chiu, W. S.; Belsey, N. A.; Garrett, N. L.; Moger, J.; Delgado-Charro, M. B.; Guy, R. H. Molecular Diffusion in the Human Nail Measured by Stimulated Raman Scattering Microscopy. *Proc. Natl. Acad. Sci. U.S.A.* **2015**, *112* (25), 7725–7730. https://doi.org/10.1073/pnas.1503791112.
(55) Ménorval, M.-A. de; Mir, L. M.; Fernández, M. L.; Reigada, R. Effects of Dimethyl Sulfoxide in Cholesterol-Containing Lipid Membranes: A Comparative Study of Experiments In Silico and with Cells. *PLOS ONE* **2012**, *7* (7), e41733. https://doi.org/10.1371/journal.pone.0041733.
(56) Malajczuk, C. J.; Stachura, S. S.; Hendry, J. O.; Mancera, R. L. Redefining the Molecular Interplay between Dimethyl Sulfoxide, Lipid Bilayers, and Dehydration. *J. Phys. Chem. B* **2022**, *126* (13), 2513–2529. https://doi.org/10.1021/acs.jpcb.2c00353.
(57) Cheng, J.-X. Coherent Anti-Stokes Raman Scattering Microscopy. *Appl Spectrosc* **2007**, *61* (9), 197–208.
(58) Samuels, F. M. D.; Stich, D. G.; Bonnart, R.; Volk, G. M.; Levinger, N. E. Non-Uniform Distribution of Cryoprotecting Agents in Rice Culture Cells Measured by CARS Microscopy. *Plants* **2021**, *10* (3), 589. https://doi.org/10.3390/plants10030589.
(59) Linkert, M.; Rueden, C. T.; Allan, C.; Burel, J.-M.; Moore, W.; Patterson, A.; Loranger, B.; Moore, J.; Neves, C.; MacDonald, D.; Tarkowska, A.; Sticco, C.; Hill, E.; Rossner, M.;

Eliceiri, K. W.; Swedlow, J. R. Metadata Matters: Access to Image Data in the Real World. *Journal of Cell Biology* **2010**, *189* (5), 777–782. https://doi.org/10.1083/jcb.201004104.
(60) de Moliner, F.; Knox, K.; Gordon, D.; Lee, M.; Tipping, W. J.; Geddis, A.; Reinders, A.; Ward, J. M.; Oparka, K.; Vendrell, M. A Palette of Minimally Tagged Sucrose Analogues for Real-Time Raman Imaging of Intracellular Plant Metabolism. *Angewandte Chemie International Edition* **2021**, *60* (14), 7637–7642. https://doi.org/10.1002/anie.202016802.
(61) Elliott, G. D.; Wang, S.; Fuller, B. J. Cryoprotectants: A Review of the Actions and Applications of Cryoprotective Solutes That Modulate Cell Recovery from Ultra-Low Temperatures. *Cryobiology* **2017**, *76*, 74–91. https://doi.org/10.1016/j.cryobiol.2017.04.004.
(62) Fuller, B. J. Cryoprotectants: The Essential Antifreezes to Protect Life in the Frozen State. *CryoLetters* **2004**, *25* (6).
(63) Best, B. P. Cryoprotectant Toxicity: Facts, Issues, and Questions. *Rejuvenation Res* **2015**, *18* (5), 422–436. https://doi.org/10.1089/rej.2014.1656.
(64) C.j, B.; K.c, S. Regeneration of Plants from Callus-Derived Protoplasts of Salpiglossis [Sinuata, Protoplast Technology]. *Journal American Society for Horticultural Science* **1981**.
(65) Li, S.; Li, Y.; Yi, R.; Liu, L.; Qu, J. Coherent Anti-Stokes Raman Scattering Microscopy and Its Applications. *Frontiers in Physics* **2020**, *8*.
(66) Freudiger, C. W.; Min, W.; Saar, B. G.; Lu, S.; Holtom, G. R.; He, C.; Tsai, J. C.; Kang, J. X.; Xie, X. S. Label-Free Biomedical Imaging with High Sensitivity by Stimulated Raman Scattering Microscopy. *Science* **2008**, *322* (5909), 1857–1861. https://doi.org/10.1126/science.1165758.
(67) Zeng, Y.; Yarbrough, J. M.; Mittal, A.; Tucker, M. P.; Vinzant, T. B.; Decker, S. R.; Himmel, M. E. In Situ Label-Free Imaging of Hemicellulose in Plant Cell Walls Using Stimulated Raman Scattering Microscopy. *Biotechnology for Biofuels* **2016**, *9* (1). https://doi.org/10.1186/s13068-016-0669-9.
(68) Mikami, H.; Shiozawa, M.; Shirai, M.; Watanabe, K. Quantitative Index of Arbitrary Molar Concentration for Coherent Anti-Stoke Raman Scattering (CARS) Spectroscopy and Microscopy. *Opt. Express, OE* **2015**, *23* (4), 5300–5311. https://doi.org/10.1364/OE.23.005300.
(69) Liu, B.; Lee, H. J.; Zhang, D.; Liao, C.-S.; Ji, N.; Xia, Y.; Cheng, J.-X. Label-Free Spectroscopic Detection of Membrane Potential Using Stimulated Raman Scattering. *Appl. Phys. Lett.* **2015**, *106* (17), 173704. https://doi.org/10.1063/1.4919104.
(70) Momoko Ikeuchi; Keiko Sugimoto; Akira Iwase. Plant Callus: Mechanisms of Induction and Repression | Plant Cell. *The Plant Cell* **2013**, *Vol. 25*, 3159–3173.

APPENDIX I: Supplementary Text and Figures for "CHAPTER 2: Non-Uniform Distribution of Cryoprotecting Agents in Rice Culture Cells Measured by CARS Microscopy"

AI.1 CARS Microscopy Instrument Description

All coherent anti-Stokes Raman scattering (CARS) images were collected at the Advanced Light Microscopy Core (ALMC), at the UC Denver, Anschutz campus. The images were acquired with the help of the ALMC personnel, Dr. Dominik Stich and Greg Glazner. A detailed description of the microscope follows here.

The Advanced Light Microscopy Core coherent anti-Stokes Raman scattering (CARS) imaging system is composed of an APE (Angewandte Physik und Elektronik GmbH, Berlin) picoEMERALD optical parametric oscillator (OPO) and an inverted Olympus IX81 microscope (Olympus Corp., Tokyo) with an Olympus FV1000 scan head (Olympus Corp., Tokyo). The APE OPO incorporates a NKT aeroPulse PS10 fiber laser (NKT Photonics A/S, Denmark) that provides a pulse train centered at 1031 nm with an 80 MHz repetition rate. A portion of the 1031 nm beam is frequency doubled to 515.5 nm and used to generate the pump beam in the OPO while the remaining 1031 nm beam comprises the Stokes beam. The OPO offers a software-controlled tunable OPO signal and OPO idler output from 700 nm to 990 nm and 1080 nm to 1950 nm, respectively. The 1031 nm beam and the OPO signal are used for CARS imaging. The pulse widths for each beam is approximately 2 ps and the spectral bandwidth of the probed CARS signal is approximately 10 cm^{-1}. The pump and Stokes beam pulse trains are overlapped temporally and spatially before exiting the OPO aperture. The beams are reduced fourfold in diameter by a telescope before being coupled into the scan head of the microscope.

From the scan head, the beams enter the microscope stand through the rear port and are reflected toward the objective by a dichroic mirror in the stand turret (Chroma t750spxrxt, lot

217722). The beams are focused into the sample by an Olympus UPlanSApo 20X, NA 0.75 air objective.

The forward CARS signal is collected by a NA 0.55 air condenser (Olympus Corp., Tokyo) and detected by an Olympus non-descanned PMT Unit (FV10MP-BXTD, Olympus Corp., Tokyo). The laser beams are rejected by a shortpass filter (Thorlabs, FES750) and a bandpass filter (Chroma HG730/50M2P, lot 248096).

In general, a CARS Stokes beam fixed at 1031 nm and a CARS Pump/Probe beam tunable from 780 nm to 960 nm can generate CARS signal in a range from 720 cm^{-1} to 3120 cm^{-1}. With the described filters in the detection path, CARS signal can be detected in the range from 1775 cm^{-1} to 2240 cm^{-1}. In these experiments the CARS Pump/Probe beam was set to 845.0 nm to detect the CARS signal of the C-D stretch vibration in d_6-DMSO at 2120 cm^{-1}.

In addition to the CARS signal, two photon autofluorescence (TPA) from the pump beam was collected in the epi direction in a range from 400 nm to 600 nm with a second non-descanned detector Unit (Olympus FV10MP- *IXD2CH*, Chroma, e600sp-2p, lot 221876). The CARS system also offers the capability of CARS imaging in epi direction and SHG imaging in forward direction, as well as normal confocal scanning imaging, see Figure AI.1. These capabilities were not used in the reported experiments.

CARS and TPA images, z-stacks and time-lapses were recorded in the FV10-ASW 4.2 acquisition software (Olympus Corp., Tokyo).

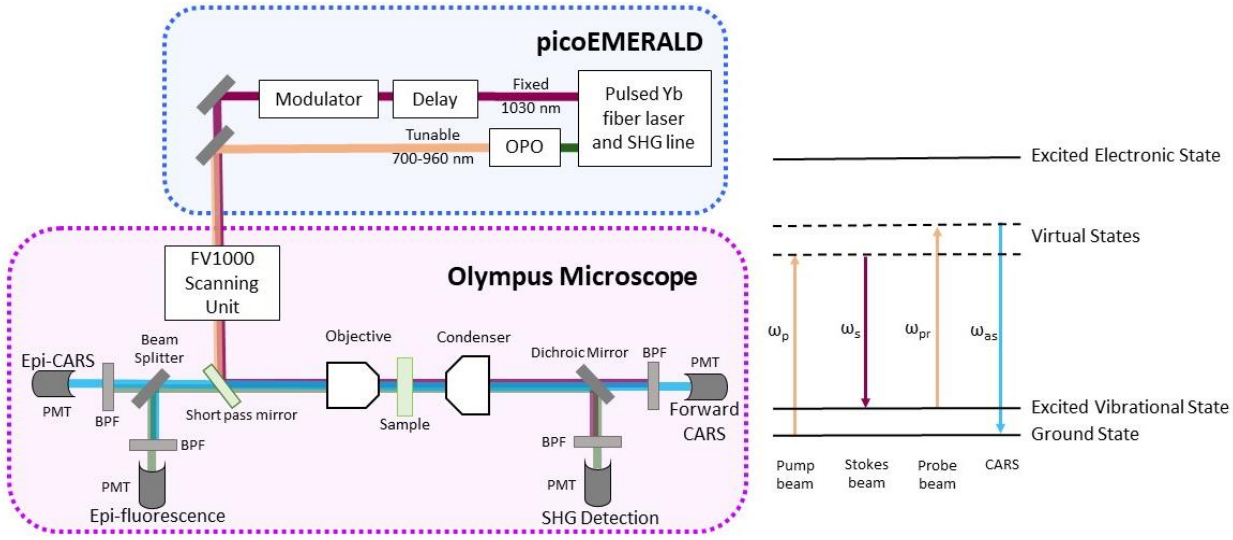

Figure AI.1: Simplified schematic of microscope set up and corresponding energy diagram of CARS process.

AI.2 Bright Field Images

Figure AI.2 shows a sample of the IKI staining experiments carried out to help determine organelle identities IKI stains starch a dark brown, and it is clear in the figure that cells either contain a few starch bodies (presumably amyloplasts) or no starch bodies. These studies lead us to believe that the primary organelles that are similar in size to those seen sequestering d_6-DMSO in the CARS images collected are likely amyloplasts.

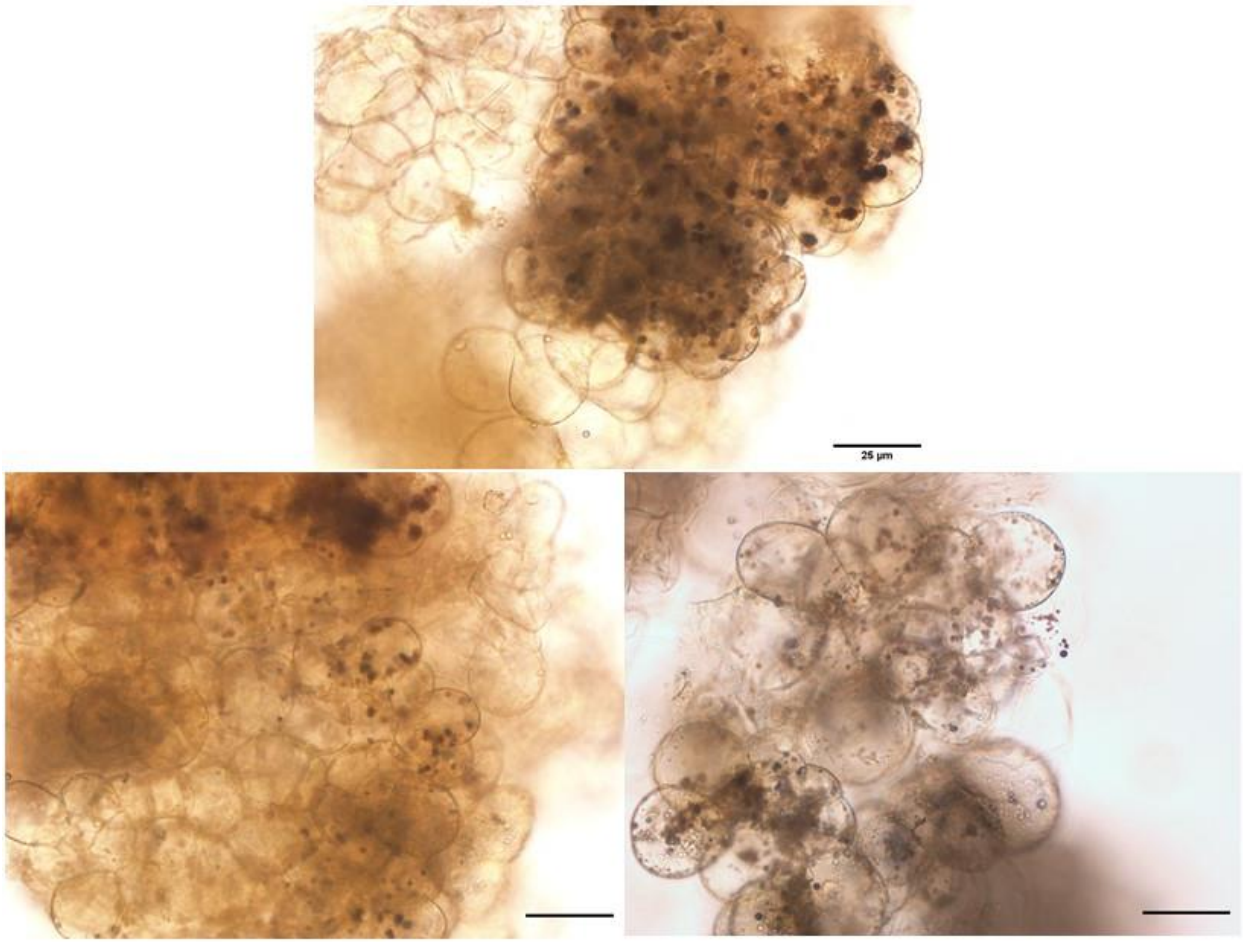

Figure AI.2: Starch containing organelles in rice callus cells stained with IKI for 5 minutes, 5 minutes and 1.5 minutes (top, bottom-left, bottom-right). All scale bars are 25 µm.

Figure AI.3 shows bright field images of callus cells being exposed to 10% DMSO. While this concentration is lower than that used in the primary CARS figure in the main text of the paper, the cellular response should be similar, if not the same, with a slightly higher DMSO concentration. The most likely difference in cellular response between a lower concentration will be to have a slightly smaller cellular response. In this case it is important to notice that the cell labelled with the pink arrow is one of the only cells obviously responding to the DMSO exposure at t = 2.2 min and that it appears to undergo plasmolysis twice. This is further evidence that directly imaging the

exact location of cryoprotectants when they are interacting with plant callus cells is important and may inform further, unusual cell behavior.

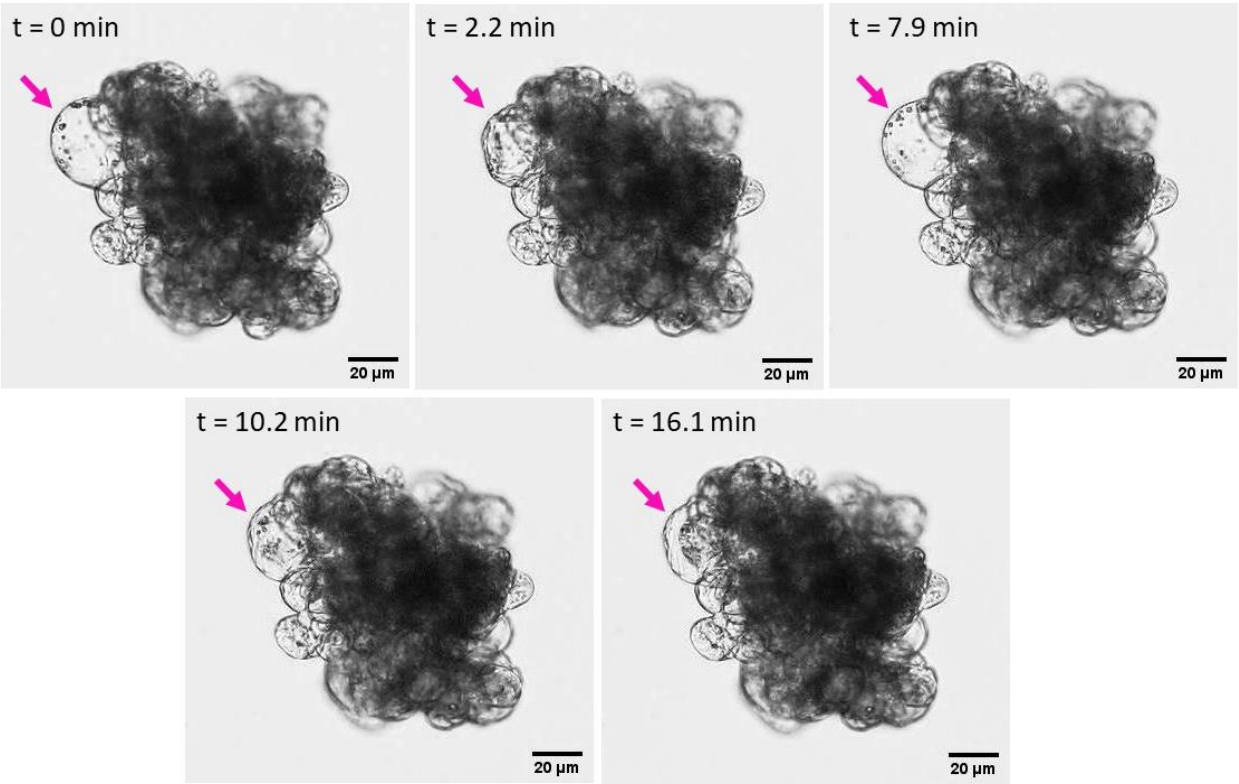

Figure AI.3: Bright field image of cells exposed to 10% DMSO in distilled water. All scale bars are 20 µm.

Figure AI.4 shows a bright field image of densely packed callus being exposed to 15% DMSO. Similar to the previous figure, only the cell labelled with the pink arrow appears to be responding as expected to the DMSO exposure, plasmolyzing and deplasmolyzing over the course

of 11 minutes. Again, this further illustrates the need for a more foundational understanding of how exactly the cryoprotectants are being distributed through the callus.

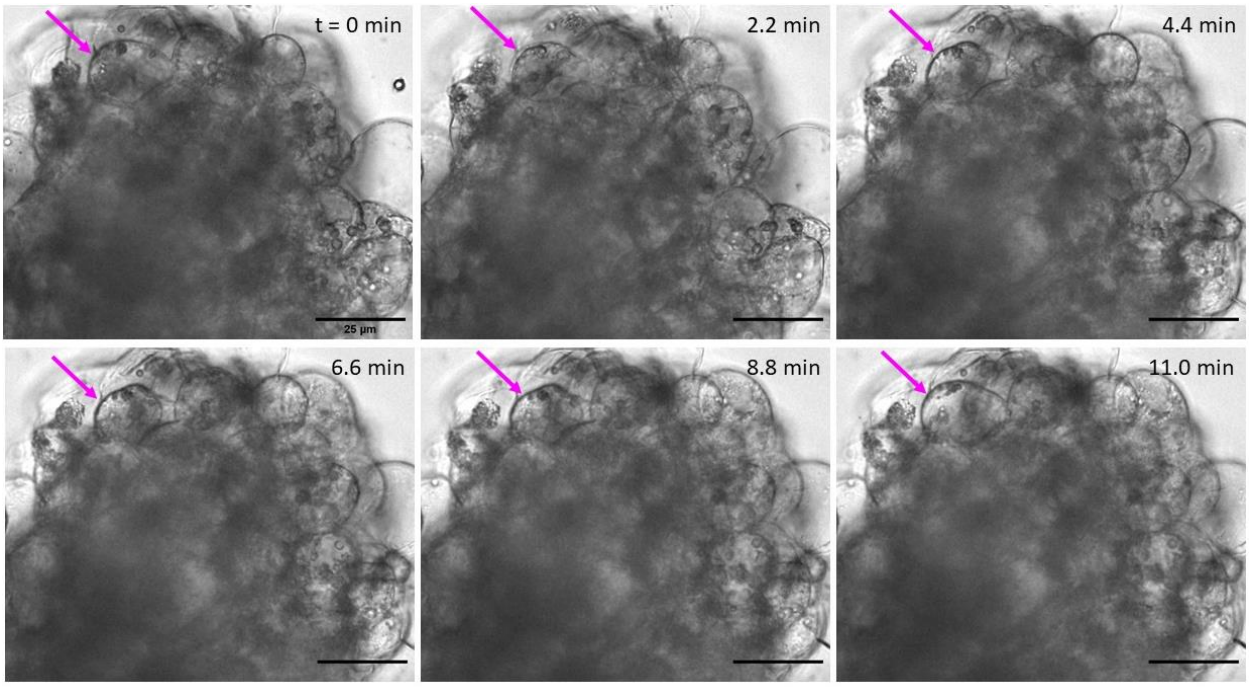

Figure AI.4: Bright field images of cells exposed to 15% DMSO in water. All scale bars are 25 µm.

AI.3 CARS Images

The following Figures AI.5-8 all show CARS data of rice callus cells after at least 3 minutes of d_6-DMSO exposure. Exposure times changed as the time to prepare the sample, find healthy cells, and begin imaging changed. All the cells shown in these figures exhibit apparent sequestering of d_6-DMSO within organelles inside the cells.

The left side of Figure AI.5 shows some callus with a particularly large cell towards the upper left. This cell is comparable in size to the one indicated in Figure AI.3, and the deplasmolysis of this cell was captured in the time-lapse images, though only one image is shown in the figure. The right side of Figure AI.5 shows the autofluorescence image captured simultaneously with the

CARS images. Looking at the autofluorescence images, it is clear that organelles are moving around within the cells, indicated the cells are likely alive.

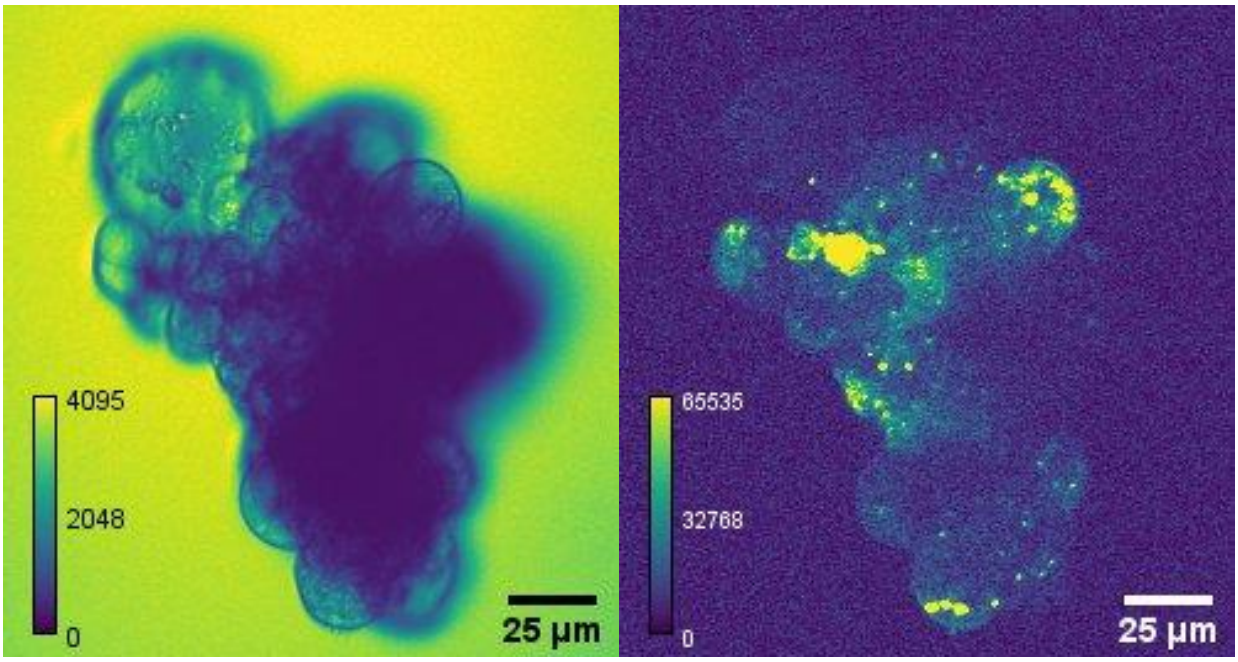

Figure AI.5: (LEFT) Rice callus after 5 minutes of 15% d6-DMSO in distilled water exposure imaged with CARS microscope. Yellow represents higher d6-DMSO signal, thus higher d6-DMSO concentration. (RIGHT) Autofluorescence image taken simultaneously with the CARS image. Images were artificially colored with ImageJ LUT, mpl-viridis (26).

Figure AI.6 shows a cluster of callus cells after 8 minutes of exposure to a mixture of 15% d_6-DMSO in a sugar solution. In this figure there appears to be differences in d_6-DMSO across the cells, interestingly with apparent lack of d_6-DMSO inside come cell cavities and higher concentration, again, in circular organelles in the cells. This figure demonstrates that non-uniformity in the cellular components may lead to increased non-uniformity of the cryoprotectant distribution within the cells.

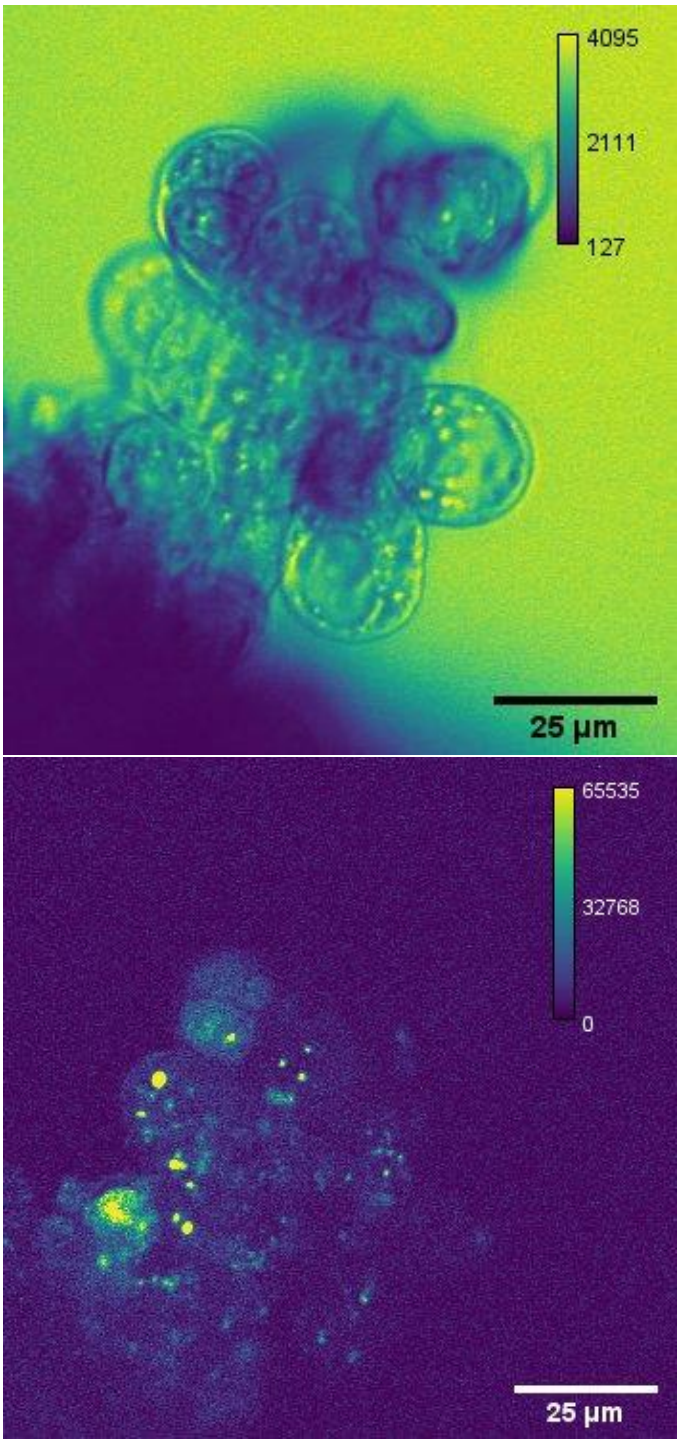

Figure AI.6: (TOP) Rice cells after 8 minutes of 15% d6-DMSO in sugar water exposure imaged with CARS microscope. Yellow represents higher d6-DMSO signal, thus higher d6-DMSO concentration. (BOTTOM) Autofluorescence image taken simultaneously as CARS data. When viewed in time-lapse, it is evident that the cells have internal movement, indicating that they are alive. Images were artificially colored with ImageJ LUT, mpl-viridis (26).

Figure AI.7 shows a CARS image of rice callus cells after 10 minutes of d_6-DMSO exposure. This figure has a range of cells in that some of them appear almost empty while others clearly contain organelles that have concentrated d_6-DMSO within them. It appears as though cells that lack organelles do have fairly uniform d_6-DMSO distribution while those cells that are densely packed with organelles have d_6-DMSO concentrating within the organelles. This contrast in cellular components and consequentially d_6-DMSO distributions within the cells further illustrates the necessity of considering that the organelle content of the cells likely will affect uniform cryoprotectant distribution within those cells. The lower image in Figure AI.7 shows the autofluorescence captured simultaneously with the CARS data.

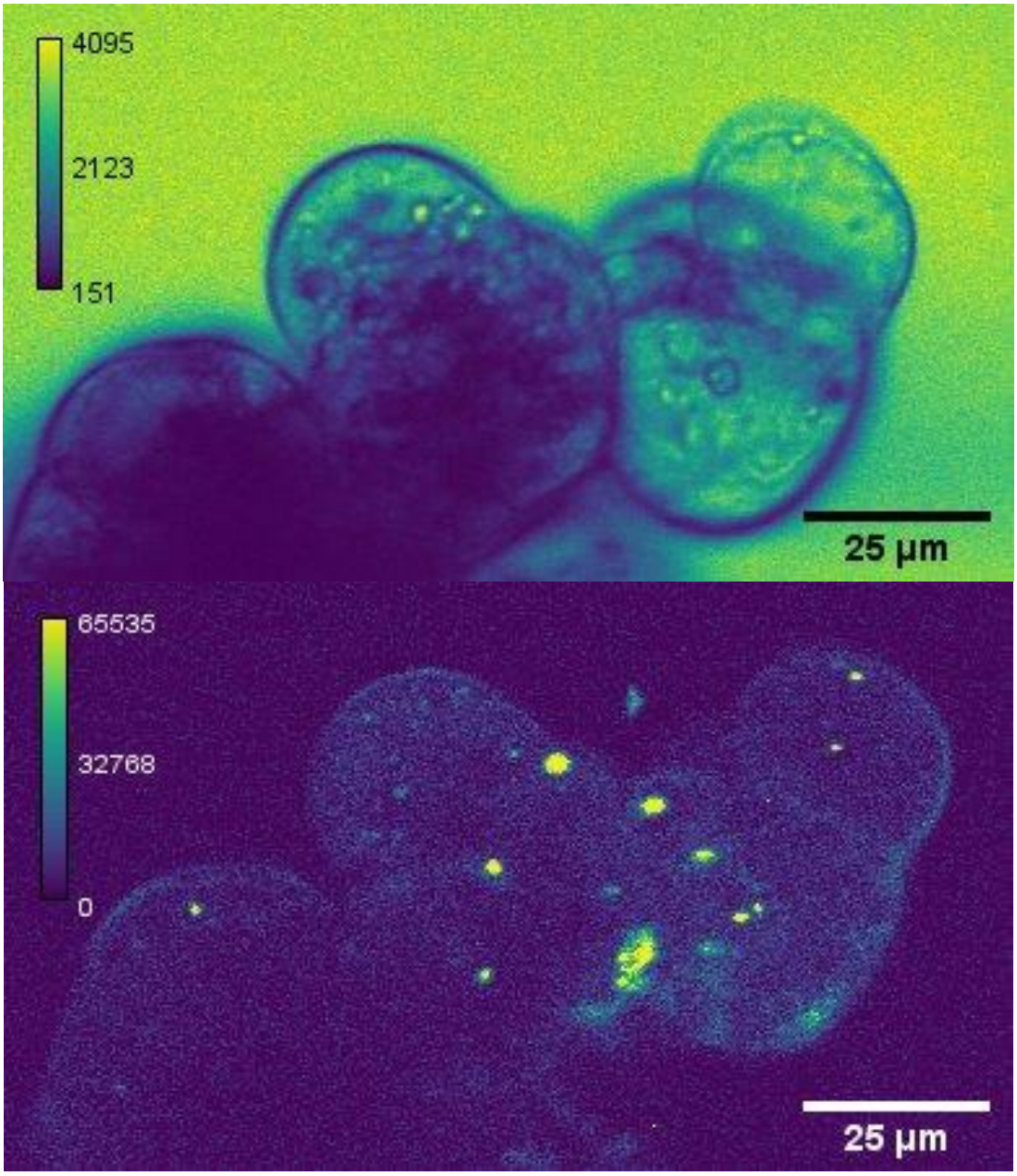

Figure AI.7: (TOP) Rice cells after 10 minutes of 15% d6-DMSO in distilled water exposure imaged with CARS microscope. Yellow represents higher d6-DMSO signal, thus higher d6-DMSO concentration. (BOTTOM) Autofluorescence captured simultaneously with the CARS data showing an image of autofluorescent components of the cells. When viewed as a time-lapse, it is clear that components of the cell are moving around, indicating the cells are likely alive. Images were artificially colored with ImageJ LUT, mpl-viridis (26).

Figure AI.8 is the same as Figure 2.2 with the addition of the pixel gray-scale value bar. This bar shows how different the gray-scale values are for the organelles contained within the outer visible cells of the callus and those in the center of the callus. The center of the callus has the

lowest values not because there is not d_6-DMSO penetrating into it, but rather because the callus is too dense for the d_6-DMSO to make it to the detector. The image below the CARS data shows the autofluorescence image of the cells captured at the same time as the CARS image. When viewed as a time lapse, it is clear that the autofluorescent parts of the cells are moving rapidly around, indicating that the cells are alive.

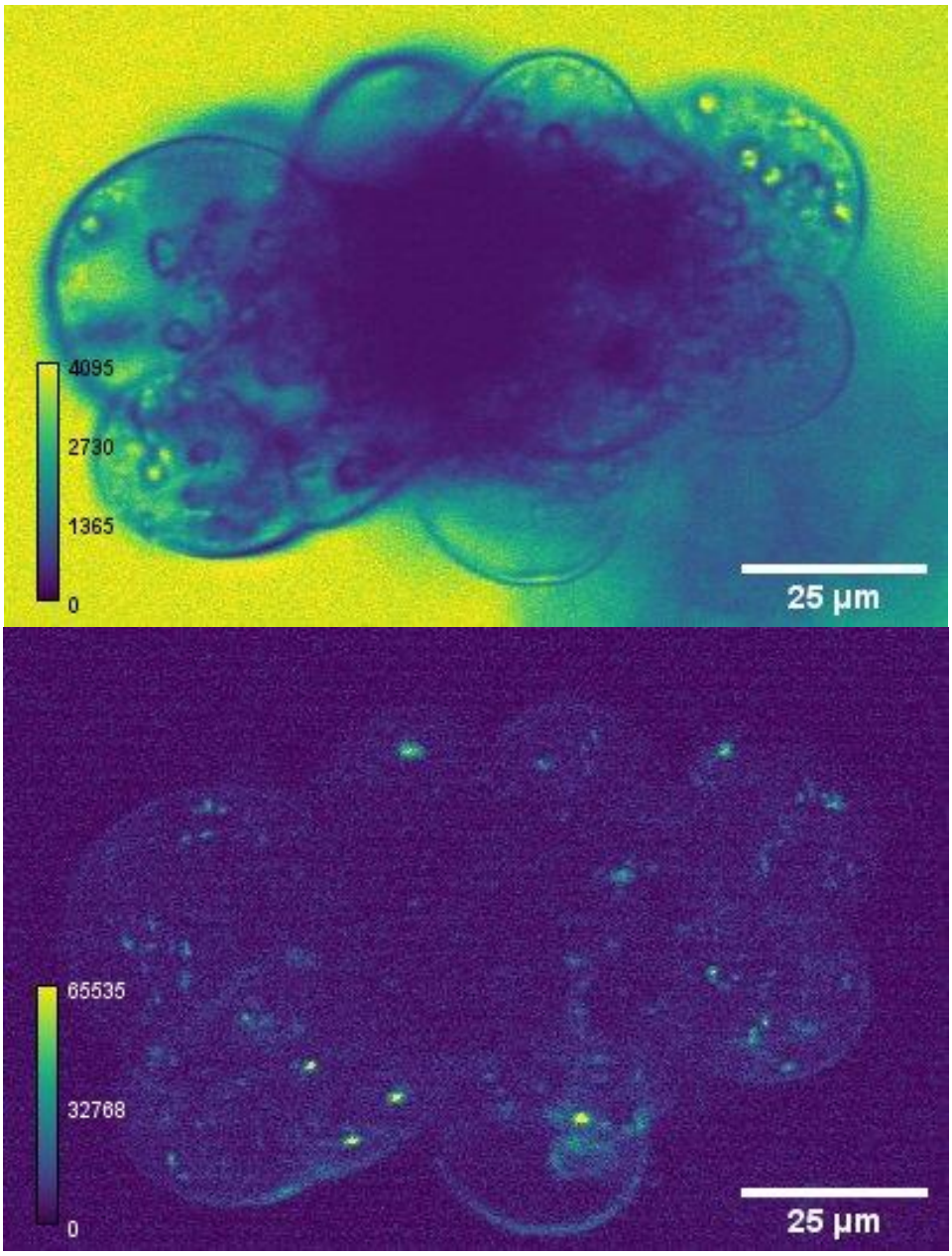

Figure AI.8: (TOP) Rice callus after 3 minutes of 15% d_6-DMSO in distilled water exposure imaged with CARS microscope. Yellow represents higher d_6-DMSO signal, thus higher d_6-DMSO

concentration. (BOTTOM) Shows autofluorescence of the cells simultaneously collected with the CARS data. When viewing the time lapse data, the autofluorescencent components move around rapidly indicating that the cells of interest are alive. Images were artificially colored with ImageJ LUT, mpl-viridis.

AI.4 Original Author Contributions

Fionna M.D. Samuels: Conceptualization, Methodology, Validation, Formal Analysis, Investigation, Resources, Writing – Original Draft, Writing – Review & Editing; Dominik G. Stich: Methodology, Resources, Software, Writing – Review & Editing; Remi Bonnart: Methodology, Resources, Writing – Review & Editing; Gayle M. Volk: Conceptualization, Writing – Review & Editing, Funding Acquisition; Nancy E. Levinger: Conceptualization, Writing – Review & Editing, Funding Acquisition, Supervision, Project Administration.

AI.4 Funding

This work received financial support from USDA NIFA Grant Number 12835363, NSF Graduate Research Fellowship Program fellow number 2019273956 (FMDS), and the Colorado State University Office of the Vice President for Research. Imaging experiments were performed in the Advanced Light Microscopy Core, part of NeuroTechnology Center at University of Colorado Anschutz Medical Campus, supported in part by Rocky Mountain Neurological Disorders Core Grant Number P30 NS048154 and by Diabetes Research Center Grant Number P30 DK116073.

APPENDIX II: Supplementary Text and Figures for "CHAPTER 3: Direct measurement of rice (*Oryza sativa*) callus cell responses to common molecular cryoprotectants"

AII.1 CARS image acquisition and analysis

The same microscope described in Appendix I was used to collect the data described in Chapter 3. This instrument generates z-stack data sets wherein images are taken at different focal planes in a sample in the z-direction. Z-stacks were occasionally collected to confirm that deuterated cryoprotectants permeated cells deeper in the cell clusters. When a z-stack was collected, the data were removed from the intensity traces, as shown in Figures 9 and 10, and Figures S2, S3 and S4 resulting in apparent blank spaces in the trace.

Before, during, and/or after data acquisition, we occasionally detune the temporal overlap between the pump and probe beams generating CARS signal so that they no longer impinge on the sample at the same time. This eliminates the possibility for the CARS process and ensures that the signal observed from the cells can be attributed to CARS signal rather than another process, like fluorescence. In these cases, the intensity data were also removed from the intensity traces.

AII.2 Supplementary Data

AII.2.1 Cell response criteria

In Chapter 3, I report the responses of rice callus cells to individual components of PVS2 and PVS3 cryoprotectant solutions measured using brightfield microscopy. We observe variable cellular responses and response times. This is consistent with previous literature that measured sweet potato suspension cell responses to cryoprotectants.[10] Unlike previous studies, the data reported here were collected as the cryoprotectant solutions flowed across the cells.[58] The resulting videos allow cellular response to be visualized in real-time. However, brightfield microscopy does not show when the cryoprotectant enters the perfusion chamber nor when the media initially

present in the perfusion chamber has been completely replaced by the cryoprotectant solution because both solutions are clear and colorless when viewed through the microscope. This makes it difficult to establish exactly when the cryoprotectant solution first enters the field of view, the true time zero. Thus, for the brightfield experiments, we estimate time zero—the time when the cryoprotectant solution enters the field of view—as the first time the cells showed any response to cryoprotectant introduction into the perfusion chamber. This generally appears as the entire cluster of cells shrinking slightly before any individual cells show a response and occurs with any cryoprotectant exposure. We note that this time could be after the cryoprotectant actually entered the perfusion chamber.

The brightfield criteria for determining how the cells respond (*i.e.*, crumpling, plasmolysis or deplasmolysis) are as follows:

1. Crumpling—the cell appears to shrink slightly and non-uniformly like crumpling a ball of paper then return to its original turgid state. The cell membrane does not clearly separate from the cell wall, but there is a clear response. The end of this response was the last frame in which the cell appeared to be swelling after the initial overall response (considered t = 0 s).
2. Plasmolysis—the cell membrane clearly separates from the cell wall leaving space between the membrane and the wall. This can be either convex or concave plasmolysis; the membrane can appear totally smooth and circular when it separates from the cell wall or it can be non-uniform and appear like places of the membrane are still stuck to the cell wall. Regardless, the majority of the cell membrane separates from the cells wall. Biologically, this response

likely occurs because water is rapidly leaving the cell. The end of this response was the last frame in which the cell membrane appeared to be shrinking after t = 0 s.

3. Deplasmolysis—the cell membrane starts from a plasmolyzed state and then returns to the cell membrane such that the cell appears similar to before exposure. This response requires that plasmolysis occurred. Previous studies have attributed this response to cryoprotectant permeation, however our study demonstrates that permeation occurs much earlier than the end of deplasmolysis. The end of this response was the last frame in which the cell appeared to be swelling after t = 0 s.

Three of the original authors (F.M.D.S, K.C.P. and S.S.) independently evaluated all the brightfield data collected and determined which cells they considered clearly visible (*i.e.*, a clear cell wall and cell membrane in the case of plasmolysis). After independently considering the data, their results were compared. Any cells that were in conflict were discussed and collectively decided upon. If a consensus could not be reached, the cell was not included in the final count.

In Chapter 3, Figure 3.6, I present response times for cells grouped for each cryoprotectant component. In Figure AII.1 we rearrange the data shown in Chapter 3 to compare the response times for each cryoprotectant as a group for each type of response. For example, Figure AII.1a. compares the end of the minimal response when exposed to DMSO (red), ethylene glycol (green) and glycerol (brown). This grouping shows the statistically significant differences between glycerol compared to both DMSO and ethylene glycol exposure.

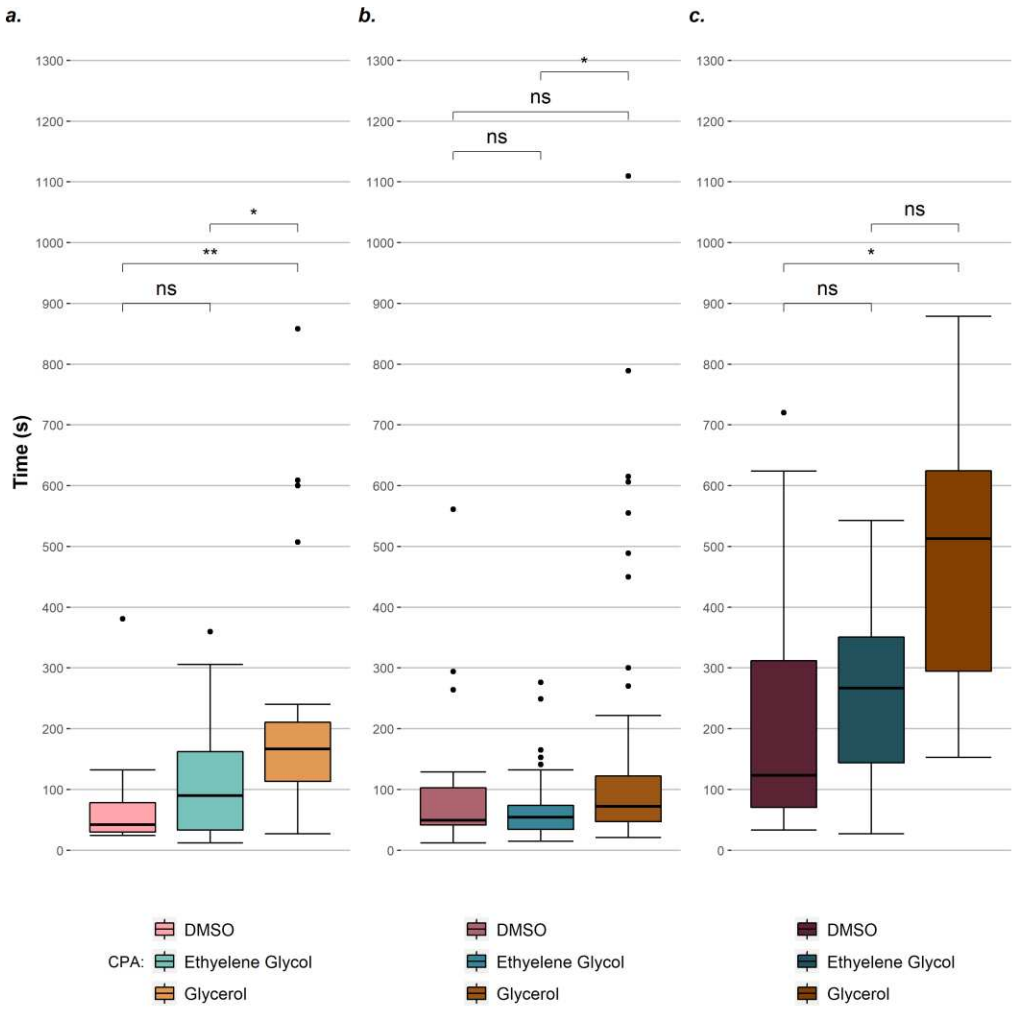

Figure AII.1: Box-and-whisker plots showing the median (line in box), interquartile range (ends of box) and 5th and 95th percentiles (whiskers) of each kind of response: a. minor response, b. plasmolysis, and c. deplasmolysis. The colors correspond to each cryoprotectant: DMSO in red tones, ethylene glycol in green tones, and glycerol in orange tones. Significance levels: ns – not significant, ∗ – p <0.05, ∗∗ – p <0.01, ∗∗∗ – p <0.001, ∗∗∗∗ – p <0.0001.

AII.2.2 CARS Response Times Boxplots

CARS data were also analyzed using the same methodology as the brightfield data to determine the end of plasmolysis and deplasmolysis. Crumpling was difficult to observe in the CARS data and was not considered. Only cells that had clear shrink/swell responses were considered because the microscope was tuned to image the deuterated cryoprotectants, so it was more difficult to clearly see the membrane. The first frame where there was an observable change in background intensity was considered t = 0 s rather than the first overall callus response. Those

time data are shown in Figure AII.2.

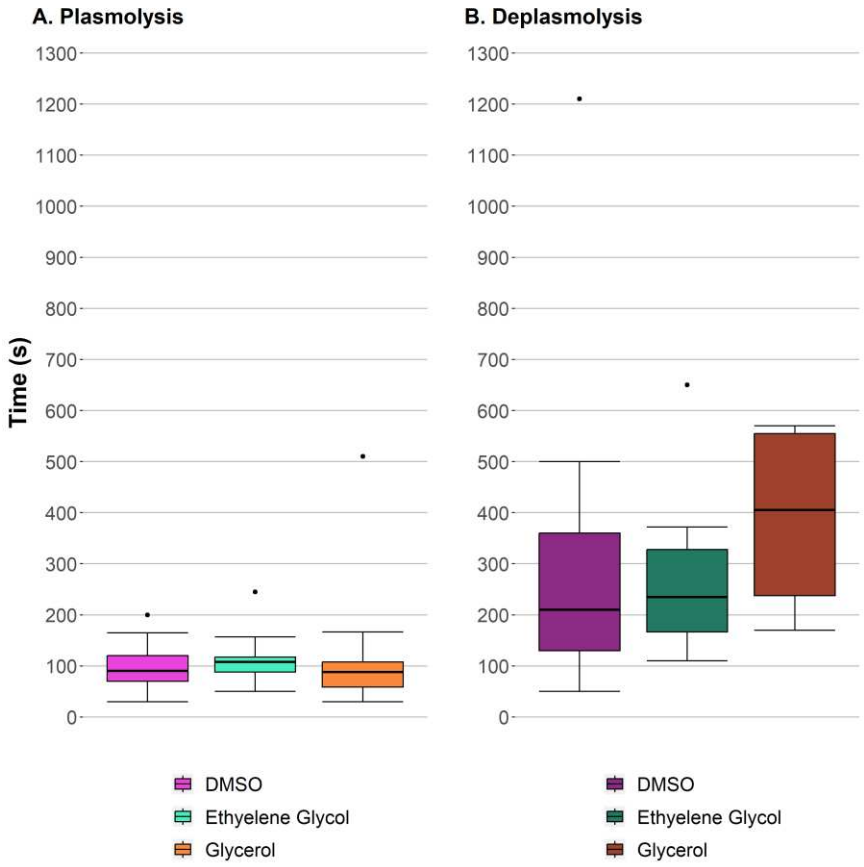

Figure AII.2: Box-and-whisker plots showing the median (line in box), interquartile range (ends of box) and 5th and 95th percentiles (whiskers) of A. plasmolysis and B. deplasmolysis from CARS data. The colors correspond to each CPA: DMSO in pink tones, ethylene glycol in green tones, and glycerol in orange tones. None of the boxplots are statistically significant.

Figure AII.3 shows the CARS and brightfield data on the same boxplot. Only the timescales of ethylene glycol plasmolysis are statistically different between CARS and brightfield data (Table AII.7) and this difference may be due to there being fewer cells included in the CARS data.

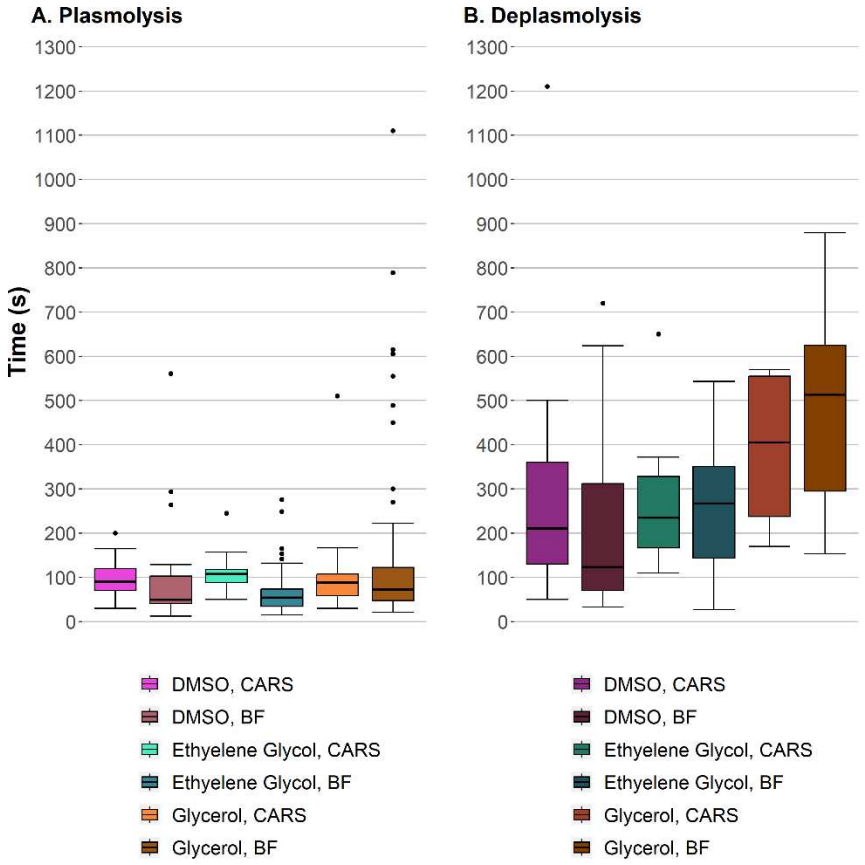

Figure AII.3: Boxplots of the CARS and brightfield cell response times. A. times for end of plasmolysis; B. times for end of deplasmolysis.

AII.2.3 CARS images and intensity traces

We present replicate data associated with additional CARS microscopy experiments performed by exposing the cells to the three different cryoprotectant solutions. Specifically, Figure AII.4 displays the response of cells to d_6-DMSO solution, Figure AII.5 shows cell responses to d_6-ethylene glycol, and Figure AII.6 shows cell responses to d_8-glycerol. Data from these experiments are included in the statistical analysis presented in Figure 3.10.

Figure AII.4 displays CARS images along with the graphical representation of seven different experiments wherein d_6-DMSO flowed across clusters of rice callus cells, similar to Figure 3.8. Each trace corresponds to a hand-selected region of interest (ROI) inside a cell (labeled C#, color), or in the background of the image (labeled BK#, grey-scale). The change in the intensity

of the background ROIs correspond to d_6-DMSO entering the perfusion chamber and replacing the media initially surrounding the cells. Time zero corresponds to the midpoint of a fit of the average background intensity (black, dashed line). The data are all shifted, as described in Chapter 3, so that each experiment has the same time zero, allowing them to be compared more readily. In Figures AII.3a and 3c, the images and graphs show d_6-DMSO flowing into the perfusion chamber and its subsequent replacement with aqueous media.

The data in Figure AII.4 show that the average intensity inside all represented cells increases over time, indicating that d_6-DMSO permeates all the cells. The cell intensities are normalized to the average background intensity, the maximum intensity of which should correspond 15% d_6-DMSO (*wt/v*) assuming the media has been entirely replaced by the d_6-DMSO solution. Few cells appear to reach the same level of intensity as the background. Further, the shape of each trace is not uniform. Although all the traces in b. and c. increase slowly before reaching a plateau around 400 s, the traces in a. and f. appear to plateau around 100 s, and the traces in e. and g. plateau at 200 s. This suggests that different cells may experience different internal concentrations of d_6-DMSO over the same amount of time.

a.

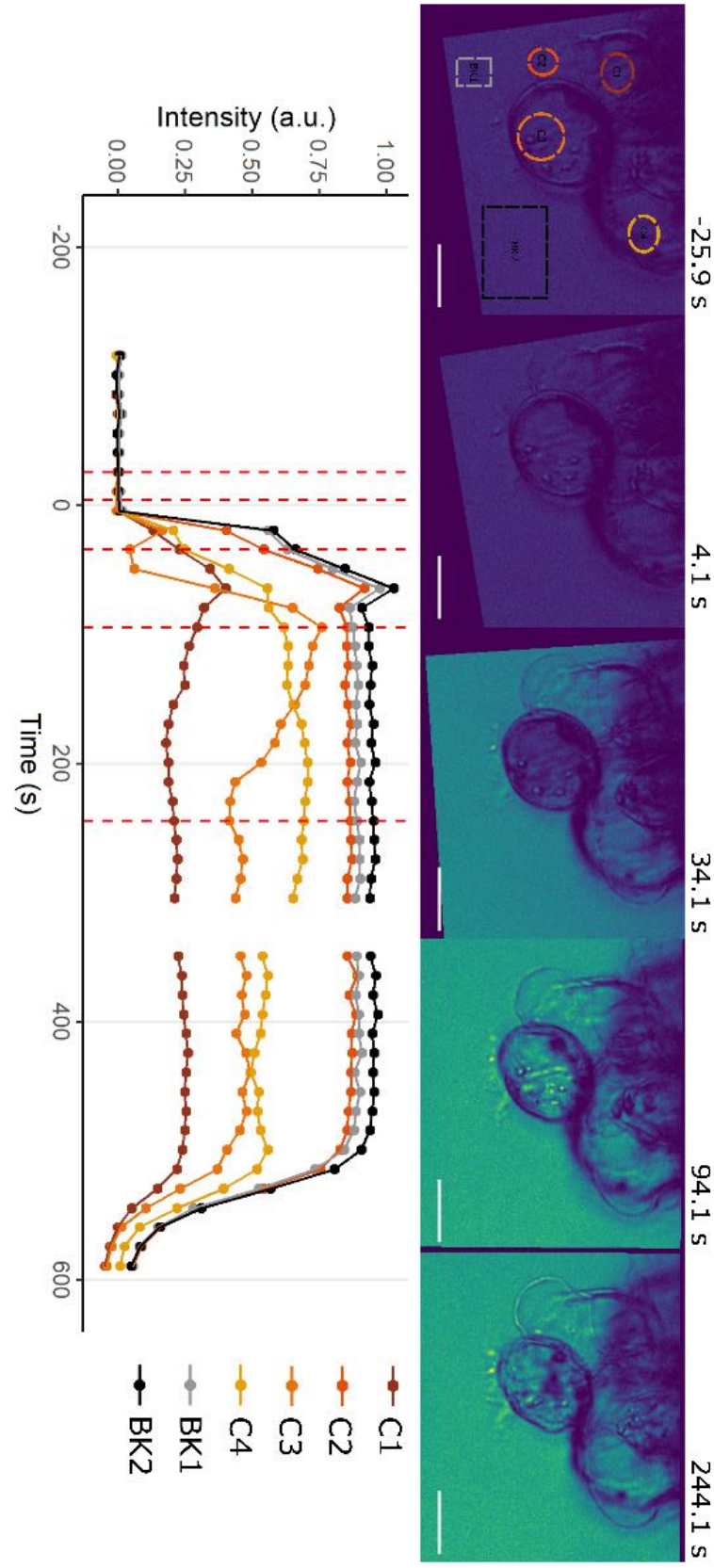
-25.9 s
4.1 s
34.1 s
94.1 s
244.1 s
Intensity (a.u.)
0.00
0.25
0.50
0.75
1.00
-200
0
200
400
600
Time (s)
C1
C2
C3
C4
BK1
BK2

b.

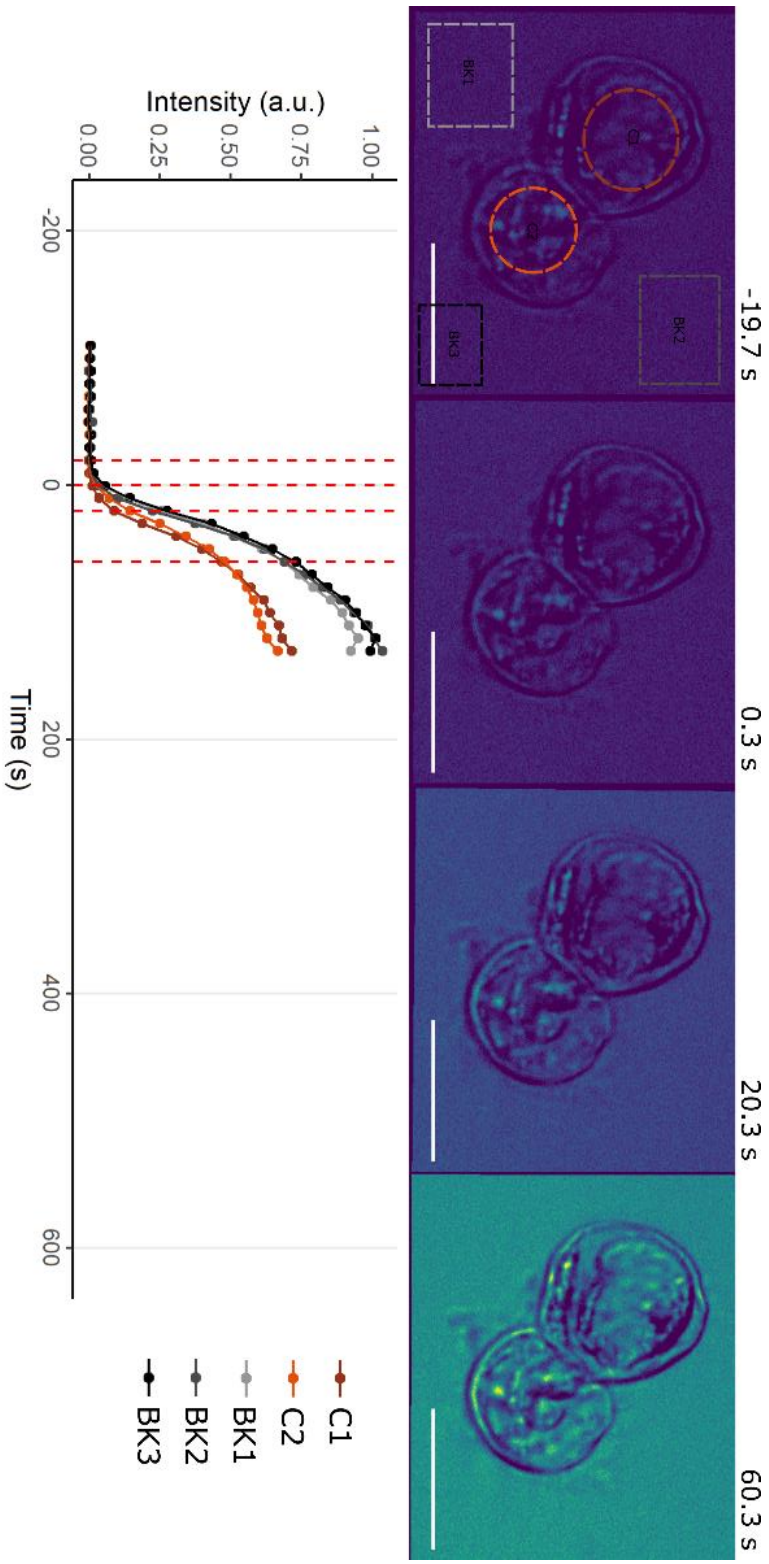
Intensity (a.u.)
0.00
0.25
0.50
0.75
1.00
-200
0
200
400
600
Time (s)
C1
C2
BK1
BK2
BK3
-19.7 s
0.3 s
20.3 s
60.3 s

c.

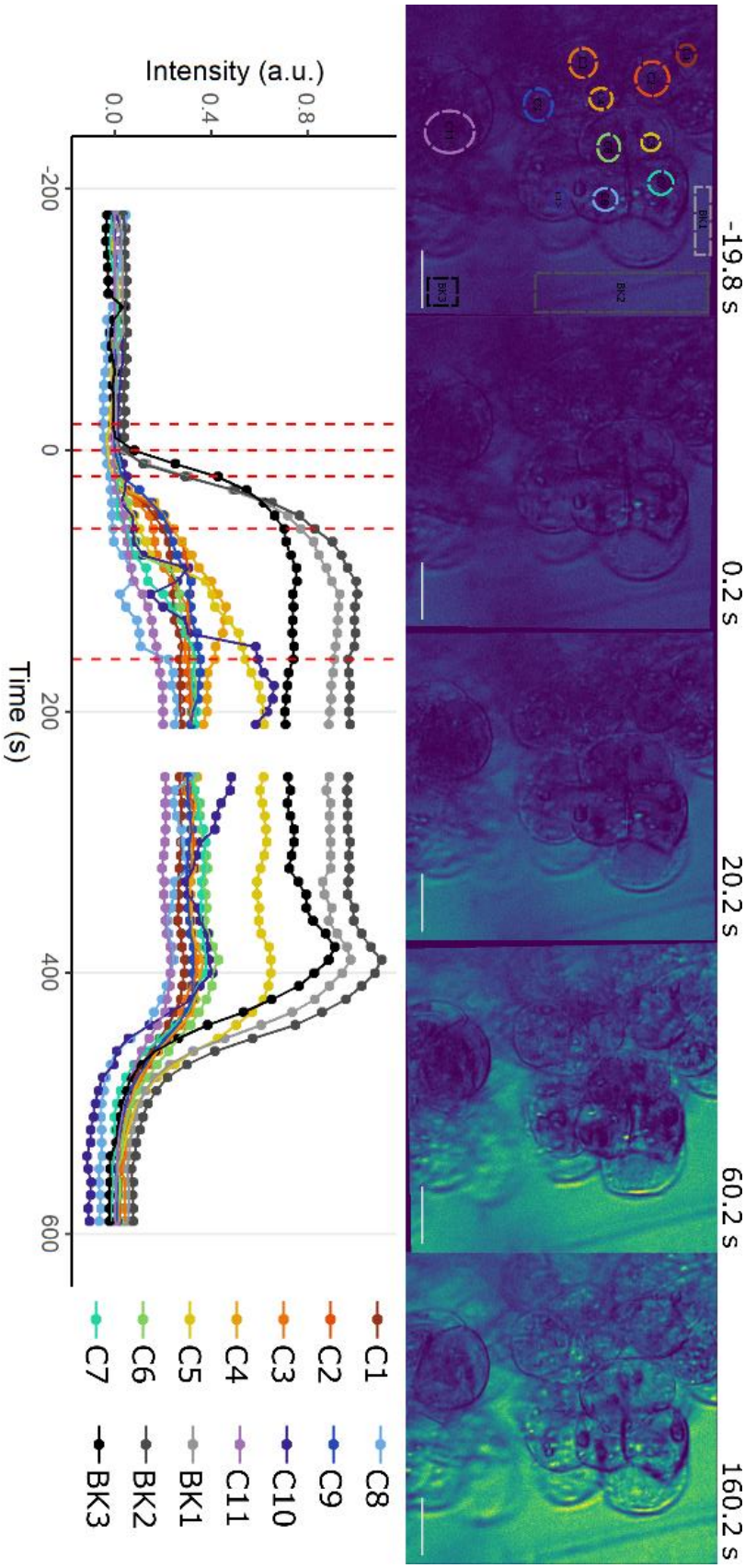
-19.8 s
0.2 s
20.2 s
60.2 s
160.2 s
Intensity (a.u.)
0.0
0.4
0.8
-200
0
200
400
600
Time (s)
C1
C2
C3
C4
C5
C6
C7
C8
C9
C10
C11
BK1
BK2
BK3

d.

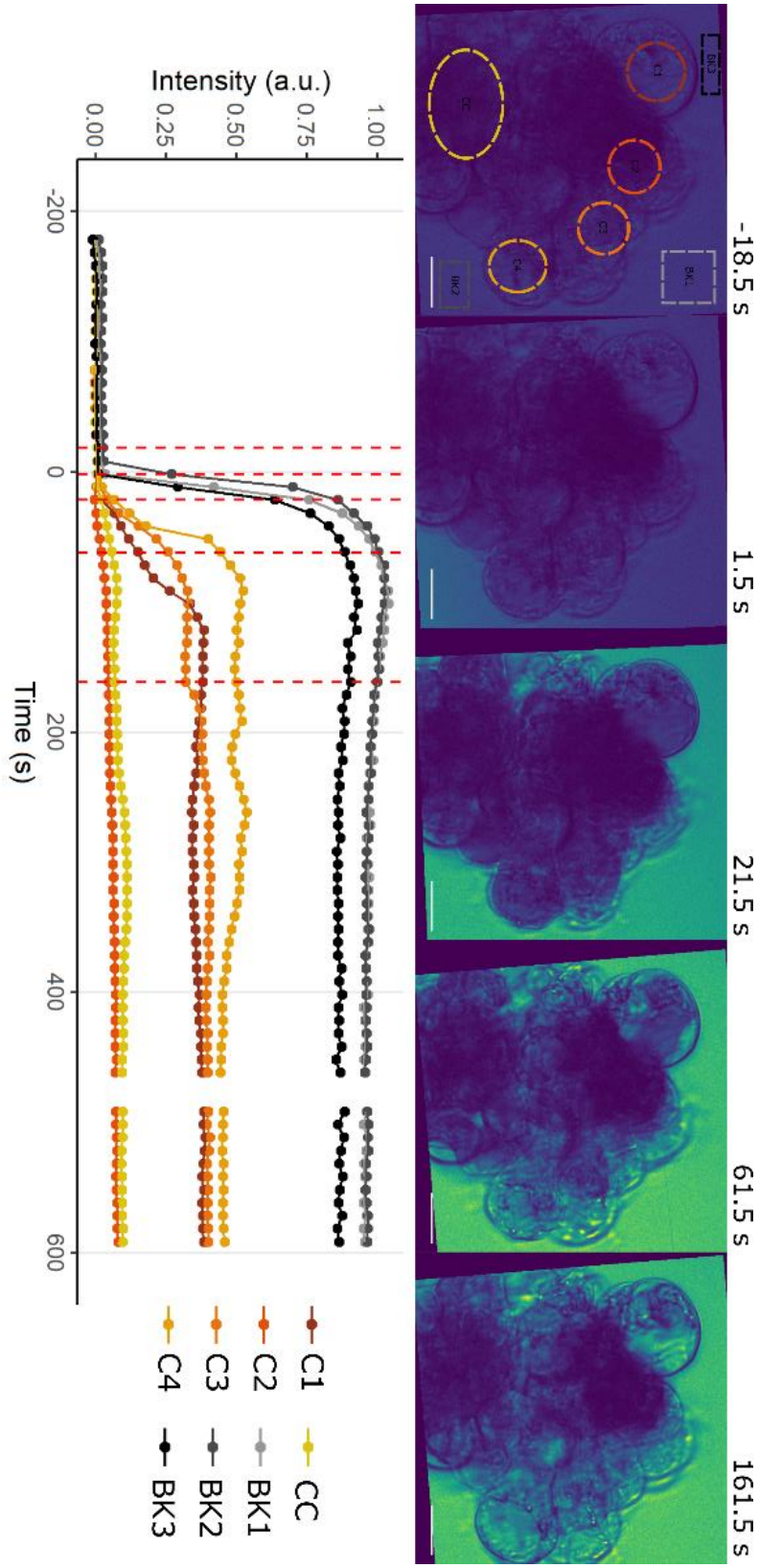
-18.5 s
1.5 s
21.5 s
61.5 s
161.5 s
Intensity (a.u.)
0.00
0.25
0.50
0.75
1.00
-200
0
200
400
600
Time (s)
C1
C2
C3
C4
CC
BK1
BK2
BK3

e.

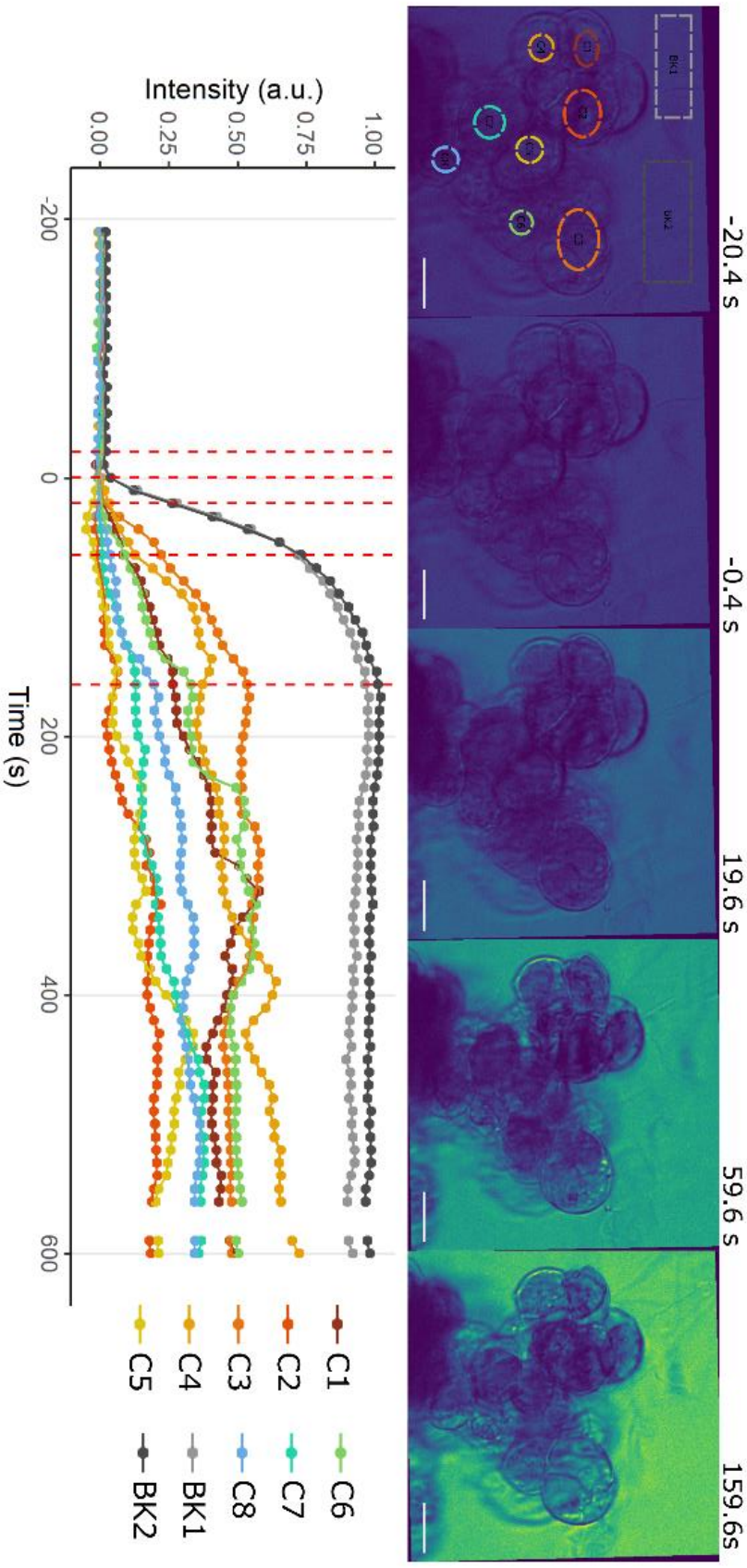
Intensity (a.u.)
0.00
0.25
0.50
0.75
1.00
-200
0
200
400
600
Time (s)
C1
C2
C3
C4
C5
C6
C7
C8
BK1
BK2
-20.4 s
-0.4 s
19.6 s
59.6 s
159.6s

f.

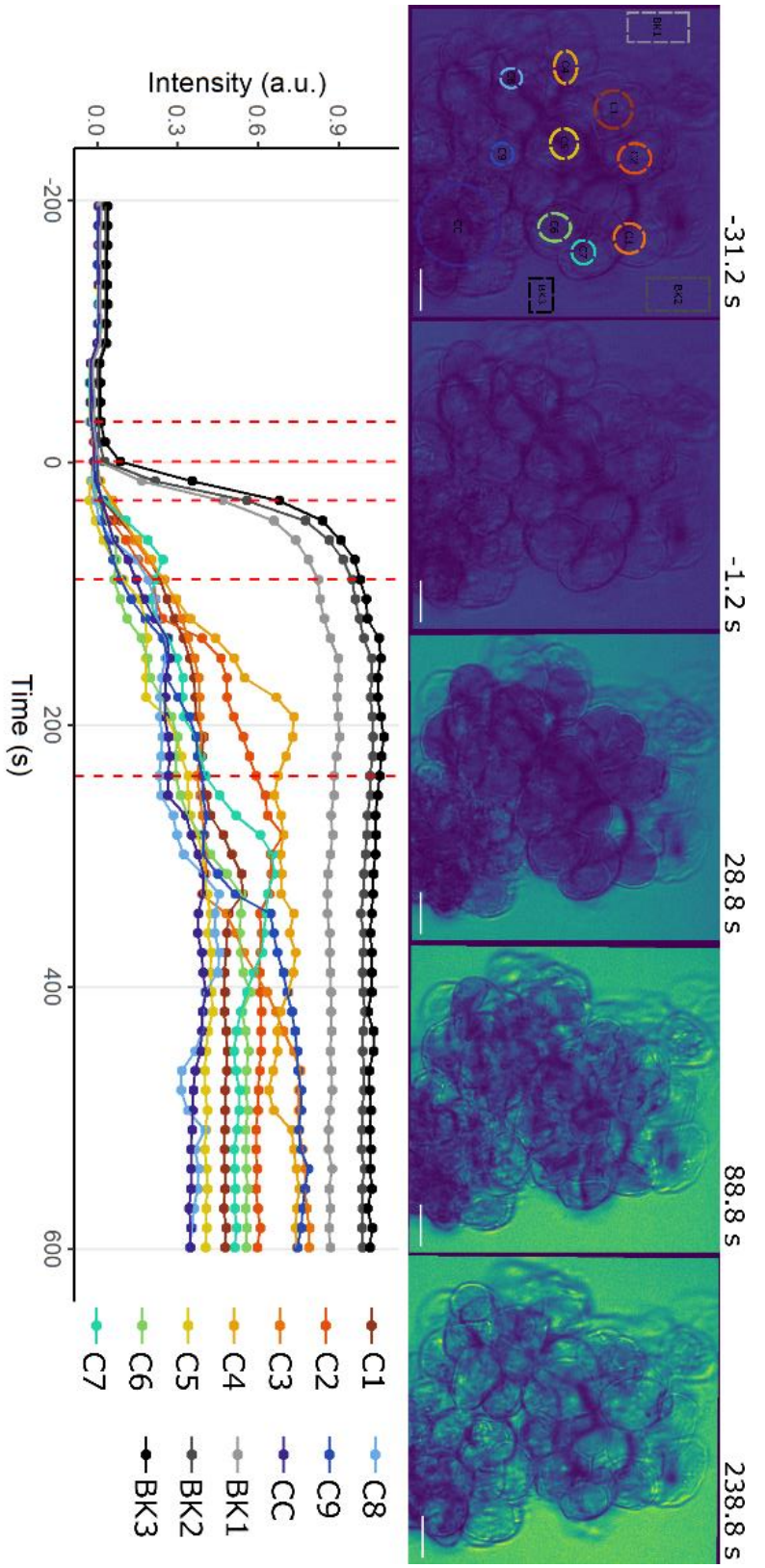

Figure AII.4: Six graphs (a-f) showing the normalized intensity (arbitrary units, a.u.) of d_6-DMSO. Each colored trace corresponds to the hand-selected region of interest shown within a cell. Each

grey-scale trace corresponds to a background ROI outside the cells. All the graphs show d_6-DMSO entering the perfusion chamber. In addition, a and c show both d_6-DMSO entering the perfusion chamber and subsequently being replaced by media within the chamber.

The data presented in Figure AII.5 show cell responses to d_6-ethylene glycol. Overall, the cell responses presented in Figure AII.5 show similar variability to cell responses resulting from exposure to d_6-DMSO, that is, they are also highly variability. Some cells appear to follow a similar shape to the background trace in time (specifically C1 in Figure AII.5 a. and C2s1 in Figure AII.5 c.), others increase in intensity before plateauing, and still others appear to dip before ultimately increasing in intensity and plateauing. Although this kind of dip appeared in the d_6-DMSO traces and was attributed to organelles or other material clumping up inside the cell and blocking (or absorbing) the CARS signal. However, cells exposed to ethylene glycol do not obviously have material inside them that condenses in this way.

a.

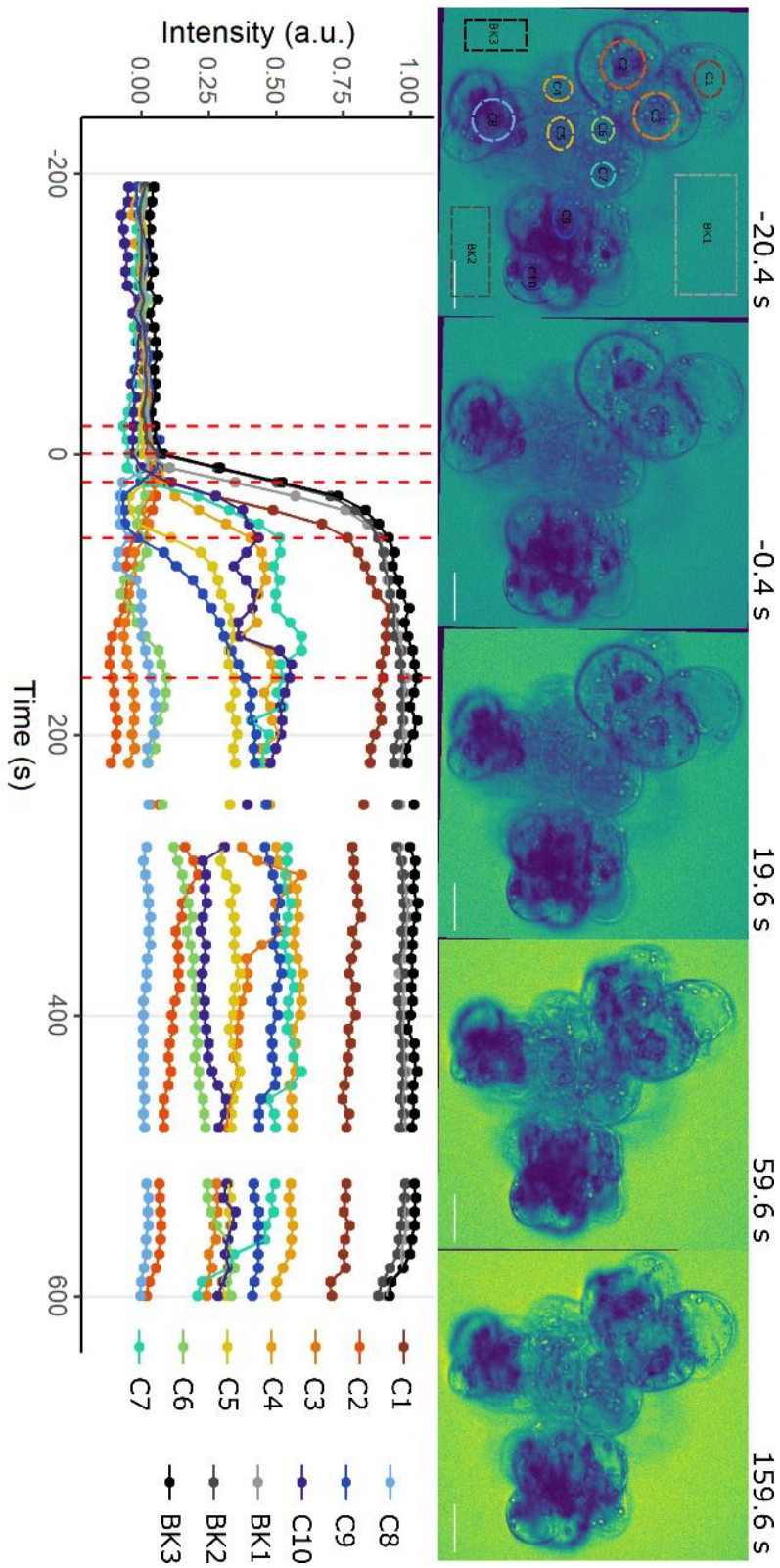
Intensity (a.u.)
0.00
0.25
0.50
0.75
1.00
-200
0
200
400
600
Time (s)
C1
C2
C3
C4
C5
C6
C7
C8
C9
C10
BK1
BK2
BK3
-20.4 s
-0.4 s
19.6 s
59.6 s
159.6 s

b.

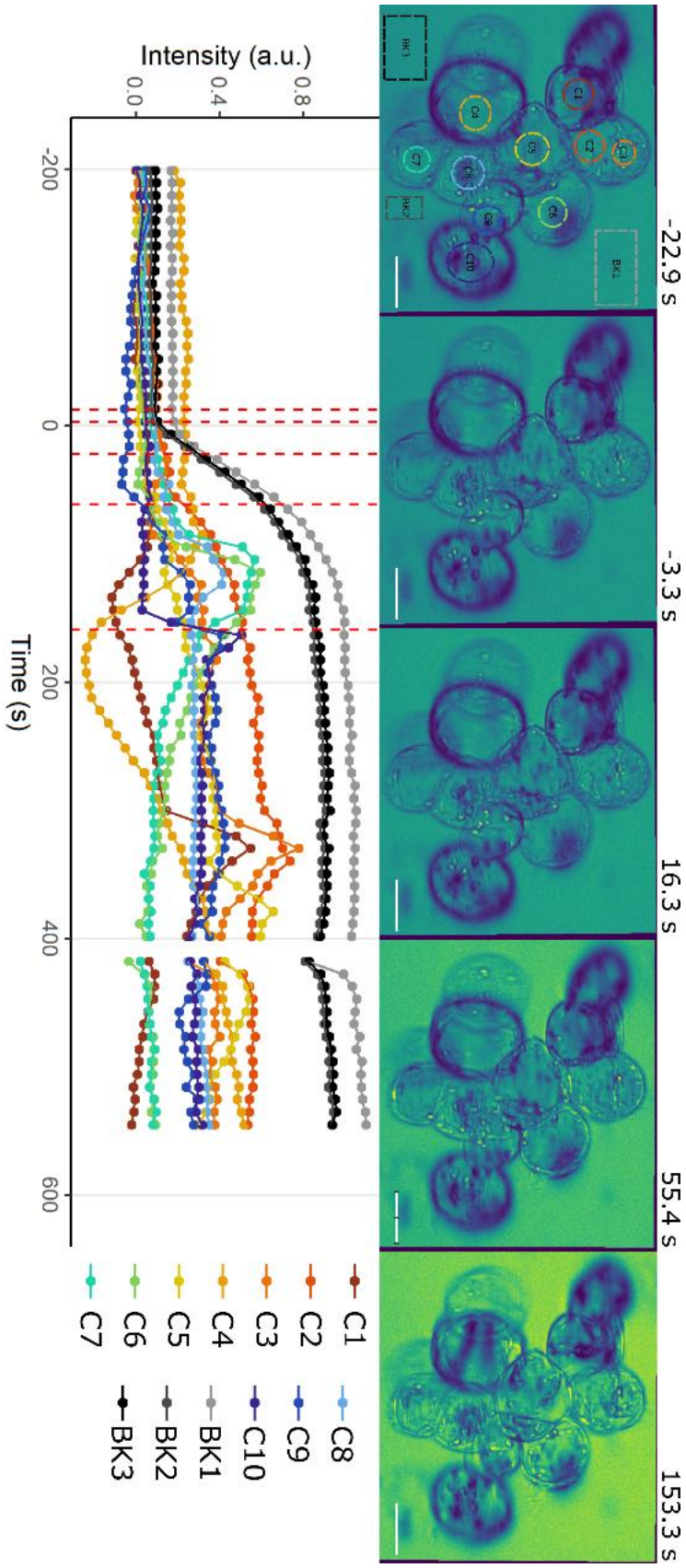
Intensity (a.u.)
0.0
0.4
0.8
-200
0
200
400
600
Time (s)
C1
C2
C3
C4
C5
C6
C7
C8
C9
C10
BK1
BK2
BK3
-22.9 s
-3.3 s
16.3 s
55.4 s
153.3 s

c.

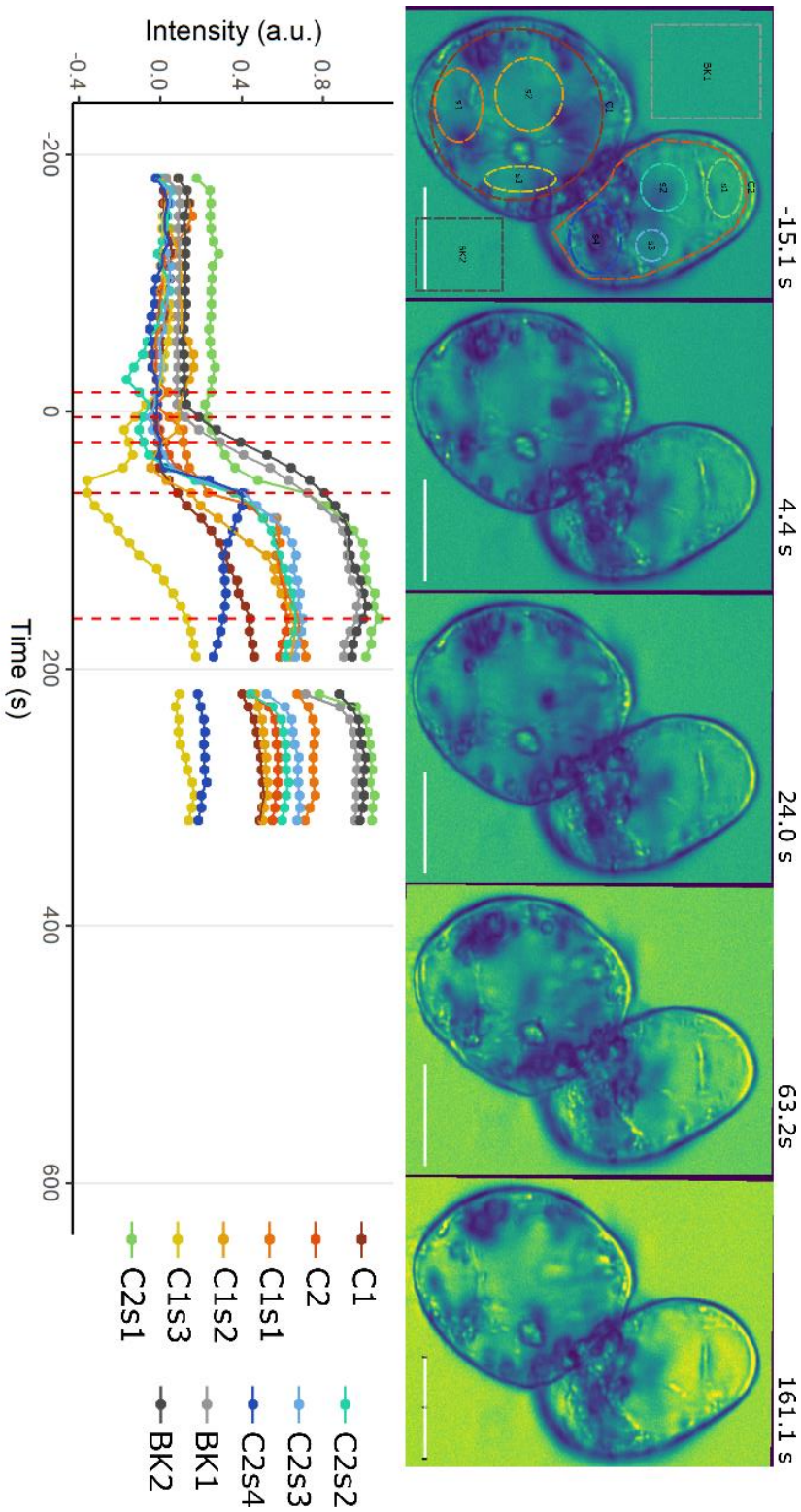

Figure AII.5: Three graphs (a.-c.) showing the normalized intensity of d_6-ethylene glycol. Each colored trace corresponds to a hand-selected region of interest within a cell. Graph c. shows regions of interest that encompass an entire cell (C1, C2) and sub-regions of interest within those cells

(C1s1, C1s2, etc.). Each grey-scale trace corresponds to a background ROI outside the cells. Although the time scale ends 600 seconds after t = 0, some experiments were allowed to run longer. All the graphs show d_6-ethylene glycol entering the perfusion chamber.

The data presented in Figure AII.6 shows cell responses to d_8-glycerol. Generally, all the intensities change in a similar manner to the previously discussed cryoprotectants: increasing then plateauing. Most cells plateau below the highest background intensities. Interestingly, one cell appears to plateau at a higher intensity than the background (Figure AII.6c., C7). Upon further investigation of the CARS images associated with that experiment, it is not clear why the signal within C7 would surpass the signal outside the cell, except perhaps because it started with large organelles blocking more of the initial laser light, making it particularly low in signal. If the organelles subsequently moved out of the ROI when the cell responded to the d_8-glycerol, this could have caused a larger difference in the signal. This would lead the final signal to appear higher than the background signal because normalization of the cell intensity leads it to start at the same point as the background signal. All the other cell traces appear to remain below the background intensity as expected.

a.

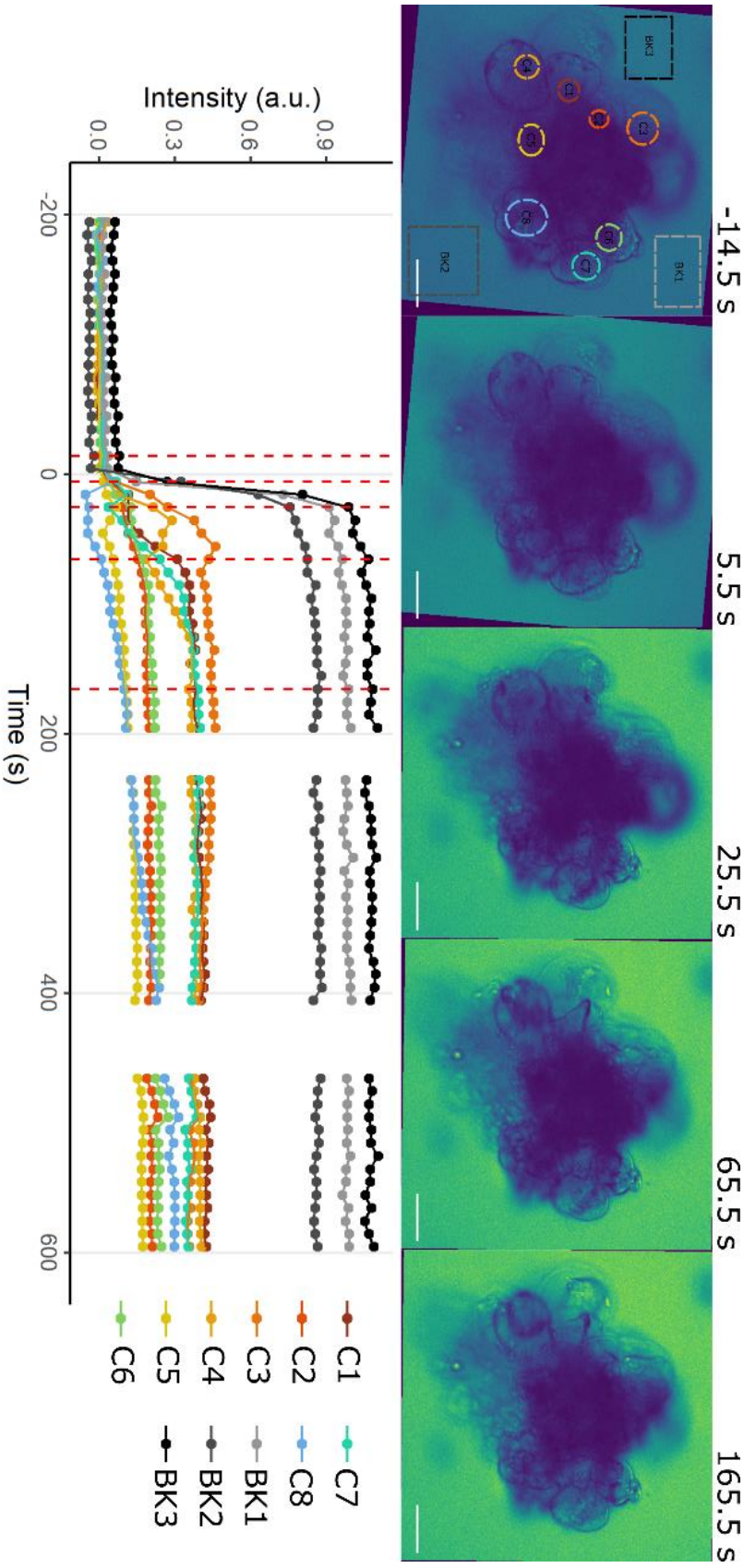
-14.5 s
5.5 s
25.5 s
65.5 s
165.5 s
BK3
BK2
BK1
C1
C2
C3
C4
C5
C6
C7
C8
Intensity (a.u.)
0.0
0.3
0.6
0.9
Time (s)
-200
0
200
400
600
C1
C2
C3
C4
C5
C6
C7
C8
BK1
BK2
BK3

b.

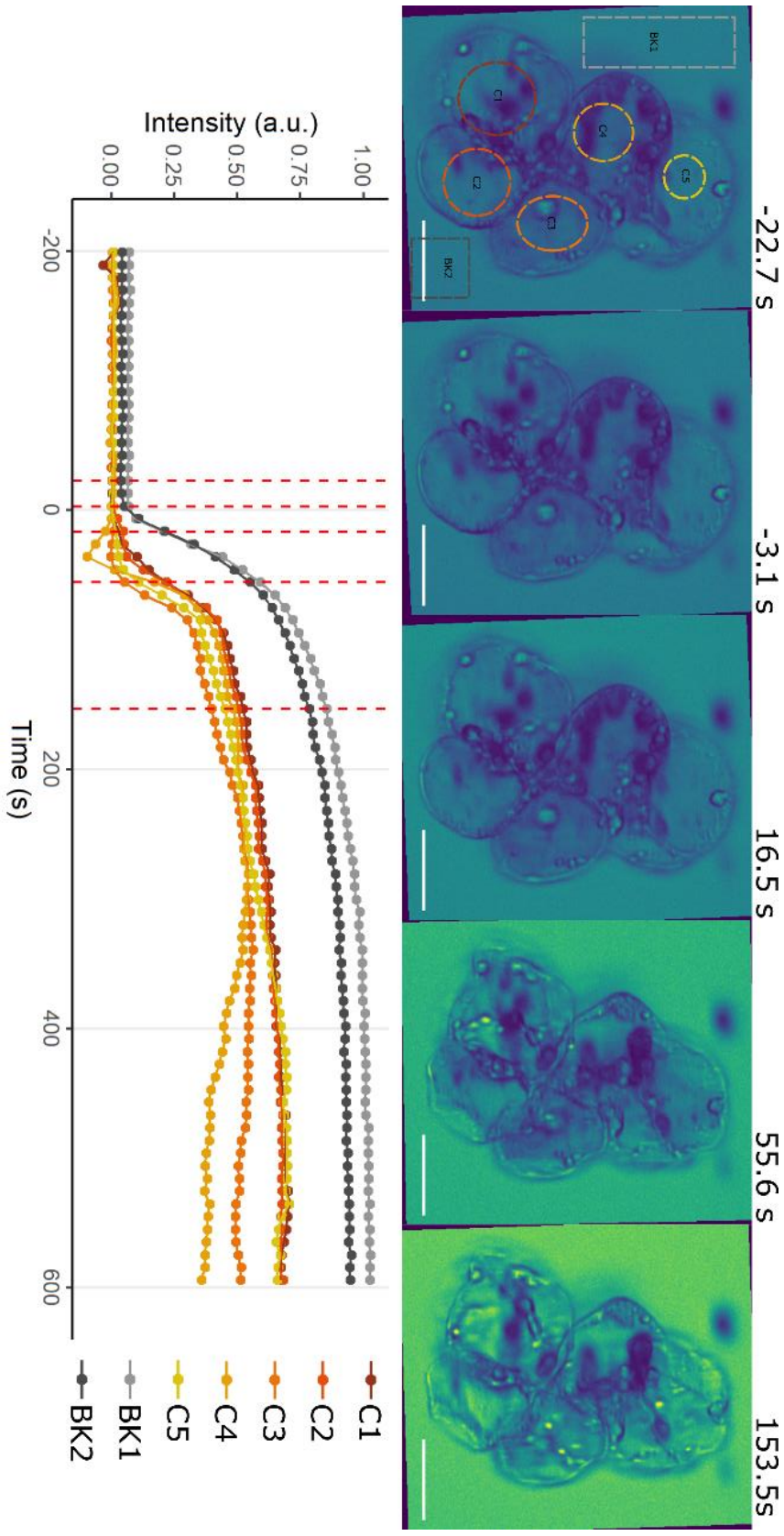
Intensity (a.u.)
0.00
0.25
0.50
0.75
1.00
-200
0
200
400
600
Time (s)
C1
C2
C3
C4
C5
BK1
BK2
-22.7 s
-3.1 s
16.5 s
55.6 s
153.5s

c.

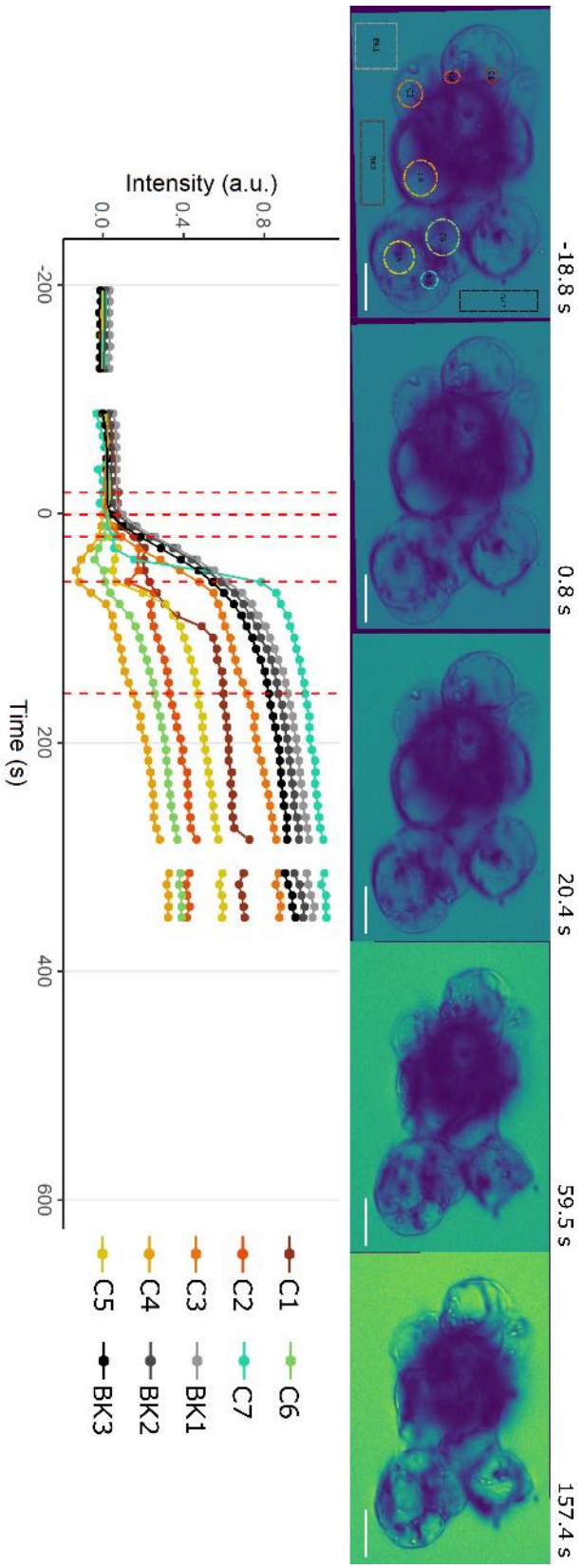

Figure AII.6: Three graphs (a.-c.) showing the normalized intensity of d_8-glycerol. Each colored trace corresponds to a hand-selected region of interest within a cell. Each grey-scale trace

corresponds to a background ROI outside the cells. Although the time scale ends 600 seconds after t = 0, some experiments were allowed to run longer. All the graphs show d_8-glycerol entering the perfusion chamber.

AII.2.4 Statistics Tables

The image acquisition parameters are described for all the presented CARS figures in Table AII.1. The same air objective was used for every acquisition. The target wavenumber is where the target vibration occurs in the spontaneous Raman spectra.

Table AII.1: The image acquisition settings for all the CARS figures presented in this work. The objective used was an air objective. pix = pixel.

Figure	**Objective**	**Image Size (microns)**	**Image Size (pix)**	**Pixel size (pix/micron)**	**Target Wavenumber (cm^{-1})**
Fig 8	20x	133.43x71.78	593x319	4.4444	2121
Fig 9	20x	84.98x76.73	515x465	6.0606	2090
Fig 10	20x	151.38x132.08	596x520	3.9370	2090
S3 a.	20x	123.30x123.30	450x381	3.6496	2121
S3 b.	20x	68.70x57.61	452x379	6.5789	2121
S3 c.	20x	135.04x135.04	640x640	4.7393	2121
S3 d.	20x	154.88x154.88	640x640	4.1322	2121
S3 e.	20x	154.88x154.88	640x640	4.1322	2121
S3 f.	20x	186.40x186.40	800x800	4.2918	2121
S4 a.	20x	162.56x162.56	640x640	3.9370	2090
S4 b.	20x	150.70x134.14	546x486	3.6232	2090
S4 c.	20x	71.45x89.93	433x545	6.0606	2090
S5 a.	20x	162.56x162.56	640x640	3.9370	2090
S5 b.	20x	93.46x107.14	396x454	4.2373	2090
S5 c.	20x	162.84x104.33	590x379	3.6232	2090

Statistics and significance testing

Table AII.2 reports the tabulated statistical values shown in the boxplots in Figure 3.6 in Chapter 3. These values were determined directly from the R program used to create Figure 3.6 whose code is available on GitHub.

Table AII.2: Statistical values for brightfield boxplots (from Figure 3.6 in Chapter 3). This includes the number of cells that experienced each response to each cryoprotectant (n), the

minimum values calculated for each response (Min), the first quartile of each response (First Quartile), the median of each response (Median), the third quartile of each response (Third Quartile), and the maximum of each response (Max). Crump. = crumpling response, Plas.= plasmolysis, deplas. = deplasmolylsis; DMSO = dimethylsulfoxide, EG = ethylene glycol, Glyc = glycerol.

	Crump. DMSO	Plas. DMSO	Deplas. DMSO	Crump. EG	Plas. EG	Deplas. EG	Crump. Glyc	Plas. Glyc	Deplas. Glyc
N	17	28	27	53	59	59	20	80	16
Min	24	12	33	12	15	27	27	21	153
First Quartile	30	40.5	70.5	33	34.5	144	100.5	46.5	283.5
Median	42	49.5	123	90	54	267	166.5	72	513
Third Quartile	78	103.5	312	162	73.5	351	220.5	124.5	634.5
Max	132	129	624	306	132	543	240	222	879

Table AII.3 shows the results from the Dunn test performed on the boxplot data in Figure 3.6 in Chapter 3. The tabulated results show the significance of every comparison, including ones that were not included in Chapter 3.

Table AII.3: Dunn test results for all brightfield data. The groupings are arbitrary and just serve show what data are being compared. The number of cells in each group is given by n1 and n2. The p-value of each comparison is reported as p and the adjusted (Benjamini-Yekutieli adjustment) p-value is p.adj. The level of significance is reported as signif.

Group1	Group2	n1	n2	p	p.adj	signif
resp_DMSO	resp_EG	17	53	0.147	0.788986	ns
resp_DMSO	resp_Glyc	17	20	0.000587	0.005885	**
resp_DMSO	plas_DMSO	17	28	0.634	1	ns
resp_DMSO	plas_EG	17	59	0.965	1	ns
resp_DMSO	plas_Glyc	17	80	0.0696	0.402198	ns
resp_DMSO	deplas_DMSO	17	27	0.000516	0.005885	**
resp_DMSO	deplas_EG	17	59	4.04×10^{-7}	6.07×10^{-6}	****
resp_DMSO	deplas_Glyc	17	16	1.05×10^{-8}	3.96×10^{-7}	****
resp_EG	resp_Glyc	53	20	0.00543	0.0429	*
resp_EG	plas_DMSO	53	28	0.269	1	ns
resp_EG	plas_EG	53	59	0.0383	0.230	ns
resp_EG	plas_Glyc	53	80	0.650	1	ns
resp_EG	deplas_DMSO	53	27	0.00455	0.0380	*
resp_EG	deplas_EG	53	59	1.66×10^{-7}	2.77×10^{-6}	****
resp_EG	deplas_Glyc	53	16	2.55×10^{-8}	7.67×10^{-7}	****

resp_Glyc	plas_DMSO	20	28	0.000744	0.00700	**
resp_Glyc	plas_EG	20	59	$1.45x10^{-5}$	0.000182	***
resp_Glyc	plas_Glyc	20	80	0.00940	0.0642	ns
resp_Glyc	deplas_DMSO	20	27	0.842	1	ns
resp_Glyc	deplas_EG	20	59	0.313	1	ns
resp_Glyc	deplas_Glyc	20	16	0.0104	0.0682	ns
plas_DMSO	plas_EG	28	59	0.558	1	ns
plas_DMSO	plas_Glyc	28	80	0.124	0.688	ns
plas_DMSO	deplas_DMSO	28	27	0.000576	0.00589	**
plas_DMSO	deplas_EG	28	59	$5.34x10^{-8}$	$1.15x10^{-6}$	****
plas_DMSO	deplas_Glyc	28	16	$3.81x10^{-9}$	$1.91x10^{-7}$	****
plas_EG	plas_Glyc	59	80	0.005893	0.044281	*
plas_EG	deplas_DMSO	59	27	$4.76x10^{-6}$	$6.51x10^{-5}$	****
plas_EG	deplas_EG	59	59	$5.91x10^{-14}$	$8.88x10^{-12}$	****
plas_EG	deplas_Glyc	59	16	$2.10x10^{-12}$	$1.58x10^{-10}$	****
plas_Glyc	deplas_DMSO	80	27	0.00798	0.0571	ns
plas_Glyc	deplas_EG	80	59	$1.13x10^{-7}$	$2.13x10^{-6}$	****
plas_Glyc	deplas_Glyc	80	16	$3.63x10^{-8}$	$9.10x10^{-7}$	****
deplas_DMSO	deplas_EG	27	59	0.169	0.875	ns
deplas_DMSO	deplas_Glyc	27	16	0.00362	0.0320	*
deplas_EG	deplas_Glyc	59	16	0.0338	0.212	ns

A tabulation of the data presented as boxplots in Figure 1.1 is shown in Table AII.4.

Table AII.4: Statistical Values for Change Point boxplots (from Figure 1.1 in Chapter 3). This includes the number of cells that experienced each response to each cryoprotectant (n), the minimum values calculated for each response (Min), the first quartile of each response (First Quartile), the median of each response (Median), the third quartile of each response (Third Quartile), and the maximum of each response (Max). Crump. = crumpling response, Plas.= plasmolysis, deplas. = deplasmolylsis; DMSO = dimethylsulfoxide, EG = ethylene glycol, Glyc = glycerol.

	Background DMSO	**Cells DMSO**	**Background EG**	**Cells EG**	**Background Glyc**	**Cells Glyc**
N	19	47	11	36	11	27
Min	-4.3	-12.5	-2.9	-3.8	-4.9	-29
First Quartile	-1.15	4.25	-2	10.15	-2.65	-1.3
Median	0	10.8	-1.6	24.7	-1.1	8.8
Third Quartile	2.15	22.4	2.3	47.7	2.8	21
Maximum	5.7	42.3	4.9	91.4	5.3	50.2

The full results of the Dunn test performed on the CARS change point data are reported in Table AII.5. These show both the significance levels shown in Figure 1.1 as well as those not displayed. For example, the changepoint of the DMSO background was statistically different than the change point of the cells exposed to ethylene glycol. These were not shown in Figure 1.1 because they are not related to each other. However, it is interesting to note that all the background changepoints are not statistically different from each other suggesting that although glycerol had a larger spread than the others, in the end they can be taken as comparable.

Table AII.5: Dunn test results for every CARS box plot. The groupings are arbitrary and just serve show what data are being compared. The number of cells in each group is given by n1 and n2. The p-value of each comparison is reported as p and the adjusted (Benjamini-Yekutieli adjustment) p-value is p.adj. The level of significance is reported as signif.

Group1	Group2	n1	n2	p	p.adj	signif
Background_DMSO	Cells_DMSO	19	47	0.000321	0.00400	**
Background_DMSO	Background_EG	19	11	0.815	1	ns
Background_DMSO	Cells_EG	19	36	2.29×10^{-8}	1.14×10^{-6}	****
Background_DMSO	Background_Glyc	19	11	0.873	1	ns
Background_DMSO	Cells_Glyc	19	27	0.00791	0.0437	*
Cells_DMSO	Background_EG	47	11	0.00145	0.0137	*
Cells_DMSO	Cells_EG	47	36	0.00616	0.0383	*
Cells_DMSO	Background_Glyc	47	11	0.00193	0.0137	*
Cells_DMSO	Cells_Glyc	47	27	0.449	1	ns
Background_EG	Cells_EG	11	36	1.19×10^{-6}	2.97×10^{-5}	****
Background_EG	Background_Glyc	11	11	0.948	1	ns
Background_EG	Cells_Glyc	11	27	0.0135	0.0670	ns
Cells_EG	Background_Glyc	36	11	1.79×10^{-6}	2.97×10^{-5}	****
Cells_EG	Cells_Glyc	36	27	0.00193	0.0137	*
Background_Glyc	Cells_Glyc	11	27	0.0167	0.0757	ns

Table AII.6 is a tabulation of the data presented in Figure AII.2 which shows the response time of cells captured with CARS microscopy.

Table AII.6: Statistical values for CARS boxplots (from Figure AII.2). This includes the number of cells that experienced each response to each cryoprotectant (n), the minimum values calculated for each response (Min), the first quartile of each response (First Quartile), the median of each response (Median), the third quartile of each response (Third Quartile), and the maximum of each

response (Max). Plas.= plasmolysis, deplas. = deplasmolylsis; DMSO = dimethylsulfoxide, EG = ethylene glycol, Glyc = glycerol.

	Plas. DMSO	Deplas. DMSO	Plas. EG	Deplas. EG	Plas. Glyc.	Deplas. Glyc.
n	33	33	20	19	21	4
Min	30	50	50	110	30	170
First Quartile	70	130	88.1	166.4	58.7	215
Median	90	210	107.7	235.0	88.1	405
Third Quartile	120	360	117.5	328.0	107.7	560
Maximum	165	500	156.6	372.0	166.4	570

Table AII.7 shows the results of a Dunn Test comparing the response times of CARS and brightfield data which are shown side-by-side in Figure AII.3.

Table AII.7: Results of a Dunn Test comparing the response times of cells from CARS and brightfield data sets. The groupings are either by CARS data or Brightfield data and show what data are being compared. The number of cells in each group is given by n (CARS) and n (BF), respectively. The p-value of each comparison is reported as p and the adjusted (Benjamini-Yekutieli adjustment) p-value is p.adj. The level of significance from the adjusted p-value is reported as sig.

CARS Data	Brightfield Data	n (CARS)	n (BF)	p	p.adj	sig.
DMSO – plasmolysis	DMSO - plasmolysis	33	28	0.080	0.56	ns
DMSO – deplasmolysis	DMSO – deplasmolysis	33	27	0.081	0.56	ns
Ethylene glycol – plasmolysis	Ethylene glycol – plasmolysis	20	59	0.0016	0.019	*
Ethylene glycol – deplasmolysis	Ethylene glycol – deplasmolysis	19	59	0.57	1.0	ns
Glycerol – plasmolysis	Glycerol – plasmolysis	21	80	0.95	1.0	ns
Glycerol – deplasmolysis	Glycerol – deplasmolysis	4	16	0.77	1.0	ns

AII.3 Original author contributions

Fionna M.D. Samuels: Conceptualization, Methodology, Validation, Formal Analysis, Investigation, Resources, Writing – Original Draft, Writing – Review & Editing; Kylie C. Pearce:

Validation, Formal Analysis, Investigation, Writing – Review & Editing; Stephanie Soderlund: Validation, Formal Analysis, Investigation, Writing – Review & Editing; Dominik G. Stich: Methodology, Resources, Software, Writing – Review & Editing; Remi Bonnart: Methodology, Resources, Writing – Review & Editing; Gayle M. Volk: Conceptualization, Writing – Review & Editing, Funding Acquisition; Nancy E. Levinger: Conceptualization, Writing – Review & Editing, Funding Acquisition, Supervision, Project Administration.

AII.4 Funding

We gratefully acknowledge financial support from USDA NIFA Grant Number 12835363, USDA ARS Non-Assistance Cooperative Agreement 58-3012-9-017. FMDS acknowledges support from the NSF Graduate Research Fellowship Program fellow number 2019273956 (FMDS). Imaging experiments were performed in the Advanced Light Microscopy Core, part of NeuroTechnology Center at University of Colorado Anschutz Medical Campus, supported in part by Rocky Mountain Neurological Disorders Core Grant Number P30 NS048154 and by Diabetes Research Center Grant Number P30 DK116073.

APPENDIX III: Supplementary Text and Figures for "CHAPTER 4: Permeation of deuterated cryoprotectants solubilized in Plant Vitrification Solution 2"

All the data shown in Chapter 4 were collected on the same instrumental set up described in Appendix I.

AIII.1 Supporting Data

AIII.1.2 CARS images and traces

Figure AIII.1 shows other experiments wherein d_6-DMSO was solvated in PVS2 and flowed across live rice cells. Each cell is identifiable by a uniquely colored region of interest (ROI). The change in average intensity within these ROI's over time is plotted below the images. The vertical dashed red lines presented in the intensity plots correspond to the images shown above the plot. In Figure AIII.1A. and B. there are multiple ROIs shown in single cells because the cell cluster moved and I manually moved the ROI such that it remained inside the cell of interest. The PVS2 solution continued to flow for the 200 s shown from each experiment displayed here and the dip in all the ROI intensities seen in Figure AIII.1C is due to a cell mass zipping behind the cluster of interest, blocking the CARS signal from reaching the detector.

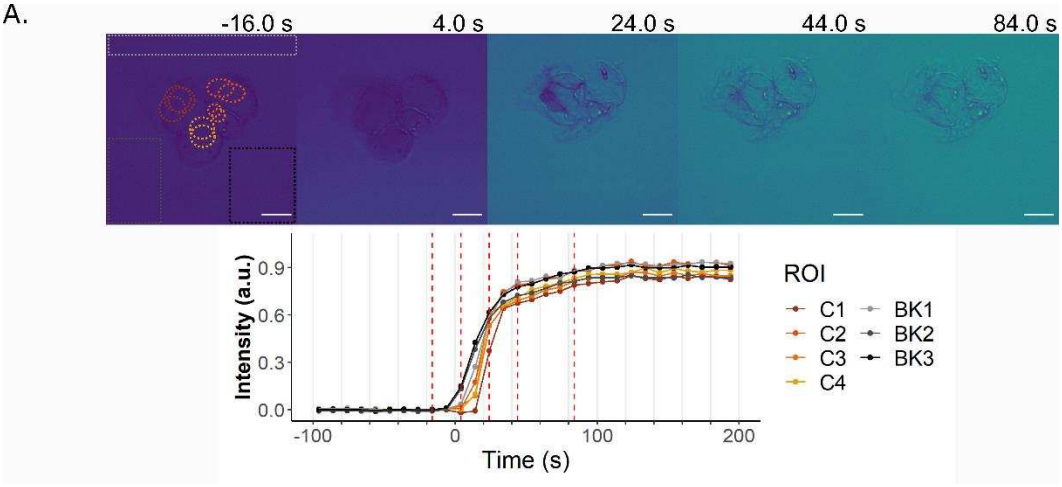

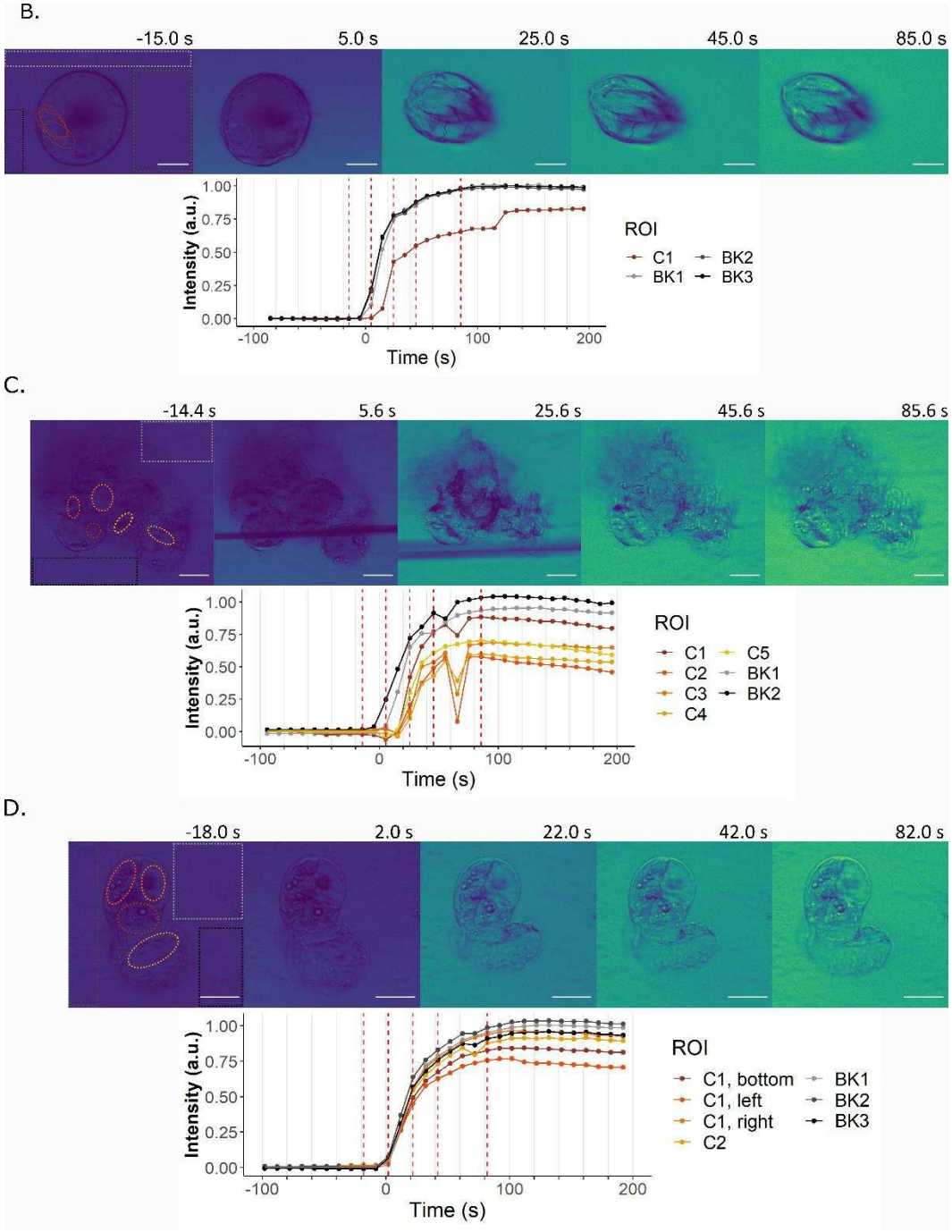

Figure AIII.1: Four graphs (A.-D.) showing the normalized intensity (arbitrary units, a.u.) of d_6-DMSO. Each colored trace corresponds to the hand-selected region of interest shown within a cell. Each grey-scale trace corresponds to a background ROI outside the cells. The multiple ROIs shown in A. and B. correspond to manually moving the ROI to ensure that it stayed within the cell membrane. This is described in more detail in the Materials and Methods section of Chapter 3. All the experiments were allowed to run longer than 200 s but maintained their asymptote. All the graphs show d_6-DMSO entering the perfusion chamber. Scale bar is 25 µm.

Figure AIII.2 shows other experiments wherein d_6-ethylene glycol was solvated in PVS2 and flowed across live rice cells. Like the previous in previous figures showing the change of CARS intensity within cells, the top half of each part of the figure shows images of the cells exposed to the PVS2 solution and the lower half of the figure parts show the change of intensity within select ROIs. In Figure III.2 A., there is another cell cluster behind the cluster of interest. This cluster blocks the CARS signal from reaching the detector and causes C1 and C2 to appear to contain much lower concentrations of d_6-ethylene glycol. However, it is more likely that these cells contain concentrations comparable to the surrounding cells.

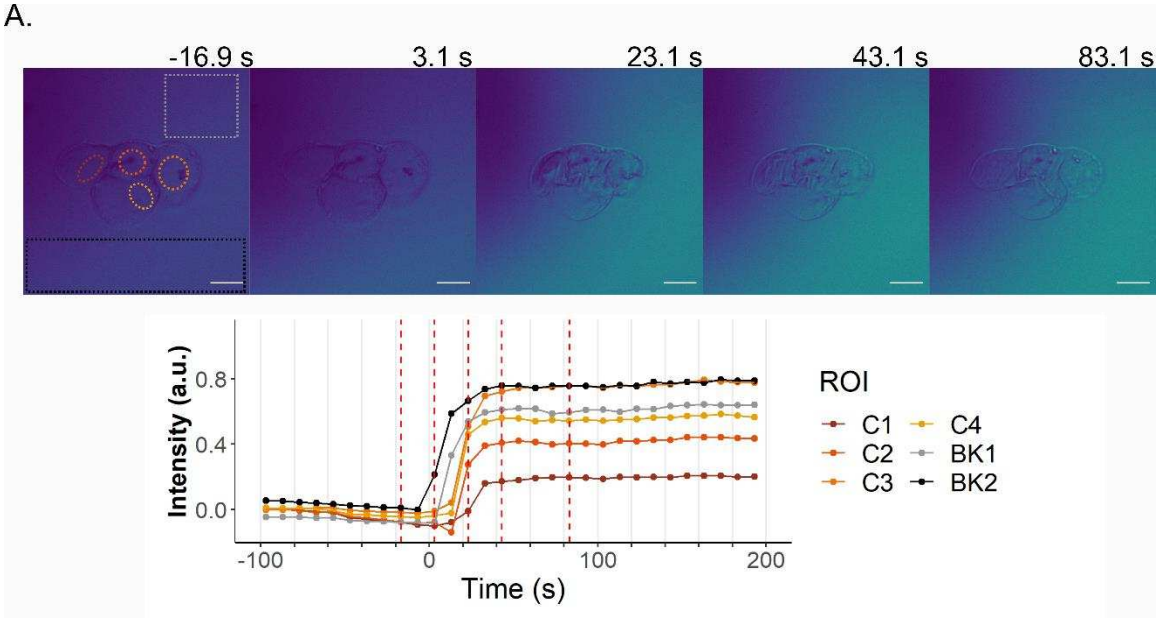

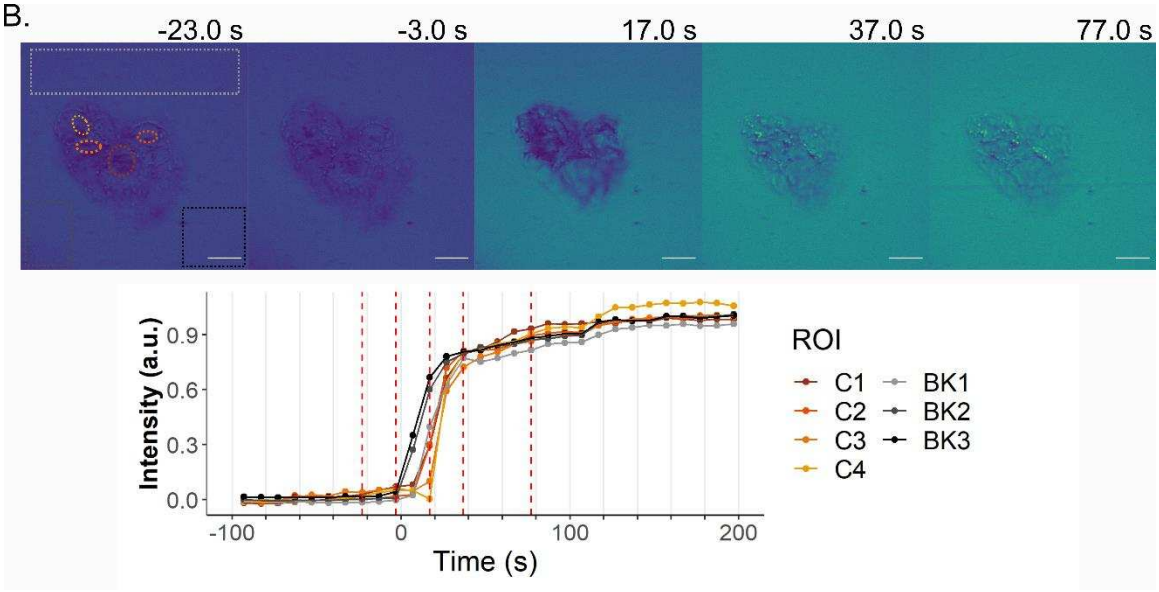

Figure AIII.2: Two graphs showing the normalized intensity of d_6-ethylene glycol. Each colored trace corresponds to a hand-selected region of interest within a cell. Each grey-scale trace corresponds to a background ROI outside the cells. All the experiments were allowed to run longer than 200 s but maintained their asymptote. All the graphs show d_6-ethylene glycol entering the perfusion chamber. Scale bar is 25 µm.

Figure AIII.3 shows additional experiments wherein d_8-glycerol was solvated in PVS2 and flowed across live rice cells. Although it appears as though the CARS intensity within these cells is further away from the background than those shown in Figure 4.1C, the background intensity from each background ROI is slightly different. When taking this into consideration, it appears like all the cells are comparable to the range of the background intensity.

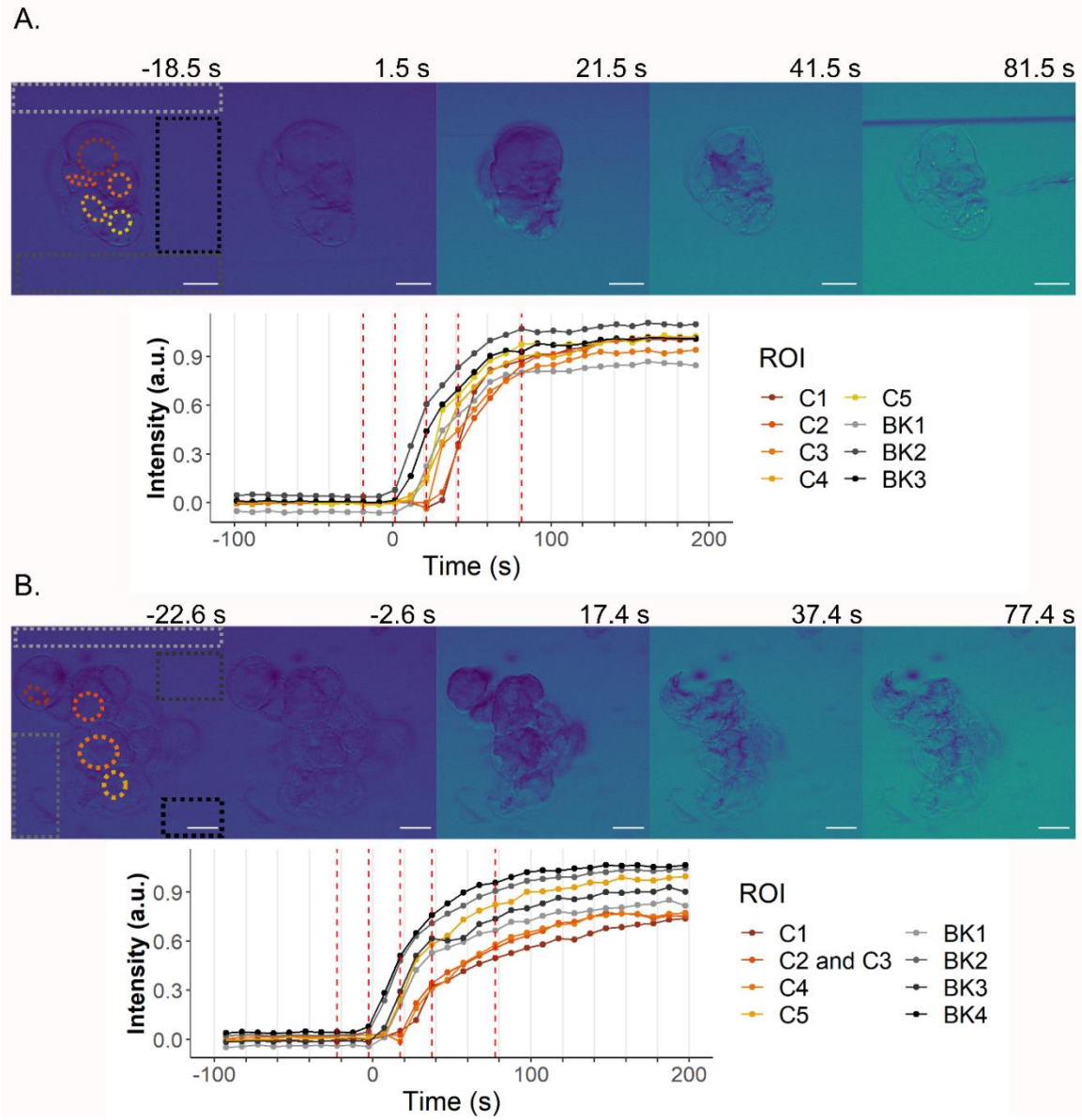

Figure AIII.3: Two graphs showing the normalized intensity of d_8-glycerol. Each colored trace corresponds to a hand-selected region of interest within a cell. Each grey-scale trace corresponds to a background ROI outside the cells. All the experiments were allowed to run longer than 200 s but maintained their asymptote. All the graphs show d_8-glycerol entering the perfusion chamber. Scale bar is 25 µm.

AIII.1.2 Statical tables

Table AIII.1 shows all the Dunn test results from the boxplot data presented in Figure 4.2 including comparisons that are not shown in Figure 4.2. From these comparisons it is clear that the timing of the first changepoint and the timing of the first cell changepoint is not dependent on

which cryoprotectant is deuterated. None of the background changepoints are statistically different from each other, which is to be expected because all the data were manipulated such that the first changepoint was considered to be t = 0s. It is more interesting that none of the first cell changepoints are different as this suggests that every cryoprotectant begins to permeate at approximately the same time. The comparisons that are statistically different between cryoprotectants are not relevant. For example, it does not matter that the first background changepoint for d_6-DMSO experiments is statistically different than the first changepoint of cells exposed to d_6-EG.

Table AIII.1: Dunn test results for all the boxplot data presented Figure 4.2. The grouping numbers are arbitrary and just serve show what data are being compared. The number of cells in each group is given by n1 and n2. The adjusted (Benjamini-Yekutieli adjustment) p-value is p.adj. The level of significance is reported as signif. The statistical comparisons that are presented in Figure AIII.4.2 are bolded.

group1	group2	n1	n2	p.adj	signif
DMSO_bk	**DMSO_cells**	**14**	**20**	**$6.5x10^{-04}$**	*******
DMSO_bk	EG_bk	14	8	1.0	ns
DMSO_bk	EG_cells	14	12	$6.5x10^{-04}$	***
DMSO_bk	glyc_bk	14	10	1.0	ns
DMSO_bk	glyc_cells	14	13	$8.4x10^{-06}$	****
DMSO_cells	EG_bk	20	8	0.0080	**
DMSO_cells	EG_cells	20	12	1.0	ns
DMSO_cells	glyc_bk	20	10	0.025	*
DMSO_cells	glyc_cells	20	13	0.41	ns
EG_bk	**EG_cells**	**8**	**12**	**0.0063**	******
EG_bk	glyc_bk	8	10	1.0	ns
EG_bk	glyc_cells	8	13	$2.6x10^{-04}$	***
EG_cells	glyc_bk	12	10	0.018	*
EG_cells	glyc_cells	12	13	1.0	ns
glyc_bk	**glyc_cells**	**10**	**13**	**$6.5x10^{-04}$**	*******

Table AIII.2 shows the Dunn test for the data presented in Figure 4.3.

Table AIII.2: Dunn test results for all the boxplot data presented Figure 4.3. The grouping numbers are arbitrary and just serve show what data are being compared. The number of cells in

each group is given by n1 and n2. The adjusted (Benjamini-Yekutieli adjustment) p-value is p.adj. The level of significance is reported as signif. The statistical comparisons that are presented in Figure AIII.4.2 are bolded.

group1	**group2**	**n1**	**n2**	**statistic**	**p.adj**	**signif**
a.respPVS2	b.stPVS2	7	71	-0.307	1	ns
a.respPVS2	c.ccPVS2	7	59	3.75	$6.5x10^{-04}$	***
a.respPVS2	d.cxPVS2	7	18	4.23	$1.1\ x10^{-04}$	***
b.stPVS2	c.ccPVS2	71	59	9.20	$5.4x10^{-19}$	****
b.stPVS2	d.cxPVS2	71	18	7.61	$2.1x10^{-13}$	****
c.ccPVS2	d.cxPVS2	59	18	1.44	0.44	ns

Table AIII.3 shows the image acquisition settings for all the CARS figures presented in chapter 4 and this appendix. The target frequency based on what molecule was being excited.

Table AIII.3: The image acquisition settings for all the CARS figures presented in chapter 4. The objective used was an air objective. pix = pixel.

Figure	**Objective**	**Image Size (pixels)**	**Pixels/Micron**	**Target Frequency (cm^{-1})**
Fig 1A	20x	508x486	3.1	2121
Fig 1B	20x	640x640	3.7	2090
Fig 1C	20x	640x640	4.5	2090
S1 A	20x	640x640	4.0	2121
S1 B	20x	611x402	4.0	2121
S1 C	20x	559x503	3.6	2121
S1 D	20x	516x487	4.6	2121
S2 A	20x	640x640	3.7	2090
S2 B	20x	640x640	3.8	2090
S3 A	20x	640x640	4.2	2090
S3 B	20x	640x640	3.7	2090

AIII.1.3 Attempts at calibration plots

Figure AIII.4 shows examples of calibration plots that were collected in an attempt to quantify the concentration of each deuterated cryoprotectant based on CARS intensity. Although the plots follow the expected quadratic relationship, with R^2 values close to 1, it is clear that it is impossible to assume that images will have same intensity for the same cryoprotectant

concentration between experiments. A logical step would be to use the calibration that corresponds to each individual experiment. However, the focal plane is inherently different between the calibration set up and the experimental set up because different slides are used in each case. Calibrations were preformed on simple coverslips while flow experiments were preformed with ibidi cells that have both more bulk and a transparent plastic top that the laser and CARS signal must go through to reach the detector. Finally, there are times during flow experiments that move behind the cluster of interest and lower the apparent concentration within the cell cluster. It would be incorrect to assume that this lower intensity signaled a lower concentration. For these reasons, the collected calibrations shown below were not used to quantify the concentration of cryoprotectants within cells. Taking a qualitative approach allows us to account for the variability between experiments.

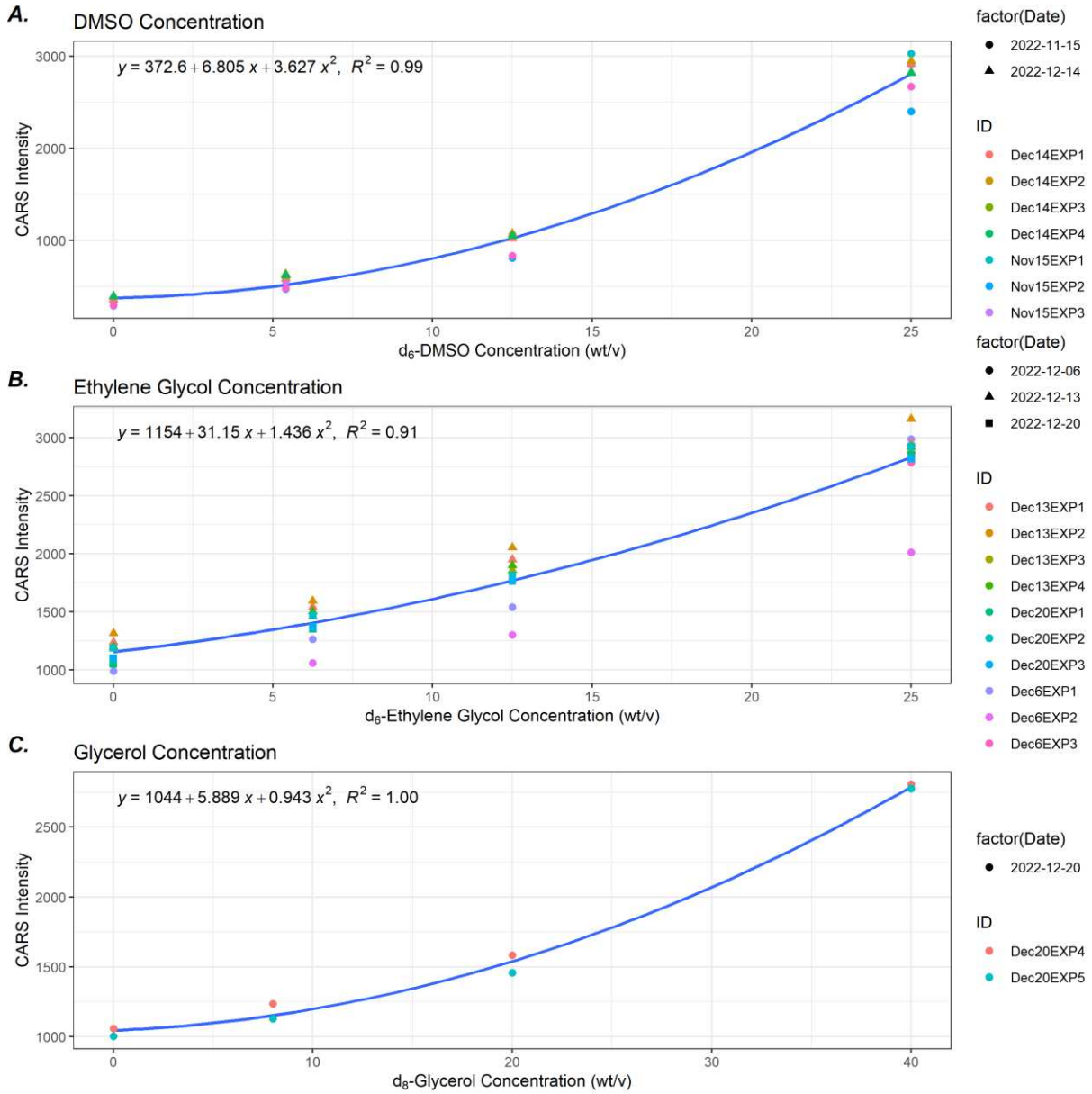

Figure AIII.4: Example calibration plots generated from data collected prior to each experiment. The shape of the points indicates the data the data were collected while the color indicates which experiment the data were collected before. The equation and R^2 value for each fitted line is presented in the top left corner of each graph.

APPENDIX IV: Homebuilt functions for data analysis presented in chapter 3 and chapter 4

There were three main sections of codes used to analyze the data presented in chapter 3. The first analyzed the brightfield data. We were interested in making a model to determine the likelihood of each response occurring after exposure to specific cryoprotectants. With the help of Michael L. Creutzinger from the Franklin A. Graybill Statistics and Data Science Laboratory at Colorado State University (RRID: SCR_022005), a generalized linear model was chosen because the data are effectively binary–either a response does or does not happen.

The second two sections were used to analyze the CARS data. First, the data had to be prepared and run through a changepoint analysis. This allowed us to follow-up by generating boxplots that illustrated how quickly the first changepoint occurred. This was attributed to the first time the intensity inside the cell increased, which we assumed was when the cryoprotectant began permeating the cell. These two sections were repeated for the data presented in chapter 4.

While the raw code is available on the Levinger Lab Github, here are my home-built functions used to analyze data presented in both chapter 3 and chapter 4.

```
#Homemade functions

# Function to subtract the min and max of the background data from cell data
norm_to_BK <- function(x, cell_data, BK_min, BK_max) {
  (cell_data[[x]] - BK_min[[x]]) / (BK_max[[x]] - BK_min[[x]])
}

#Segmented fit function
# Function to fit segmented linear pieces.
BPsegment <- function(DF, pred) {

  par(mar=c(1,1,1,1))
  plot.new()
  sigfit <- list()
  fitList <- list()

  x <- DF$Time # The data frame has to contain Time as a column
  DF <- DF %>% dplyr::select(-contains("Time")) # remove the Time column from
```

```
the data before looping
  par(mfrow=c(ncol(DF),2))
  for (i in 1:ncol(DF)) {
    y <- DF[i]
    y <- unlist(y)
    #fit simple linear regression model
    fit <-lm(y ~ x)
    #fit piece wise regression model to original model, estimating one or
multiple breakpoints
    segmented.fit <- segmented(fit, seg.Z = ~x, psi = pred)
    fitList[[i]] <- segmented.fit
    summary_BP <- summary(segmented.fit)
    Estimates <- as.data.frame(summary_BP$psi)
    sigfit[[i]] <- (Estimates$Est.)

    plot(x, y, pch=16, col='steelblue')
    plot(segmented.fit, add=T)
    plot(resid(segmented.fit))
  }

  sigfit <- as.data.frame(do.call(rbind, sigfit))
  colnames(sigfit) <- NULL
  sigfit <- t(sigfit)
  colnames(sigfit) <- colnames(DF)
  sigfit <- as.data.frame((sigfit))

}

#Need to find the difference between the average of the cell intensities
before t = 0 and the background intensities. The assumption is that the
background is a higher intensity than the cells.
bump_up <- function(x, cells, bk) {
  # x is the list of original cell data you want to modify
  # cells is the list of average of the cell data before t = 0
  # bk is the list of  average of all the bk ROIs before t = 0
  difflist <- list()
  bumped <- list()

  for (i in names(cells)) {
    diff <- cells[[i]] - bk[[i]] #find the difference between the background
average and the cell average
    difflist[[i]] <- abs(diff) #absolute value of that difference
  }

  for (i in names(difflist)) {
    for (j in 1:ncol(x[[i]])) {
      bumped[[i]][j] <- x[[i]][,j] + difflist[[i]][j]}
    #add the difference to the original cell data

  }
```

```
  for (i in names(x)) {
    names(bumped[[i]]) <- names(x[[i]])
    #add in the names so everything matches
  }

  bumped
}

#to solve for x, we use the standard for solving a quadratic equation, only
the positive version because we should not have negative concentrations.
#intensity = b2*(concentration)^2 + b1*(concentration) + b0
#b0 = c; b1 = b; b2 = a
# conc = [(-1*b1)+sqrt((b1^2)-(4*b2*(b0-Intensity))]/(2*b2)
#from https://terpconnect.umd.edu/~toh/models/CalibrationCurve.html and
https://www.wolframalpha.com/input?i=solve+for+x+where+y+%3D+a*x%5E2+%2B+b*x+
%2Bc

Intensity_to_Conc <- function(x, b0, b1, b2) {
  ((-1*b1)+sqrt((b1^2)-(4*b2*(b0-x))))/(2*b2)
}

# Need to write a function that finds the quadratic coefficients for every
data set
# This R function spits out a table with the columns labelled from the ID
variable you use.
# based on the function y = a*x^2 + b*x + c, row 1 = c, row 2 = b, and row 3
= a

quad_coeff <- function(calibration) {

  #adding in a column of square concentrations
  calibration$Concentration2 <- calibration$Concentration^2

  #splitting dataframe so it's only the ID, Mean, Concentration and
Concentration2
  new_df <- subset(calibration, select = c("ID", "Mean", "Concentration",
"Concentration2"))

  #split calibration into a list based off of the ID variable
  cal_list <- split(new_df, f = new_df$ID)
  quadfit <- list()
  sigfit <- list()
  plot.new()

    for (i in 1:length(cal_list)) {
    df <- as.data.frame(cal_list[[i]])

    #fit simple quadratic regression model
    fit <-lm(Mean ~ Concentration + Concentration2, data = df)
```

```
    quadfit[[i]] <- fit
    summary_Quad <- summary(fit)

    Estimates <- as.data.frame(summary_Quad$coefficients)
    sigfit[[i]] <- (Estimates$Estimate)


    #plot(x, y, pch=16, col='steelblue')
    #plot(segmented.fit, add=T)

    #plot(resid(segmented.fit))
  }

  sigfit <- as.data.frame(do.call(rbind, sigfit))
  colnames(sigfit) <- NULL
  sigfit <- t(sigfit)
  colnames(sigfit) <- names(cal_list)
  rownames(sigfit) <- c("c", "b", "a")

  sigfit <- as.data.frame((sigfit))

}

#Use the following function to import a file that has multiple sheets. Each
Sheet should be one experiment
#importing data
read_allsheets_excel <- function(filename, tibble = TRUE) {
  sheets <- readxl::excel_sheets(filename)
  x <- lapply(sheets, function(X) readxl::read_excel(filename, sheet = X))
  if(!tibble) x <- lapply(x, as.data.frame)
  names(x) <- sheets
  x
}

#Function to shift data to a set t = 0. CPA is the list of times from each
experiment. xmid is a list that contains the value you wish to shift by. In
this case, that will be the change point.
TimeShift <- function(x, CPA, xmid) {
  (CPA[[x]]["Time"] - xmid[[x]])
}

#Write a function that allows me to convert everything to concentration based
on the coeff data frames
conc_convert <- function(x, coeff){
  # x is the list of intensties you want to convert
  # coeff is the list of coeffients you want to use to convert it
  # the coeff list should have the same names in the same order as the x list
  # coeff is also assumed to be in the order c, b, a (based on the normal
quadratic equation)
```

```
  # if a NaN is produced, that means that the root is imaginary. We assume
that this means the value is below the calibration curve and we can safely
assume that the concentration is 0%
  converted <- list()

  for (i in names(coeff)) {
    #b0 = c; b1 = b; b2 = a
    b0 <- coeff[[i]][1]
    b1 <- coeff[[i]][2]
    b2 <- coeff[[i]][3]

    for (j in 1:ncol(x[[i]])) {
      #This takes the values pulled from coeff and finds the conc of each
column in a list
      converted[[i]][j] <- ((-1*b1)+sqrt(((b1^2)-(4*b2*(b0-
x[[i]][,j])))))/(2*b2)

    }
    #put back in the original names
    names(converted[[i]]) <- names(x[[i]])
  }
  #output the new list
  converted
}
```

APPENDIX V: Growing and maintaining *Orzya sativa* (Asian rice) cell cultures

Note: This is the basic procedure I used to maintain the cells for all cell experiments described in chapterS 2, 3 and 4.

Safety Statement

Always use proper PPE when following these instructions or anytime in your life. The plant cells we use pose no threat to humans nor plants as they are non-infected rice callus cells, but if any cells or media come in contact with skin wash well with soap and water. Do not ingest anything mentioned here; if ingestion occurs contact a medical doctor. If anything comes in contact with your eyes, use an eye wash immediately and contact a medical doctor for further instruction. Glassware that comes out of the autoclave may be >100 °C and cause burns if not properly handled with a heat glove. If burned by glass, run under cold water and contact medical doctor if you suffered a severe burn. See safety data sheets of listed chemicals for more specifics on those hazards.

Background

We used rice callus cells (*Orzya sativa*) for all cryopreservation experiments. Callus cells are created from injuring a plant which causes de-differentiation of the cells allowing them to be cultured.[70] These callus cells were frozen in the 1980s, as explained by Finkle and Ulrich.[47] They were thawed in 2018 by Gayle Volk and Remi Bonnart at the USDA National Laboratory for Genetic Resource Preservation (Fort Collins, CO, USA). The cells that we have are the A7 mutation. This labelling system doesn't appear anywhere in the literature about these cells, so it's hard to say the exact mutation in this strain.

This document describes the methods we use to propagate the rice callus cells, including preparing cells in suspension and on plates. For both suspension and plated cells, use the following media recipe, taking care to add agar only when making solid media plates:

Media

Ingredients

1/2X Murashige & Skoog (MS) macro elements*

1X MS Microelements and vitamins*

*rather than using two separate things, I purchased HiMedia MS PT046 which has this same formulation (1/2X macro, 1X micro) but in one bottle. Follow the bottle instructions for the amount of MS powder to add to the media solution you are making.

146 mg/L L-Glutamine

1 mg/L 2,4-dichlorophenoxyacetic Acid (2,4-D)

1 mg/L Indoleacetic Acid (IAA)

1 mg/L Kinetin

30 g/L Sucrose

7 g/L Agar **(omitted for suspension cultures)**

pH 5.7 after autoclaving, pH 6.5 before autoclaving

Directions

Using the above recipe, you can make as much media as you need by multiplying the amount of each component by the volume of media you are trying to make. For the MS salts, the appropriate amount to use will be printed on the chemical bottle(s).

1. Add all the dry chemicals in appropriate amounts to a volumetric flask that corresponds to how much media you are making.

2. Fill volumetric flask to mark with distilled water.
3. Take volumetric flask from wet chemistry lab to the cell culture facility (CCF) using appropriate secondary containment.
4. In CCF, collect autoclave safe bottles, and fill appropriate number of bottles with the prepared media. Autoclave bottles should be filled such that there is room for the liquid to boil without spilling out of the bottle – only fill to the highest volume mark.
5. Cap the autoclave bottles so that they are NOT fully closed. Gas should be able to escape from the bottle.
6. Place a piece of autoclave tape across the cap of the bottle.
7. Place bottles in a metal tray such that they are not touching and place the metal tray in the autoclave in the CCF. If you are making large amounts of media, you may have to use the departmental autoclave which has its own instructions elsewhere.
8. Program autoclave for a liquid run. Both autoclaves are useable, use the autoclave's manual to determine how to use whichever one you choose to use. The liquid program takes about 2 hours to complete and cool to a point where the bottles can be handled with a heat glove.
9. After the program finishes, and the autoclave bottles are cool enough to handle, remove them from the autoclave.
10. **Suspension Media** can be immediately placed in the refrigerator. If you are splitting cells on the same day as making media, allow the media to cool to at least room temperature before using on the cells.
11. **Solid Media** needs to be poured into petri dishes (plates) before it cools. Pour the plates in the biosafety cabinet, using appropriate protocols to prepare the cabinet beforehand. The media should fill the bottom part of the petri dish about halfway.

12. **Solid Media** plates should be allowed to cool in the biosafety cabinet with their lids partially off to minimize condensation. After they have completely set (10-30 min), put their lids on and store in the refrigerator upside down, so that the lid is on the bottom and the solid media is on top.
13. Media (solid or liquid) can be stored in the refrigerator for up to a month. If the liquid media becomes cloudy and you are unable to make more, autoclave it before using. Otherwise, autoclave it before pouring it down the drain. Solid media plates can be disposed of in the biohazard waste.

Disposal

1. **Liquid Media** containing cells should be autoclaved and bleached before being poured down the drain. See the disposal of suspension cells for more detail.
2. **Solid Media** plates can be disposed of in the hazardous waste in the CCF. This gets autoclaved in the departmental autoclave when it is filled.

Making Plated Cell Cultures

You can start a plate from a suspension culture (Steps 1-6). Plated cells need to be split every few weeks if they are growing (Steps 7-8). Everything should be done in a biosafety hood or similarly sterile area to minimize the amount of contamination that will get into your culture.

Directions

1. Prepare biosafety cabinet.
2. Prepare your materials by spraying everything with 70% EtOH:
    a. Spray 2 large filter papers of any weight and place in biosafety cabinet to dry.
    b. Spray forceps or tweezers and place in biosafety cabinet to dry.

c. Spray spatula and place in cabinet to dry. I recommend a spatula that has a scooped end.

d. Cell cultures you will be using.

3. Take suspension cells and allow the cells to settle as much as possible. Gently decant as much of the liquid as possible into an autoclave bottle.
4. Use a spatula to remove cells and place on the dry filter paper. The point of this is to remove as much of the liquid media as possible from the cells. Gently squish the liquid out of the cell mass and move the cells around on the filter paper to essentially pat them dry.
5. Take about 1 cm^3 (approximately a g) of cells and use forceps to place onto solid media plate.
6. Gently pat the cells into the plate with the forceps so that they are securely stuck on the solid media. They should not be embedded in the media.
7. Remove the newly plated cells and wipe with a KimWipe dampened with 70% EtOH.
8. Secure the plate lid to the bottom of the plate by wrapping it around the seam with parafilm.
9. Label the plate with the cell strain, date, and researcher's initials around the top of the lid. Ex: A7 Rice Cells, 9/17/20, FDS
10. Place into a dark, room temperature space (can be the drawer in the CCF or can be anywhere wrapped in foil) and allow to grow.
11. After a few weeks, take new growth off the callus and place onto a new plate as described in Step 6. You should not have to remove more than a pea sized amount of callus for each plate.
12. Gently push the new callus into the plate so that it sticks and is fairly flat.
13. Repeat Steps 7 – 8 every few weeks, or as you see new growth on the callus.

Disposal

1. Put old cell plates into the biohazard waste bin in the CCF. Do not allow this bin to overflow. If it is full it will need to be autoclaved in the departmental autoclave.

Making Suspension Cell Cultures

Suspension cultures only use liquid media, so you don't need solid media plates. You can start a suspension culture from a plated culture (Steps 1-8). Once started, suspension cultures need to have their media changed every 1-2 weeks (Steps 8-12). As stated in the previous section, steps should be completed in a biosafety hood or other sterile environment that has been prepared appropriately.

1. Prepare biosafety cabinet.
2. Prepare the materials you will need:
    a. Spray out the inside of the Erlenmeyer flasks you will be using to create your suspension cultures with 70% EtOH. I suggest using 100 mL flasks.
    b. Place the Erlenmeyer flasks upside down on a KimWipe in the biosafety cabinet to remove as much of the residual EtOH.
    c. Clean forceps with 70% EtOH.
    d. Collect solid media plates with cells that you will be using – you should use cells that are recently grown, not cells that have just been plated. Spray these with 70% EtOH before putting in biosafety cabinet.
    e. Grab cooled liquid media and spray bottle with 70% EtOH before placing in biosafety cabinet.
3. Place a small amount of cells from a plated culture into an Erlenmeyer flask, approximately 1 cm^3 (this equates to about a gram).

4. Fill the Erlenmeyer to approximately the 75 mL mark with the cooled liquid media.
5. Before removing suspension cultures from the good, place a small piece of foil cleaned with 70% EtOH over their openings.
6. After removing the flasks from the hood, wrap the bottom part of the foil with parafilm so that it is sealed.
7. Label the flasks with the cell strain, date and your initials (ex. A7 Rice Cells, 9/17/20, FDS)
8. Cover flasks in foil and place on shaker at 140 rpm.
9. After 1-2 weeks of shaking, remove from the shaker to replace the media.
10. To replace the media, take suspension cells into hood and decant the old media.
11. If the cells are growing well, remove a portion of them and place into a new Erlenmeyer flask, like in Step 3. Fill flasks to 75 mL mark.
12. Cover Erlenmeyer flasks with foil as before, and label correctly, before placing on the shaker at 140 rpm.

Disposal

1. Take any media containing cells and autoclave:
    a. **Media in Erlenmeyer flasks** should have a piece of foil over the opening and a piece of autoclave tape across the foil. The flasks should be placed in an autoclave tray such that they do not touch.
    b. **Media in Autoclave bottles** should have their caps slightly unscrewed and a piece of autoclave tape across the cap. The bottles should be placed in an autoclave tray such that they do not touch.

2. After autoclaving, allow to cool, and add bleach so that you've created approximately a 20% bleach solution. For example, if you have 75 mL of media containing cells, add approximately 20 mL of bleach.
3. Allow bleach solution to sit for an hour to really ensure everything is killed. Pour down the drain with the tap on so that there is a lot of water going down the drain.
4. Use a sponge and a spatula to clean the sides of any flasks or bottles that still have cells stuck in them. Wrap the sponge around the spatula so that it becomes similar to a pipe cleaner.

13. Allow flask or bottle to dry upside down in appropriate cabinet:
    a. **Erlenmeyer flasks** go into the Levinger Group cabinet.
    b. **Autoclave bottles** go into the cabinet directly right of the sink.

APPENDIX VI: How to conduct cell experiments described in chapterS 2, 3 and 4

Note: These are examples of the experiments conducted, they were not necessarily conducted in this order and the cryoprotectant mixture of interest changed. However, a calibration of each deuterated cryoprotectant was performed prior to every experiment.

EXP 1: Calibration of 15% d_6-Ethylene Glycol

Take full FOV images from highest concentration to lowest concentration. Concentrations should be 20%, 15%, 10%, 7.5% and 0%. After tuning the HV, gain, and offset to the appropriate levels, record each and do not change for the rest of the experiments.

EXP 2: Static image of 15% d_6-EG exposed cells

Place small amount of callus in vial and expose it to 15% d_6-EG solution. Record the time exposure started and the time the first image was acquired. After taking the first image, take an image of the cells with the time delay set to 0. Try to minimize the number of µm/pixel by zooming into the cell of choice – this should be around 0.250 µm. This experiment can serve as a baseline for what to expect the cells to look like after exposure.

EXP 3: Flow time series of 15% d_6-EG

Place a small amount of callus in a vial and fully cover it with MS media solution. Perturb the sample, then pipette the liquid media and cells into the chamber of the ibidi cell. Carefully place the prepared PLL cover slip on top to the channel. Flip the whole chamber over and press down onto the table, protecting it with a KimWipe, to fully seal the chamber.

If you are pushing solutions through the ibidi cell, prepare your media syringe, attach it to the appropriate tubing and fill the tubing so that it drips. Attach the tubing to the ibidi cell carefully,

trying to minimize any bubbles formed. Connect the waste tubing to the ibidi cell and then to a waste vial.

If you are pulling solutions through the ibidi cell, prepare your media vial. Ensure that media fills the tubing completely and there is at least 0.2 mL of media in the syringe—it will not pull if it is empty. Connect the tubing to the ibidi cell and put the cell on the microscope stage piece.

Place the whole perfusion set up onto the CARS microscope with the syringe pump on the right side of the microscope.

Collect your data! First ensure that the beam block is in, and the system shutter is on. Then turn on the syringe pump and pull media through the ibidi chamber. This ensures that any cells that have not properly adhered are not chosen as the cells to be imaged. Use the transmission light and the oculars to find the cells you want to image. These cells should look turgid and have some internal movement. Additionally, they should not be blocked by cells behind themselves. Take your time to find cells that look good. Focus on the cells and the re-collimate the light (the ibidi cells change how the beam needs to be collimated).

If your cells are good, turn off the transmission light, push in the transmission setting on the microscope, and cover it so that it is enclosed. Remove the beam block and turn the system shutter off. Turn on XY-Repeat and open the shutter. You should be able to see them enough to focus on the cells better, though it should not look like there is any signal and everything should be dark and shadow-y.

Begin the image acquisition. Your settings should be set up so that each frame is taken in about 10 s (with Kelaman averaging). Set the time acquisition to go for approximately 20 min. Press go.

If you are pushing solutions through the ibidi cell, prep your 15% d_6-EG syringe with about 2 mL of solution. Once prepared, remove the media syringe from the pump, and carefully remove the

tubing from the syringe. This should be done to minimize bubbles, so the tubing should be pointed down while the syringe is pointed up. Place the tubing on the EG syringe and put the syringe on the pump. Turn the pump on and note the time slice where you replaced the syringe.

Alternatively, if you are pulling solutions through the ibidi cell, prep your 15% d_6-ethylene glycol vial. Turn off the syringe pump before changing your media vial to your ethylene glycol vial to ensure that a bubble does not form. Place the tubing in the appropriate vial and turn the pump back on.

Allow at least 1 mL of CPA solution to flow through the set up. This ensures that it is full before you turn it off. Do not allow the syringe to empty. Once 1-1.5 mL has flowed through the system, turn the pump off and leave it for the rest of the experiment.

Let the experiment run!

After the experiment is done, take a regular brightfield image.

LIST OF ABBREVIATIONS

CARS	coherent anti-Stokes Raman scattering
SRS	simulated Raman scattering
BF	brightfield
IR	infrared
PMT	photo multiplier tube
BPF	band pass filter
BK#	background number…
C#	cell number…
plas	plasmolysis
deplas	deplasmolysis
PVS2	Plant Vitrification Solution 2
PVS3	Plant Vitrification Solution 3
DMSO	dimethyl sulfoxide
EG	ethylene glycol
Glyc (or glyc)	glycerol
EtOH	ethanol
PLL	poly-L-lysine
d_n-	deuterated… (for example, d_6-DMSO is deuterated dimethyl sulfoxide)
wt/v	weight by volume
cm^{-1}	wavenumbers
°C	degrees Celsius
s	second(s)
hr	hour(s)
g	gram(s)
mg	milligram(s)
L	liter
mL	milliliter

cm	centimeters
µm	micrometers
nm	nanometers
rpm	rotations per minute
pix	pixel(s)
a.u.	arbitrary units
min	minimum
max	maximum
PPE	personal protective equipment
CSU	Colorado State University
CCF	Cell Culture Facility (CSU)
ALMC	Advanced Light Microscopy Core (Colorado University, Denver)
USDA	United States Department of Agriculture
NIFA	National Institute of Food and Agriculture
AAAS	American Association for the Advancement of Science
NSF	National Science Foundation